TESTING POTENTIAL GROUNDWATER RESERVOIR CONNECTIVITY USING ISOTOPES IN THE SOUTH-CENTRAL KAROO REGION

By

Sinazo Dlakavu

Submitted in fulfilment of the requirements of a Masters degree in Geology/Geoscience at the Nelson Mandela University

April 2019

Supervisor: Prof MJ de Wit

NELSON MANDELA UNIVERSITY
AEON AFRICA EARTH OBSERVATORY NETWORK
NRF National Research Foundation
iThemba LABS Laboratory for Accelerator Based Sciences

NELSON MANDELA
UNIVERSITY

DEPARTMENT OF ACADEMIC ADMINISTRATION
EXAMINATION SECTION
SUMMERSTARND NORTH CAMPUS
PO Box 77000
Nelson Mandela Metropolitan University
Port Elizabeth
6013

Enquiries: Postgraduate Examination Officer

DECLARATION BY CANDIDATE

NAME: Sinazo Dlakavu

STUDENT NUMBER: s214391396

QUALIFICATION: MSc Geology

TITLE OF PROJECT: Testing potential groundwater reservoir connectivity using isotopes in the south-central Karoo region.

DECLARATION:

In accordance with Rule G4.6.3, I hereby declare that the above-mentioned treatise/ dissertation/ thesis is my own work and that it has not previously been submitted for assessment to another University or for another qualification.

SIGNATURE: 

DATE: 19 March 2019

Acknowledgements

Umntu Ngumntu Ngabantu

I would like to thank my family for their patience, support and prayers. I would especially like to thank my mother and sisters for persevering in their work places and showing me the importance of never giving up. My youngest brother was always encouraging throughout this journey as well and was even willing to become my field assistant when I could not find one. I wish my father was still alive to see how far we have all come as a family (May his soul rest in peace).

My family, AmaJwarha Amakhulu

I would like to thank Professor Maarten de Wit my supervisor for always encouraging me and for ensuring that I had funding. I appreciate Mr. Barry Morkel's hard work as he obtained land owner contact details so that the groundwater team could collect samples in the Karoo Basin. I am also grateful to every land owner who welcomed my field assistants (Richard Campbell and Manyano Makhuzeni, whom I would like to thank as well) and me in their properties to collect groundwater samples.

I would like to thank Mr. Butler, Mr. Mabitsela and Mr. Malinga of iThemba Labs for analysing my groundwater samples and for sharing their knowledge with me when I visited the laboratory. I would like to thank Bastien Linol for helping me edit some chapters. I would like to thank Thomas Muedi for showing me how to use QGIS and Inkscape. Last but not least, I would like to thank Emily Bosire for her administrative assistance as she helped me plan field trips and procure everything I needed for this project.

Abstract

Documenting areas with natural groundwater reservior connectivity using isotopes before the anticipated shale gas development in the Karoo Basin of South Africa could contribute to developing legislative framework for hydraulic fracturing. In this study, groundwater dynamics (primarily connectivity between old/deep and low temperature modern/shallow (<25°C) groundwater) are studied using isotopes (^{14}C, $\delta^{18}O$-$\delta^{2}H$, ^{3}H, and $\delta^{13}C$) in conjunction with geochemical parameters (sampling depth (masl) and (mbgl), temperature (°C), Electrical Conductivity (EC) (µS/m) and sustainable yield (l/s)). Previous groundwater studies conducted in the Karoo Basin suggest that ^{14}C (pMC) has the least overlap among isotope signature constraints between the different aquifer/groundwater groups. The outcomes of ^{14}C analysis for this study suggest that one groundwater sample is an old/deep groundwater sample (<53 pMC), and that three groundwater samples are composed of shallow/young groundwater mixed with old/deep groundwater (<74 pMC). These four relatively older samples have calculated ^{14}C ages ≥ 1700 years and were collected from boreholes that are north-east of the Cape Mountains (~50 km). The position of these samples suggests that deep-seated faults within the Cape Mountains and the basement of the southern Karoo Basin act as preferential pathways for deep groundwater migration (as is consistent with existing deep geophysical data) to shallower depths (<60 mbgl) where it cools and/or mixes with low temperature groundwater (<25°C). Three more groundwater samples were found to match the relatively old calculated ^{14}C ages (≥ 1700 years) of the groundwater samples collected close to the Cape Mountains even though they have modern ^{14}C (pMC) concentrations (>74 pMC). This implies that adjusting the ^{14}C content in Dissolved Inorganic Carbon (DIC) based on its dilution by ^{14}C free carbonates is influential in controlling the mixed groundwater ages, and that relatively older groundwater occurs at shallow depths in other parts of the study area possibly due to linked fault systems between deep and shallow aquifers. $\delta^{18}O$-$\delta^{2}H$ relationships for the sampled groundwater suggest that groundwater samples collected within the main drainage of the Great Fish River plot close to the Global Meteoric Water Line (GMWL) indicating that the recharge water to this groundwater does not experience significant evaporation. The average isotope composition of the recharging water for the all of the sampled groundwater is -7.90 ‰ and -46.72 ‰ for $\delta^{18}O$ and $\delta^{2}H$, respectively. This result plots halfway between rainwater ^{18}O-^{2}H relationship lines for the Indian Ocean and the Atlantic Ocean. This suggests that the rainwater from which the sampled groundwater was derived from evolved from both the Indian and Atlantic Ocean waters.

List of Figures

List of Tables

List of Equations

Table of Contents

1. Introduction

The prospect of shale gas development in the Karoo Basin of South Africa has raised concerns over the threat that hydraulic fracturing may inflict on groundwater (van Tonder et al. 2013; Murray et al. 2015). One of these threats is the potential for induced propagation of preferential pathways between shallow (< 300 m) and deep aquifers/groundwater reservoirs (> 300 m) (Academy of Science of South Africa (ASSAf) 2016). Preferential pathways may be instrumental in connecting deep and shallow groundwater reservoirs/aquifers and thus polluting shallow potable groundwater by carrying fracking fluids and groundwater from deep aquifers (which is usually saline) to shallower depths (Myers 2012; Warner et al. 2012; ASSAf 2016). This project attempts to document area(s) with potential reservoir connectivity before shale gas development in the south-central part of the Karoo Basin using $\delta^{18}O$, $\delta^{2}H$, ^{13}C, ^{3}H and ^{14}C. Van Tonder et al. (2013) speculated that in the Karoo Basin groundwater abstraction boreholes drilled along preferential pathways such as a fault or a dyke intersecting the fracked reservoir and situated at approximately 6 km from a shale gas well pad could be polluted in less than 2 months.

Previous studies conducted in the Cape Mountains and the Karoo Basin have shown that thermal springs (> 25°C) are likely representatives of old groundwater that has migrated from deep aquifers to shallow aquifers, thus providing evidence that natural reservoir connectivity occurs at various locations in the Karoo Basin and Cape Mountains. Such studies were conducted using isotopes (e.g. Mazor & Verhagen 1983; Egle 1996; Diamond & Harris 2000; Swana 2016) and magnetotelluric (MT) surveys (e.g. Weckmann et al. 2012). Figure 1-1 is a simplified geological map showing the localities of thermal springs that have been documented to conduct old groundwater from deep aquifers. It is important to note that although temperature plays an important role in delineating groundwater from different aquifer depths, old groundwater from deep aquifers does not always have high temperatures (>25°C) (Murray et al. 2015 p.viii). According to Miller et al. (2015), Murray et al. (2015) and Swana (2016), old groundwater from deep aquifers has isotope signatures of -6.7 to -7.7 ‰ for $\delta^{18}O$; -39 ‰ for $\delta^{2}H$; 0 to 0.5 TU for ^{3}H and 20 to 53 pMC for ^{14}C (Figure 1-1). Mixed (mixture between old and modern groundwater) groundwater has isotope signatures of -4.9 to -5.7 ‰ for $\delta^{18}O$; -28 for $\delta^{2}H$; 0.1 to 0.9 TU for ^{3}H (TU) and 50 to 74 pMC for ^{14}C. Shallow/modern groundwater has isotope signatures of -4.9 to 0.4 ‰ for $\delta^{18}O$; -30 to 0 ‰ for $\delta^{2}H$; 0.5 to 3.1 TU for ^{3}H and 74 to 94 pMC for ^{14}C.

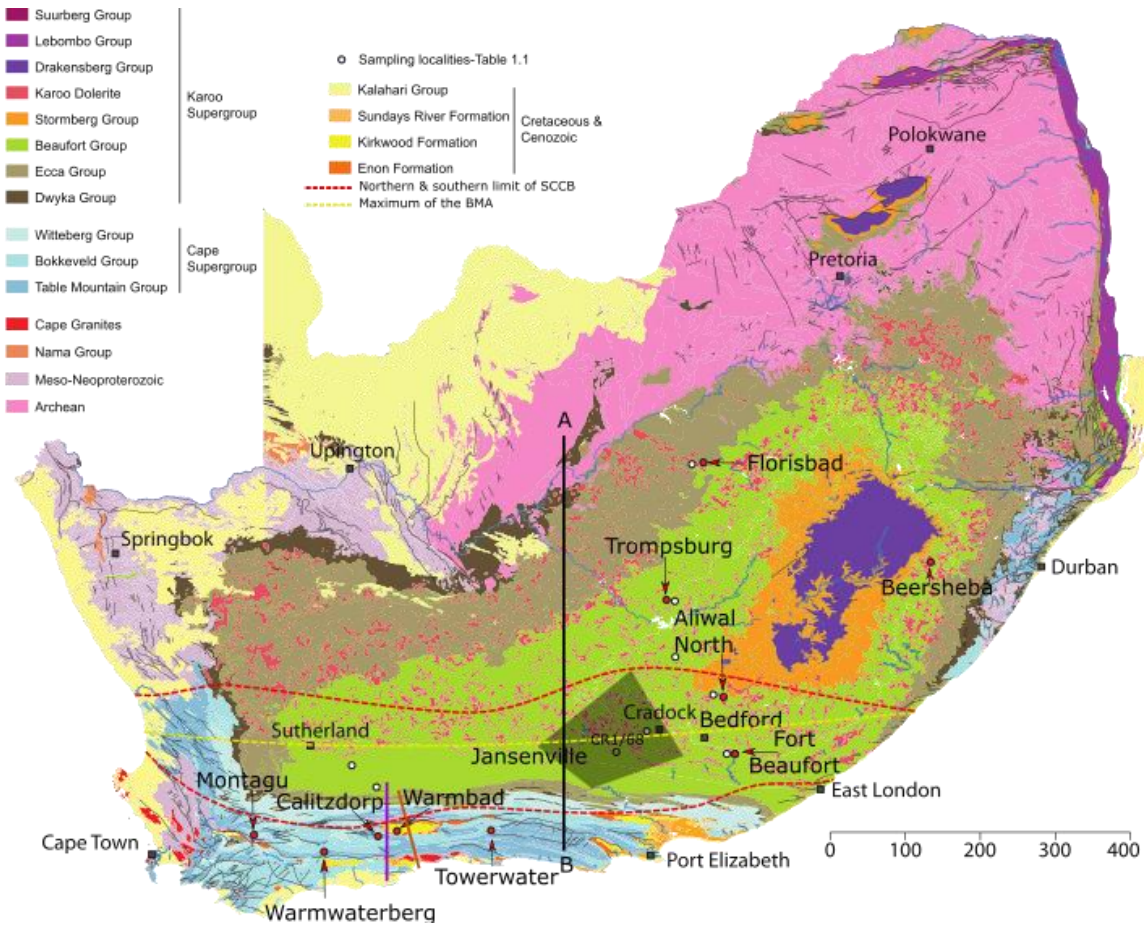

Figure 1-1: Simplified geological map of South Africa showing the locations of thermal springs where groundwater from deep aquifers are known to have migrated to shallow aquifers (red labelled dots), groundwater sampling locations for Table 1-1 isotope studies, the BMA (Beattie Magnetic Anomaly) and SCCB (Southern Cape Conductive Belt). Also shown on the map is the study area (shaded black) and the positions of lines for a N-S geological cross section of the geology of the Karoo Basin (A-B) (Figure 3-2), and for MT surveys conducted in the southern part of the Karoo Basin and Cape Mountains (see Figure 2-9-orange line & Figure 2-10-purple line) (modified from Linol & de Wit 2016).

Table 1-1: Groundwater isotope signatures from eight localities in the Karoo Basin (data from Miller et al. 2015; Murray et al. 2015; Swana 2016).

Groundwater Type	$\delta^{18}O$ (‰)	$\delta^{2}H$ (‰)	^{3}H (TU)	^{14}C (pMC)	Alkalinity (mg/L HCO_3^-)
Shallow/modern	-4.9 to 0.4	-30 to 0	0.5 to 3.1	74 to 94	236 to 764
Mixed	-4.9 to -5.7	-28	0.1 to 0.9	50 to 74	167 to 403
Deep/old	-6.7 to -7.7	-39	0 to 0.5	20 to 53	20 to 228

Jasechko et al. (2018) state that, “the vulnerability of groundwater to contamination is closely related to its age”. Using isotopes, the relative age of groundwater can usually be deduced and if older groundwater occurs at shallower depths it is possible that there is aquifer connectivity in the area (e.g. Miller et al. 2015). The measurement of the success rates of various isotopes in distinguishing deep/old groundwater from shallow/modern groundwater in the Karoo Basin is largely based on the correlation of different isotopes with groundwater temperature (Figure 1-2 to Figure 1-5). ^{14}C and ^{18}O-^{2}H are defined as having a 100% success rate in defining groundwater age in the Karoo Basin, ^{3}H is labelled as having a 50-75% success rate and $\delta^{13}C$ is termed as having a less than 50% success rate (Murray et al. 2015). ^{14}C (pMC) has the strongest correlation with temperature (R^2 = 0.47-Figure 1-2); this is followed by $\delta^{18}O$ (‰) (R^2 = 0.38-Figure 1-3A), then ^{3}H (TU) (R^2 = 0.19-Figure 1-4A), and finally $\delta^{13}C$ (‰) which has the poorest/weakest linear correlation with temperature (R^2 = 0.11-Figure 1-5A). The correlation between ^{14}C and other isotopes is also shown from Figure 1-3(B) to Figure 1-5(B). $\delta^{18}O$ (‰) vs. ^{14}C (pMC) has the strongest linear correlation (R^2 = 0.52) and $\delta^{13}C$ vs. ^{14}C (pMC) has the weakest linear correlation (R^2 = 0.01). Although certain isotopes (e.g. $\delta^{13}C$ (‰) have low success rates in delineating deep/old groundwater, they can be instrumental in studying additional aspects of groundwater such as groundwater mineralisation and groundwater recharge (Murray et al. 2015).

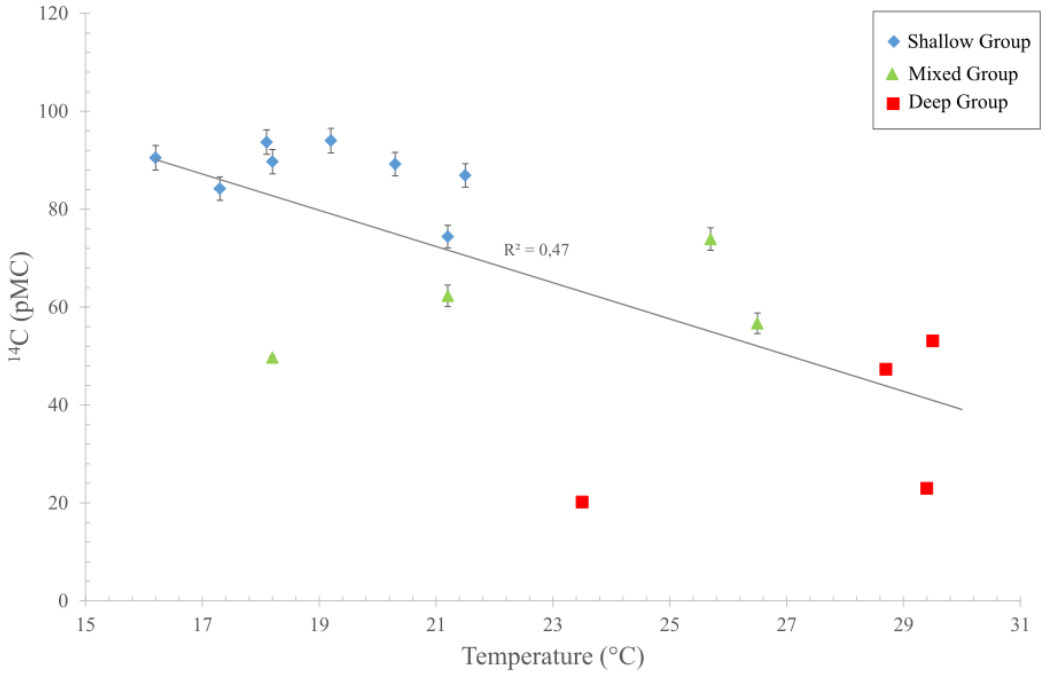

Figure 1-2: ^{14}C (pMC) vs. Temperature (°C) (R^2 = 0.47) for the three aquifer depth groundwater groups in the Karoo Basin (modified from Swana 2016).

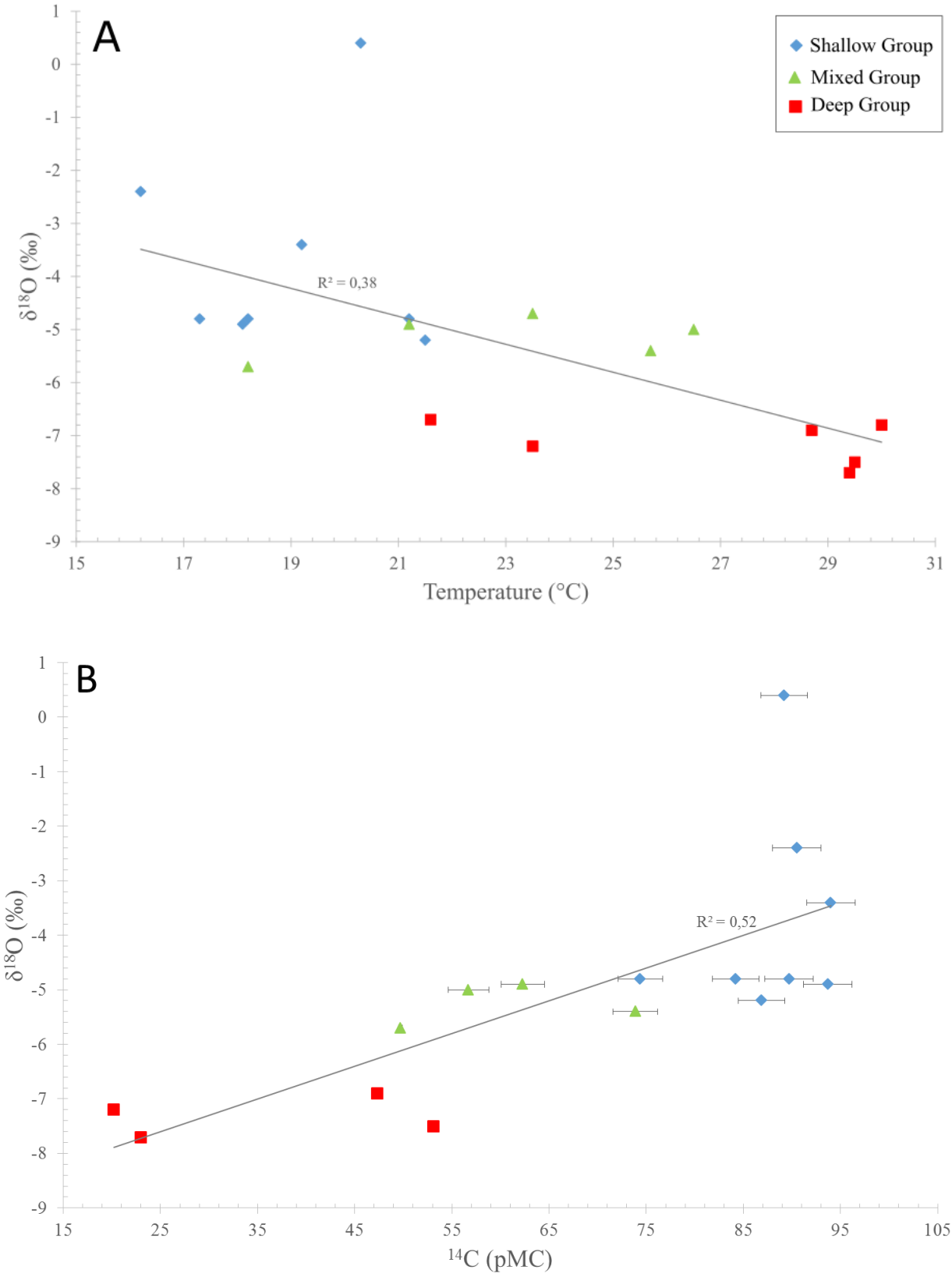

Figure 1-3: $\delta^{18}O$ (‰) vs. Temperature (°C) (R^2 = 0.38) (A) and ^{14}C (pMC) (R^2 = 0.52) (B) for the three aquifer depth groundwater groups in the Karoo Basin (modified from Swana 2016).

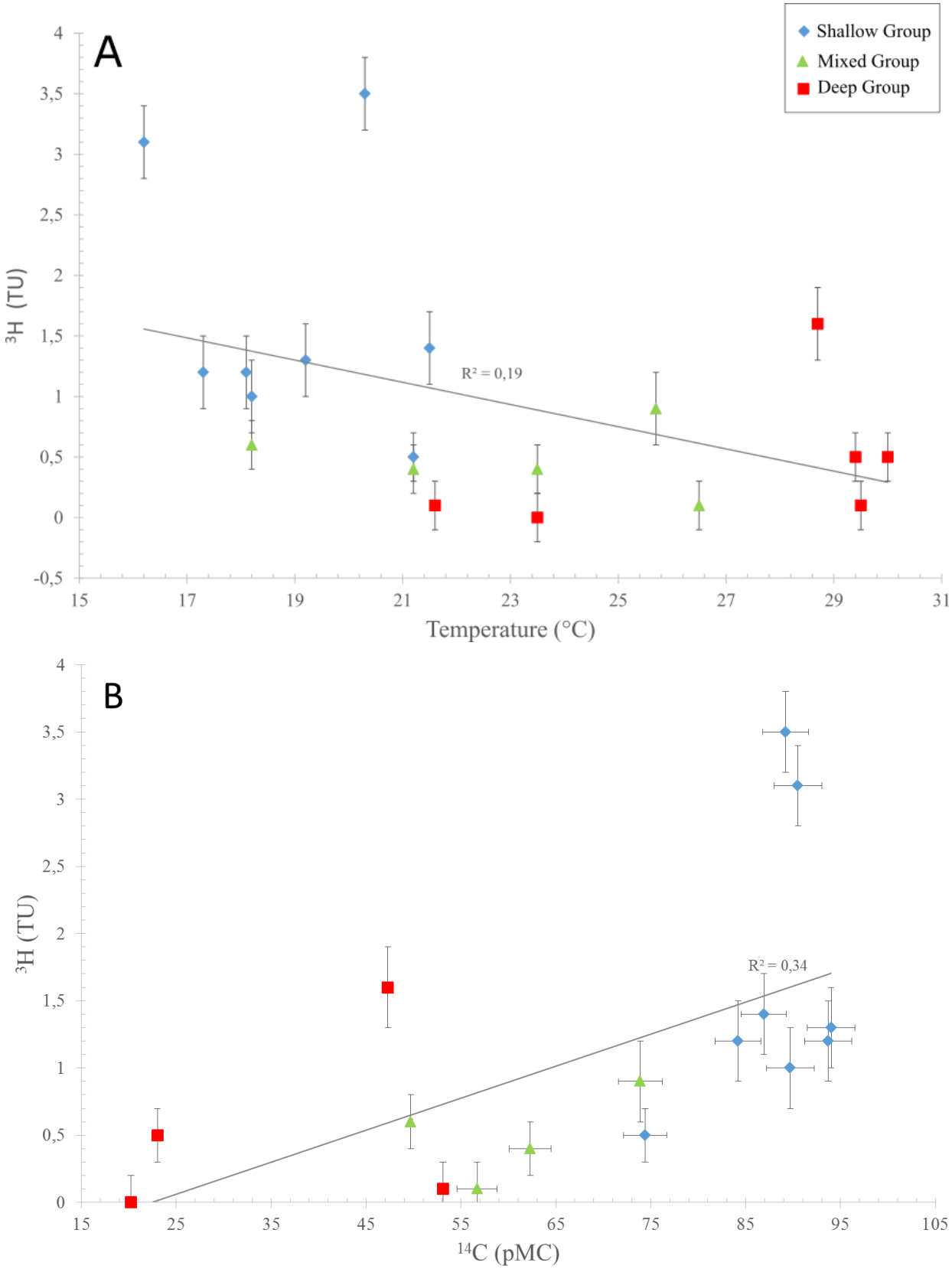

Figure 1-4: ^{3}H (TU) vs. Temperature (°C) (R^2 = 0.19) (A) and ^{14}C (pMC) (R^2 = 0.34) (B) for the three aquifer depth groundwater groups in the Karoo Basin (modified from Swana 2016).

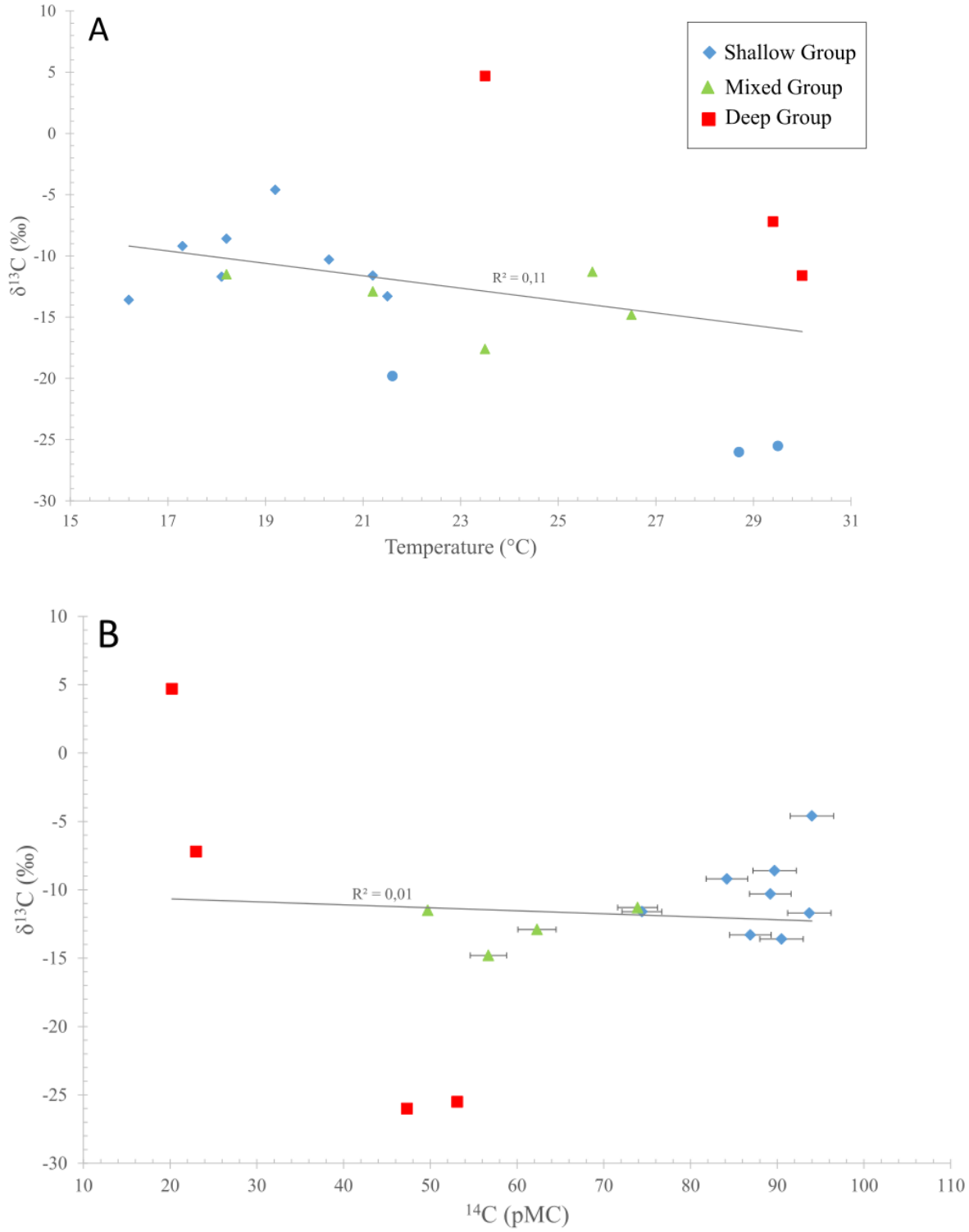

Figure 1-5: $\delta^{13}C$ (‰) vs. Temperature (°C) (R^2 = 0.11) (A) and 14C (pMC) (R^2 = 0.01) (B) for the three aquifer depth groundwater groups in the Karoo Basin (modified from Swana 2016).

1.1. Aims and Objectives

Various thermal springs have been identified as representatives of deep groundwater that has migrated to shallow aquifers in the Karoo Basin (e.g. Diamond & Harris 2000; Swana, 2016; Weckmann et al. 2012). This suggests that upward flow occurs within Karoo Basin aquifers. The Karoo Groundwater Expert Group (KGEG) (2013) postulates that some old groundwater from deep aquifers cools during its upward migration to shallower depths. Groundwater consumers in the Karoo Basin and South Africa as a whole may in turn utilize this cool groundwater (< 25°C) (Department of Water Affairs and Forestry (DWAF) 1996) without knowing that it might be connected to deep groundwater reservoirs. This could be a problem should shale gas development be implemented in the Karoo Basin because hydraulic fracturing may induce new preferential pathways between deep and shallow groundwater reservoirs, thereby further promoting groundwater reservoir connectivity. This could in turn lead to the pollution of potable groundwater from deep saline waters and fracking fluids. Therefore, it is important that areas with natural reservoir connectivity between cool (<25°C) possibly potable groundwater and old groundwater likely from deep aquifers are documented before the on-set of shale gas development, so that extra caution could be taken around these areas when conducting hydraulic fracturing.

The main aim of this thesis is to investigate possible connections between deep groundwater reservoirs and cool (<25°C) groundwater from shallow aquifers before the on-set of the anticipated shale gas development in a selected area of the south-central Karoo Basin (in the Eastern Cape). The first objective of the study is conducting a hydrocensus in order to identify suitable groundwater sampling locations in an area demarcated for baseline studies by Africa Earth Observatory Network - Earth Stewardship Science Research Institute (AEON-ESSRI). The second objective is to define the age of the water samples and evaluate groundwater dynamics such as groundwater recharge and salinization.

1.2. Outline of the Thesis (Thesis Structure)

This thesis is divided into 8 chapters. The first chapter is an introductory chapter establishing the basis of the main topic. Chapter 2 is a review of the available literature relevant for this thesis. Chapter 3 is an assessment of the study area. Chapter 4 is technical chapter that describes the methodologies used in this study. Chapter 5 provides the research results. Chapter 6 is a

discussion of the results. Finally, Chapter 7 and Chapter 8 are conclusions and recommendations chapters, respectively:

- Chapter 1 introduces MT and isotope research studies conducted in the Cape Mountains and Karoo Basin that provide evidence for reservoir connectivity. This chapter also details the aims and objectives of this project.
- Chapter 2 provides a background and essential information to this research. It reviews literature pertaining to: Critical Zone (CZ) research, the importance of groundwater, hydraulic fracturing prospects in the Karoo Basin, MT research, and the different isotopes used in this study ($\delta^{18}O$, $\delta^{2}H$, $\delta^{13}C_{DIC}$, ^{14}C and ^{3}H).
- Chapter 3 gives an account of the study area. This chapter is divided into five sections, discussing the geology, geohydrology, vegetation, population and access to water resources and land use within the study area.
- Chapter 4 describes the methodologies of the project. This chapter is divided into three sections, namely: hydrocensus, sampling and laboratory analysis.
- Chapter 5 provides the results. This chapter is divided into 3 sections namely: hydrocensus maps and EC profiles; laboratory and field results and isotope results.
- Chapter 6 discusses the research results. Evidence for reservoir connectivity is argued using ^{14}C results. The groundwater recharge and salinization mechanisms are discussed based on $\delta^{18}O$ and EC results, and $\delta^{13}C_{DIC}$ results are used to evaluate the mineralisation of the analysed groundwater.
- Chapter 7 provides a consolidation of all the important aspects gained from the isotope results. This chapter also provides a conceptual model that demarcates where natural reservoir connectivity within the study area possibly occurs, and consolidates the overall outcomes of this research project.
- Chapter 8 recommends future research questions that need to be considered to lessen the potential impact that hydraulic fracturing may pose to potable groundwater. Recommendations include using transdisciplinary research methodologies to identify more areas with reservoir connectivity in the Karoo Basin before the on-set of hydraulic fracturing; and to advise the South African government in developing a legislative framework that deals with the potential for groundwater contamination in such areas.

2. Background and Essential Information

The AEON-ESSRI of Nelson Mandela University (NMU) has initiated a natural baseline scheme across the Karoo Basin before the potential on-set of hydraulic fracturing. This includes research in the fields of geology, groundwater/water-well chemistry, geophysics, biology, health and socio-economic systems[1]. This ensuing project falls under the groundwater/water-well chemistry section of this AEON-ESSRI baseline research project. Reference will be made to studies in the fields of geology, geophysics and biology because AEON-ESSRI is focused on transdisciplinarity. Transdiscplinarity is important for research conducted in the Critical Zone (CZ) (see section below) because it allows researchers from different fields to share ideas and data in order to solve environmental and social problems (Parsekian et al. 2014). In order to highlight the interaction of different aspects or spheres in the CZ, the effect that the detonation of nuclear bombs in the 1960s has on groundwater is discussed extensively in this chapter (see sections 2.7.2 and 2.8.2).

2.1. Groundwater in the Earth's Critical Zone (CZ)

Various researchers (e.g. Brantley et al. 2007; National Research Council (NRC) 2009; Parsekian et al. 2014; Dhansay 2017) define the CZ as a life-supporting layer of the Earth that reaches from the top of the vegetation down through soil, weathered rock, and fractured bedrock and to the lower limits of groundwater (Figure 2-1). This layer is regulated by the complex interactions between rock, soil, water, air and living organisms, which all work to determine the availability of life sustaining resources such as water (Brantley et al. 2007). It is therefore important that the individual interfaces in the CZ are sufficiently defined because this provides common ground effective for transdisciplinary research (Lin 2010). Transdisciplinary research assists with understanding the CZ from different perspectives and scales. This is an important aspect for groundwater research because groundwater is a part of the hydrologic cycle, which forms an environmental gradient that can profoundly shape CZ evolution socially and environmentally at continental to global scales (Fan 2015). The following section summarises the origin of groundwater from precipitation in South Africa. This provides an understanding of the connections between groundwater and rainfall patterns within the CZ in South Africa.

[1] To view scientific reports done by AEON-ESSRI visit http://aeon.org.za/report-series/

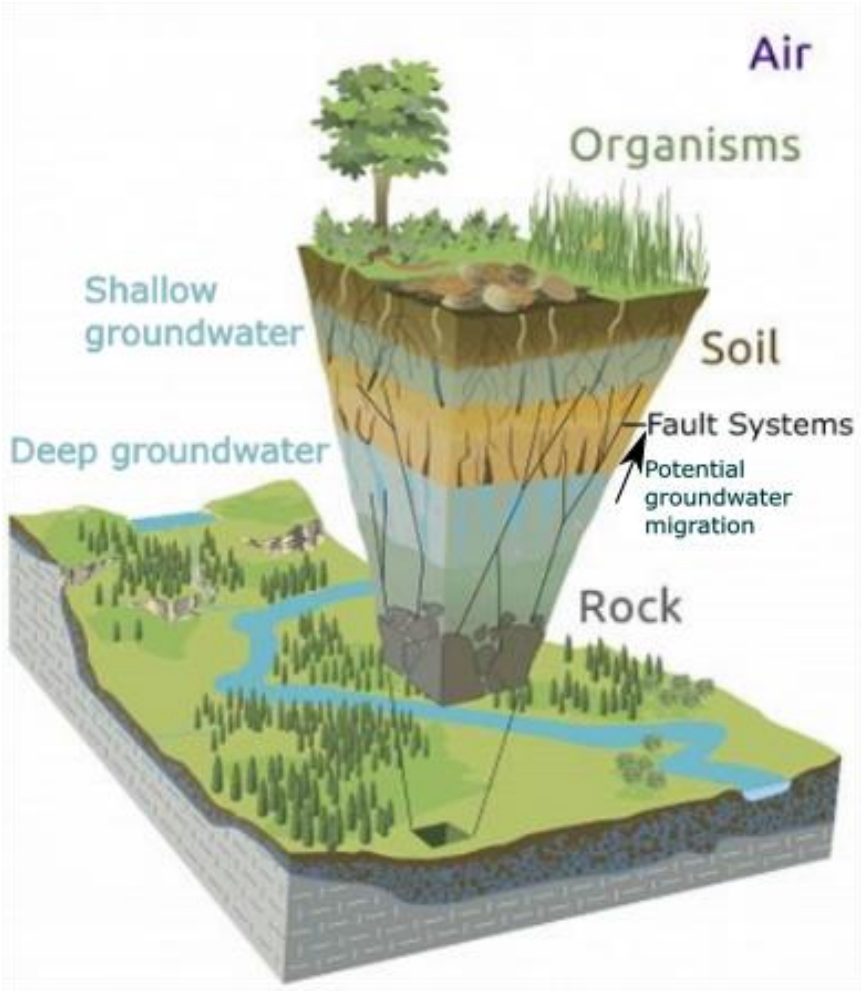

Figure 2-1: Schematic section of the Critical Zone (modified from Chorover et al. 2007). Also shown are fault systems which may act as preferential pathways for deep groundwater migration from deep aquifers to shallow aquifers. For isotope concentrations of deep and shallow groundwater in the Karoo Basin refer to Table 1-1.

2.2. Origin and Distribution of Precipitation Across South Africa

Groundwater isotope research conducted in South Africa must be linked to a robust understanding of rainfall variability. South Africa is a 1 219 912 km^2 landmass located at the southern tip of the African continent (between latitudes 22° and 35°S, and longitudes 16° and 33°E). The country constitutes an elevated (~ 1500 masl) wedge-like land mass that is outlined by a thin coastal strip and a steep prominent escarpment that flanks the interior Karoo and Kalahari basins (van Wyk et al. 2011). The factors affecting the weather of South Africa and thus rainfall trends include: the Indian and Atlantic oceans; the latitudinal position; the altitude

and the interior plateau of the country (Eamus 2006). The latitudinal position of South Africa implies that the country's climate is influenced by subtropical high pressure systems and therefore experiences a predominantly sub-tropical climate (Kruger et al. 2010; Engelbrecht & Landman 2016). These high pressure systems lead to the subsidence of air over southern Africa, thereby overpowering cloud formation and rainfall. This results in the semi-arid climate across the country (Figure 2-2) (Davis 2010) with a total South African rainfall ca. 497 mm. This means South Africa is approximately two times drier than the rest of the world, which has a yearly rainfall average of 860 mm (Herbst 2013; Swatuk 2017). On Figure 2-2 it is shown that the eastern side of South Africa receives relatively more rainfall (>450 mm/year) than the rest of the country. This is partly due to higher elevations in that area (Jury 2013; Simon et al. 2015).

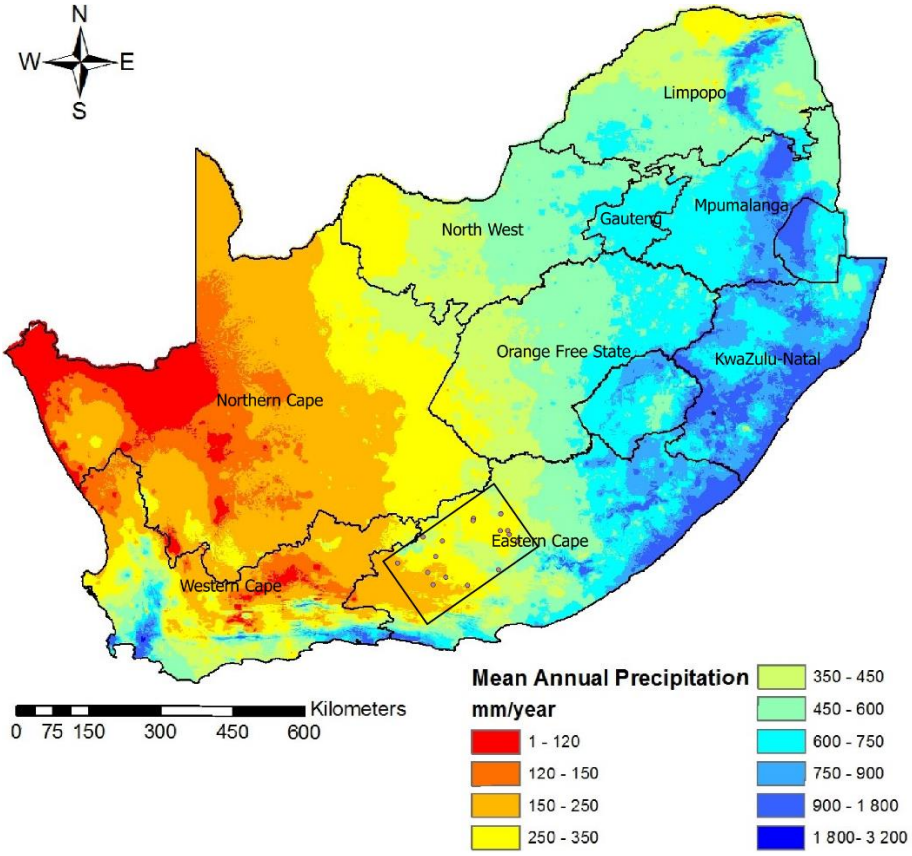

Figure 2-2: Map of South Africa and its provinces with the average annual precipitation in mm/year (modified from Lynch 2004). Also shown on the map is the demarcation of the study area (black rectangle with purple dots symbolising groundwater sample localities).

In South Africa, precipitation originates as evaporated water from the surrounding Atlantic and Indian Oceans (Thomas & Shaw 1991; van Wyk et al. 2011; Diamond 2014). It is largely distributed between winter and summer through the seasonal north-south migration of the

Intertropical Convergence Zone (ITCZ), the Subtropical High Pressure Zone (SHPZ) and the Temperate Zone (Antarctic low-pressure system) (Kruger et al. 2010; van Wyk et al. 2011) (Figure 2-3).

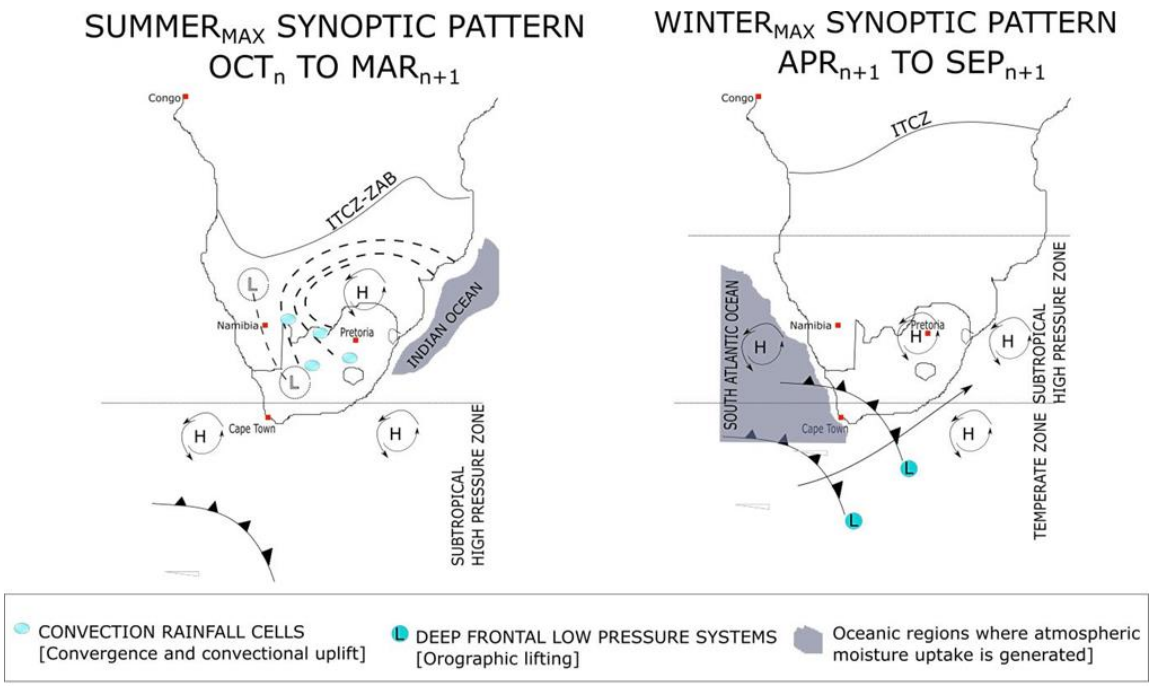

Figure 2-3: Synoptic patterns over Southern Africa during summer and winter seasons in relation to the generation of airborne moisture and the general migration pathways (modified from van Wyk et al. 2011).

Peak summer rainfall occurs when the ITCZ migrates to its most southerly position north of the Angola-Namibia boarder, where it connects with the southerly Zaire Air Boundary (ZAB) (Kruger et al. 2010; van Wyk et al. 2011; Garstang et al. 2014). The ZAB is a region of low pressure that brings wet weather to the Congo region (Cai et al. 2017). It separates the ITCZ from a continental thermal low pressure system (the Kalahari Trough) (Thomas & Shaw, 1991; van Wyk et al. 2011), which develops around January to March over the western side of southern Africa due to extremely heated surface temperatures (van Wyk et al. 2011). The ITCZ-ZAB carries moist air from the equatorial Atlantic and Indian oceans. This air is supported by convergent trade winds, which are generated by an interior, moderate high pressure anticyclonic system oscillating over the north-eastern part of the sub-continent (Thomas & Shaw 1991). This anticyclonic system drives both western and eastern airflow

components. The upper, easterly humid air masses migrate into the Kalahari Trough and form an oscillating low-pressure system that extends from northern Namibia and passes the southern Cape coastal regions during its maximum dominance. Rainstorms are in the form of isolated thunderstorm activated by convectional uplift. Regionally, these storm systems are associated in long trough lines, referred to as line storms, and slowly move from northwest to southeast over southern Africa depending on the consistency of the Kalahari low-pressure system (Kruger et al. 2010). "During an episodic extremely humid event, a band of heavy rain clouds with regional rainfall dominates the summer synoptic picture for a number of successive days, during which rainfall intensities can be significantly high. The magnitude of rainfall intensities during these periods is such that effective groundwater recharge occurs" (van Wyk et al. 2011).

According to van Wyk et al. (2011), winter rainfall occurs when the vertical and horizontal components of the equatorial and southern air circulation system move northwards (Figure 2-3). During this time, southern Africa's weather pattern is controlled by the SHPZ, a zone characterised by three distinguished anticyclones situated across the sub-continent (i.e. South Atlantic, the Botswana/Kalahari and the Indian Ocean Anticyclones). The significant northward movement of the South Atlantic zone brings deep Antarctic air masses that pass the southern tip of South Africa (Reason & Jagaadheesha 2005). Westerly winds in this zone bear the cold Antarctic air masses as cold fronts to the western coastal and immediate inland regions of southern Africa. Cold, polar air masses may however resettle over large portions of southern Africa depending on the physical position and strength of the Botswana/Kalahari Anticyclone (Tadross & Johnston 2012). Cold front centres commonly pass within 10° south of the South African coast. These generate the winter airborne moisture (Figure 2-3). Conventional warm oceanic evaporative principles do not exclusively account for all airborne moisture generation in the Temperate Zone. Low altitude gale force winds mechanically force maritime moisture directly into these low-lying dry air masses. Once on land, orographic uplift caused by rising land surfaces away from the seaboard, initiates a characteristic NaCl precipitation. This precipitation characterises groundwater recharged in winter. Below is an account of the importance of groundwater (van Wyk et al. 2011).

2.3. The Importance of Groundwater and the Shortcomings of Groundwater Development in South Africa

Water in itself is one of the most important resources on earth, as it supports life. However, potable and easily accessible water is not evenly distributed on the planet, partly because the largest freshwater reserve (~67%) is bound in ice and permanent snow cover in the Antarctic; Arctic; and in continental mountains (Shiklomanov 1993). Groundwater is most important because it represents the biggest portion of freshwater on earth (Figure 2-4) (Shiklomanov 1993; Mook 2000; Aggarwal 2013). Groundwater in both renewable and non-renewable aquifers accounts for about 95% of accessible fresh water and supplies more than half of all domestic and irrigation water used around the world (Braune et al. 2014).

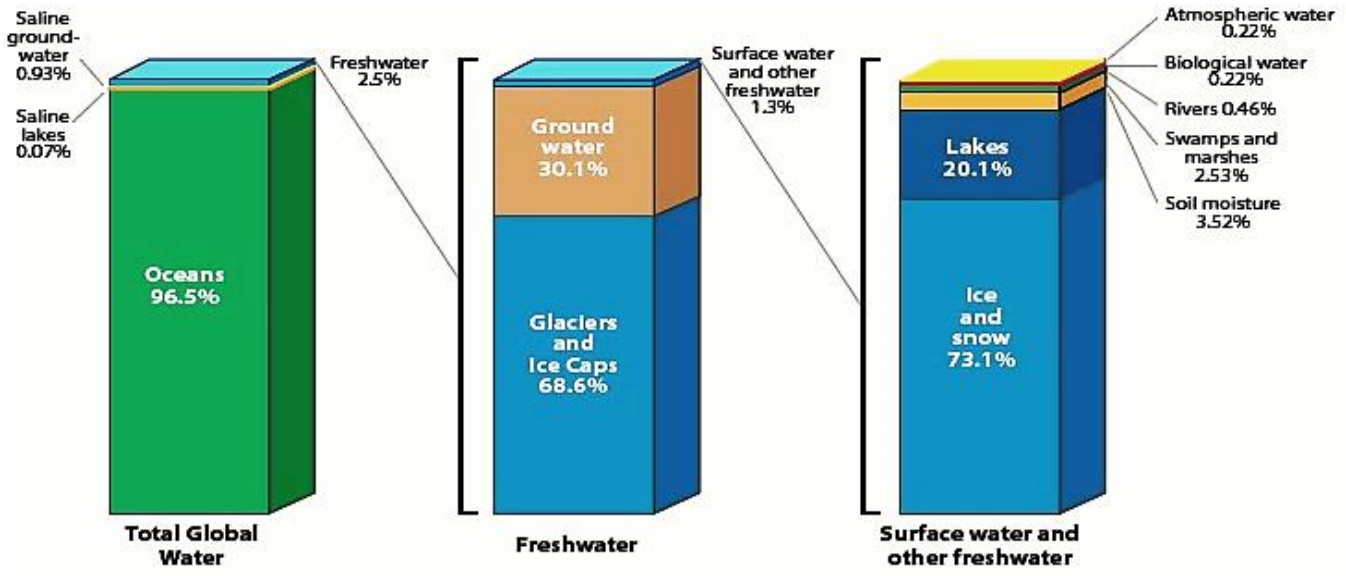

Figure 2-4: Distribution of Earth's Water (from Shiklomanov 1993). Groundwater represents the largest freshwater reserve on Earth.

In the 1960s, groundwater abstraction increased exponentially worldwide, mainly as a result of use for agriculture. This development is sometimes termed the 'silent revolution' and was executed without integrated planning or management. Although the silent revolution kick-started the 'green revolution'[2], which brought about greater food security (Braune et al. 2014),

[2] The Green Revolution refers to a set of research and the deployment of technology transfer initiatives between the 1930s and the late 1960s. This increased agricultural production (due to groundwater accessibility and

the previous lack of proper management by social and institutional dimensions deems groundwater a poorly understood water resource worldwide, especially in Africa (Aggarwal 2013; Braune et al. 2014). The African continent has used only 5% of its available groundwater resources due to lack of human and financial resources to deal with the spatial and temporal variability of water availability (Braune et al. 2014). There is thus an emerging understanding that local groundwater resources (developed through increased groundwater research) will have to play an increasingly tactical part in socio-economic development, specifically for the most vulnerable and most abandoned rural communities in Africa (African Ministries' Council on Water (AMCOW 2008; Aggarwal 2013). For example, groundwater research conducted using isotopes uncovered aspects such as groundwater flow patterns and contamination levels for aquifers in the Sahel, North Africa. This information is valuable for the Sahel because government across that area can use it to site boreholes in suitable areas which the community can utilise for a long period (Gil 2017).

In South Africa, groundwater has long represented an important aspect of social development. For example, pre-colonial settlements in South Africa were influenced by the availability of water. As such, "the very first permanent European settlement, Cape Town, was chosen over Saldanha Bay with its better harbour, on the presence of excellent quality perennial water coming from the springs at the foot of Table Mountain" (Diamond 2014). Nowadays, groundwater is estimated to contribute 15% to the total South African water budget (Department of Water and Sanitation 2016). The Department of Water and Sanitation (2016; 2018) estimates that the agricultural sector uses the largest portion (~66%) of this total groundwater budget (Figure 2-5). However, Braune et al. (2014) postulate that it is difficult to quantify the amount of water used by the agricultural sector. This is because most farm owners still believe that they own groundwater in their properties (according to the Water Act of 1956) and are therefore hesitant to register it according to the provisions of the National Water Act of 1998, which declares groundwater a public natural resource for which the government is the custodian (Braune et al. 2014).

implementation of artificial fertilisers) worldwide, particularly in the developing world beginning in the late 1960s (Braune et al. 2014).

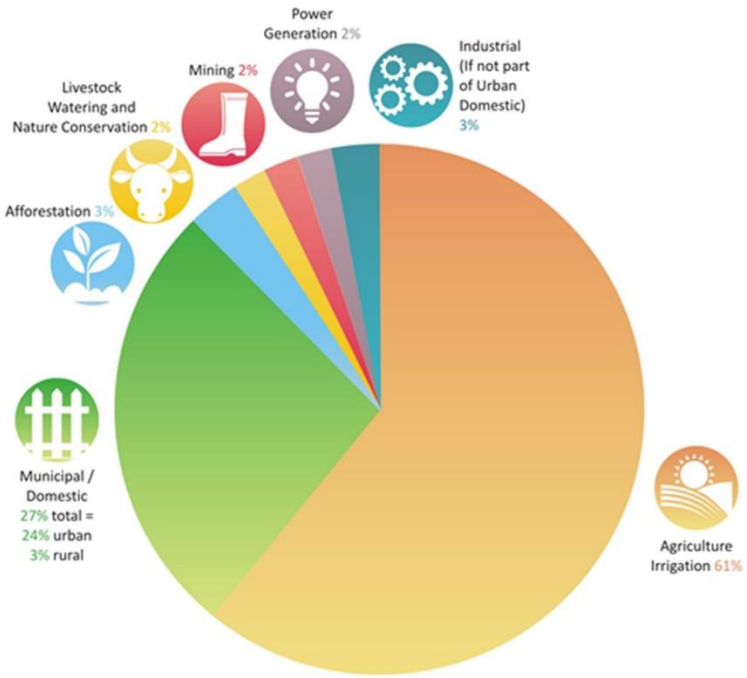

Figure 2-5: Breakdown of groundwater use for different economic sectors in South Africa (Department of Water and Sanitation 2018).

The total estimated volume of available, renewable groundwater is 10 343 million m^3/a or 7 500 million m^3/a under drought conditions in South Africa. Total groundwater consumption is between 2 000 and 4 000 million m^3/a (Adams 2011). Further, groundwater provides water supply to approximately 22% of South African towns as a sole source and another 34% in combination with surface water (Braune et al. 2014; Department of Water and Sanitation, 2016). These statistics show that there is (still) a dire need to develop and protect groundwater resources in South Africa. This can only be done through thorough research conducted by qualified water scientists. However, the water science research community in South Africa is still in its infancy (Braune et al. 2014). The community was smaller in past and as such hindered the implementation of the National Water Act of 1998 and hurt groundwater research. As a result, the South African public has insufficient knowledge about groundwater (Braune et al. 2014, Ground Water Division (GWD) of the Geological Society of South Africa (GSSA), 2008). However, the prospect of shale gas development in the Karoo (see section below) is refocusing attention to groundwater research due to the desire to secure sufficient potable water resources for future generations in the event that hydraulic fracturing is implemented. In the Karoo, groundwater represents a strategic water resource due to the low annual rainfall (Figure

2-2) and high evaporation rates (especially in the western part of the basin) (Woodford & Chevallier 2002; Department of Water and Sanitation 2016 p.23). Du Toit (2013) postulates that, "of the 34 sizable towns within or close to the Karoo Basin's shale gas exploration concessions, 31 depend wholly or partially on underground aquifers for drinking water. Only Cradock, Cookhouse and Adelaide draw their water solely from rivers for drinking water". The following section introduces the practise of hydraulic fracturing to harvest shale gas and the prospects of shale gas development in the Karoo Basin.

2.4. Hydraulic Fracturing Prospects in the Karoo Basin

Hydraulic fracturing is an oil and gas extraction technique (Kargbo et al. 2010; Academy of Science of South Africa (ASSAf) 2016; Soeder 2017). The process of hydraulic fracturing produces fractures in rock formations to stimulate the flow of natural gas or oil, increasing the volumes that can be recovered (Figure 2-6) (Soeder 2017). Production wells may be drilled vertically thousands of meters (2 to 4 km) below the land surface and may include horizontal or directional sections extending thousands of meters (up to ~eight km) (Davies et al. 2014). Fractures are created by pumping large quantities of fluids at high pressure into the target rock formation. Hydraulic fracturing fluids commonly consist of water, proppant and chemical additives that open and enlarge fractures within the rock formation. These fractures can extend several hundred meters away from the well (Kargbo et al. 2010). Hydraulic fracturing has been used in the oil and gas industry for more than 50 years and, in the last 20 years, together with the practice of horizontal drilling, has been instrumental in making the unconventional exploitation of shale gas reserves technically and economically viable worldwide (Department of Mineral Resources (DMR) 2012). Soeder (2012) reported that, active drilling projects are underway or planned in Britain, Canada, Ukraine, South Africa, several North African countries, and Argentina. One of the threats hydraulic fracturing poses on the environment is the potential for the migration of fracking fluids into potable water reserviors. Normally, the production well is sealed with multiple cement and steel casing layers. However, Ingraffea et al. (2014) show that cement and steel casing fail sometimes (Figure 2-6). This is why areas with increased groundwater contamination risk (due to natural connectivity) need to be identified so that better performing well casings can be installed in these areas.

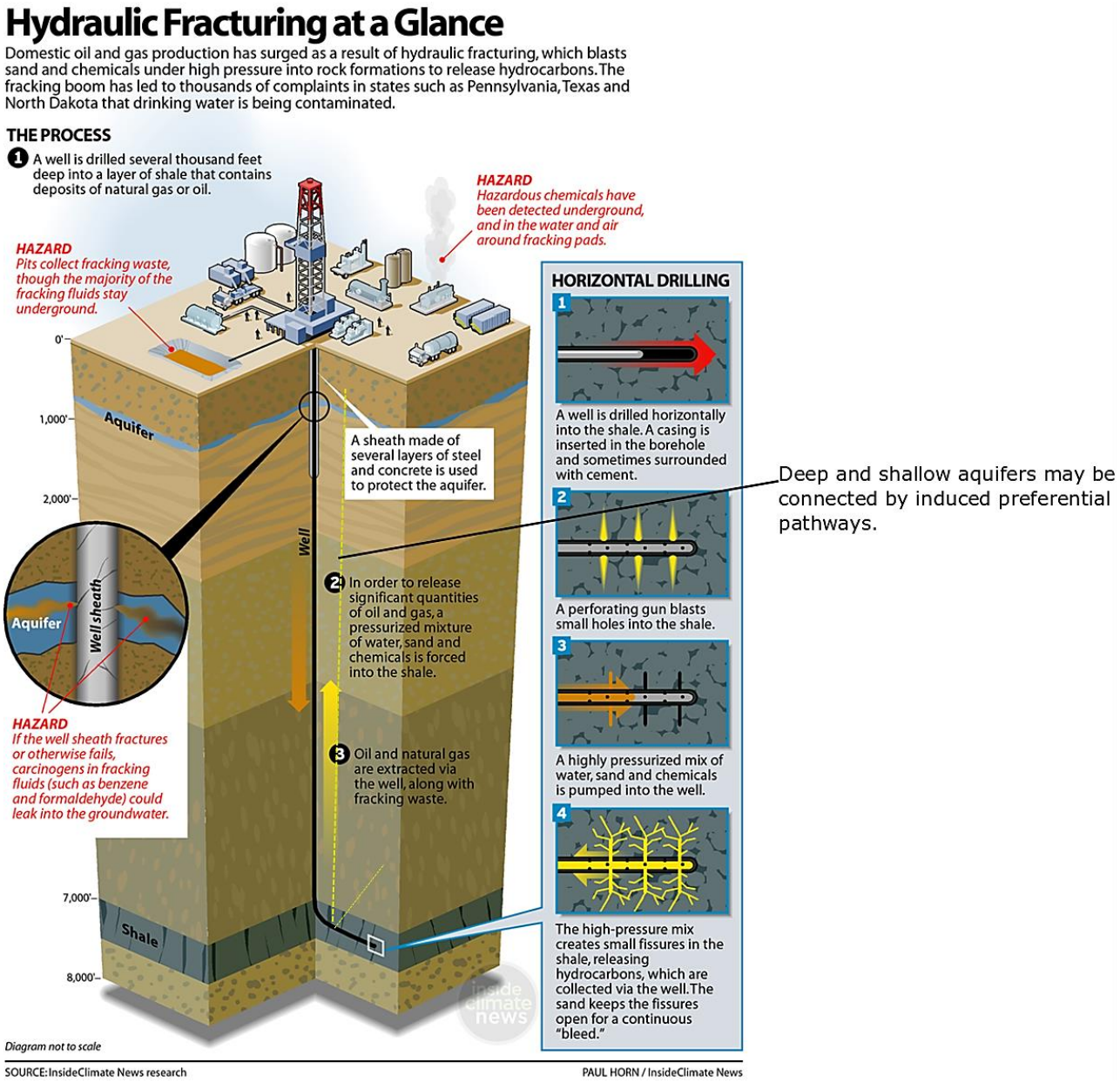

Figure 2-6: The process of hydraulic fracturing (modified from https://insideclimatenews.org/content/infographic-hydraulic-fracturing-explained-health-risks). Also shown is the potential for fracking fluid migration to potable groundwater reservoirs (note scales are in feet).

In South Africa, a renewed interest in shale gas development (targeting the Whitehill Formation) emerged between 2008 and 2010 when Bundu Gas and Oil submitted an exploration licence application for an area in the Karoo Basin (DMR 2012). In July 2012, the DMR released an investigation on the prospects of hydraulic fracturing. This was followed by lifting a ban on the processing of exploration licence applications. After lifting this ban, a

number of South African citizen groups demonstrated their objection towards this decision outside parliament (Figure 2-7). The protests were mostly driven by environmental concerns such as potential groundwater pollution through the propagation of preferential pathways during hydraulic fracturing. This is a valid concern for the Karoo Basin because MT research has shown that deep saline groundwater migration may have occurred naturally (see section below). Water consumption is also a concern because as mentioned earlier South Africa is a dry country (Figure 2-2) and it has been shown that hydraulic fracturing water use estimates range from 1 400 m^3 to 33 900 m^3 per shale gas well in the USA (Clark et al. 2013; Gallegos et al. 2015).

Figure 2-7: South African anti-fracking protest outside Parliament buildings in Cape Town (from https://www.businesslive.co.za/bd/national/science-and-environment/2017-09-01-sa-needs-fracking-police-scientists-warn/).

Although there is currently no consensus on the recoverable shale gas amount in the Karoo Basin (estimated between 20 to 400 Tcf) (DMR 2012), shale gas development in South Africa could improve the economy through increased job creation and industrialisation (Morkel & de Wit 2017). Also, South Africa is a coal dependent country with energy demands that exceed

supply as demonstrated by the previous implementation of 'load shedding[3]' and the fact that there are parts of South Africa that are still without electricity (Netshishivhe 2014). Introducing shale gas to the energy mix could assist with meeting energy demands and may assist with decreasing South Africa's carbon intensity and greenhouse gas emissions (National Planning Commission (NPC) 2011). Engelder (2013) shows that shale gas development coupled with wind energy in America had an impact in decreasing CO_2 emissions from energy demands. However, it may be hard to track the environmental footprint of shale gas development once it has been implemented. This is because the CZ of the earth (see section 2.1) is a complex system that has many influences. These influences (for example climate change) may affect the environment in ways that are similar to hydraulic fracturing (e.g. water pollution or water shortages (Vörösmarty et al. 2000). Therefore, assessing the environment before the implementation of hydraulic fracturing will help with identifying the source of the influence and this may in turn assist with conceptualising ways to deal with the problems. South Africa, at this stage is fortunate because it has an opportunity to develop and conduct environmental baselines before possible shale gas development. This will allow monitoring of its environment before implementation. This might even lead to a solution that enables South Africa to develop shale gas without compromising the natural environment.

In 2015, a team of scientific councils collectively known as the SEA (Strategic Environmental Assessment) was commissioned by the Department of Environmental Affairs. The SEA states that the National Development Plan of 2012 and the Constitution of South Africa (Act 108 of 1996) will guide the process of shale gas development to ensure that it is executed in an ethical, responsible and transparent manner. The SEA focussed on an area in the south-central part of the Karoo Basin (Figure 2-8). This area has attracted a lot of interest because it is where major oil companies (e.g. Bundu Gas and Oil; Shell etc.) have submitted exploration licence applications.

[3] Load shedding is a measure of last resort to prevent the collapse of the power system country-wide (http://www.eskom.co.za/documents/LoadSheddingFAQ.pdf)

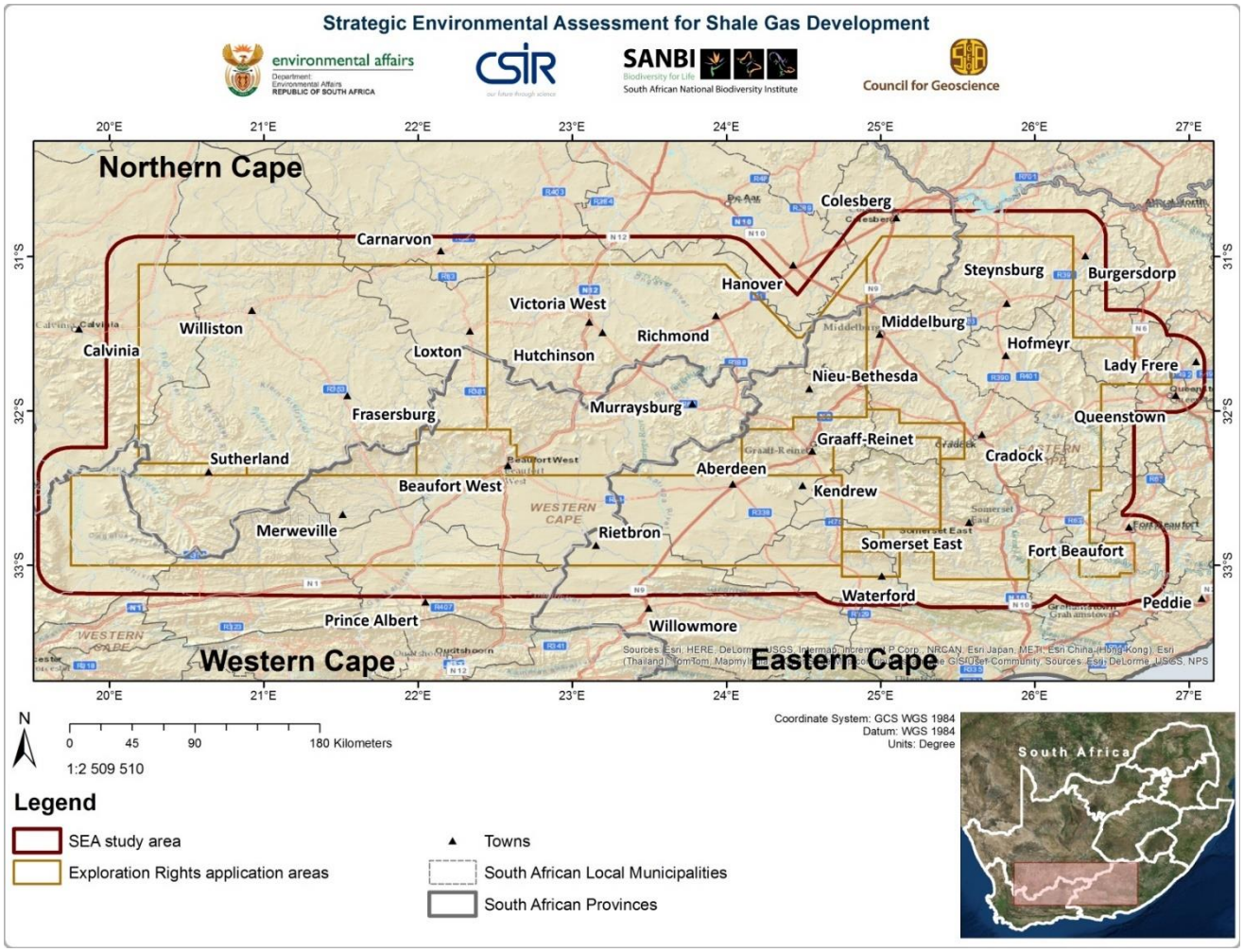

Figure 2-8: Proposed SEA study area. The study area encompasses 171 811 km^2 (from http://seasgd.csir.co.za/).

2.5. Magnetotelluric (MT) Research in the Cape Mountains and Southern Karoo Reveals Possibility for Aquifer Connectivity

Magnetotellurics (MT or the magnetotelluric method) is a geophysical technique that makes use of the fluctuations in the natural electromagnetic fields around the Earth. The fluctuations of these electromagnetic fields can be determined at the surface of the earth by measuring electrical impedance which is a function of the conductivity of the rocks in the subsurface (Sims & Bostick 1969; Naidu 2012). MT investigations reach depths between 300 and 10000 m or even deeper with long-period soundings (Horton & Hoffman 1962). Magnetotelluric techniques became popular after Cagniard (1953) gave a quantitative description of the relationship between the electric and magnetic fields at the surface of a horizontally layered

earth (Sims & Bostick, 1969). Fast forward to the 2000's, MT has proven to be an important aspect of subsurface research in South Africa (e.g. Weckmann et al. 2007; Lindeque & de Wit 2009; Branch 2013).

The electrical resistivity (inverse of conductivity, measured in Ω.m) of the upper few kilometres of the Earth's upper crust is largely controlled by the presence of interconnected aqueous fluids (Unsworth et al. 2005). The resistivity of a rock formation is thus a function of: lithology, porosity (often occupied by fluid), and permeability (degree of interconnectivity between pores). This resistivity can be measured using geophysical techniques such as: electrical resistivity depth probing; natural gamma logging; seismic down-hole logging; magnetotellurics etc. Magnetotellurics is preferred for deeper subsurface surveys and is particularly suited for studying deep saline groundwater migration (Unsworth et al. 2005; Naidu 2012).

In South Africa, MT research was conducted on lines that traverse both the BMA (Beattie Magnetic Anomaly) and the SCCB (Southern Cape Conductive Belt) to learn more about the subsurface structure of the southern Karoo and the Cape Mountains (Figure 1-1). The work done using MT surveys has proven to be beneficial for delineating where highly conductive areas (possibly saline groundwater reservoirs) occur deep below the Karoo Basin and the Cape Mountains. While studying the BMA and the SCCB using magnetotellurics, Weckmann et al. (2012) noted that there might be a sub-vertical fault reaching close to the surface through the Cape Mountains which is tapping into a deep saline groundwater reservoir. This is highlighted by the existence of hot springs (which are also highly conductive) near the village of Warmbad (~ 300 km south-west from the study area) (Figure 2-9).

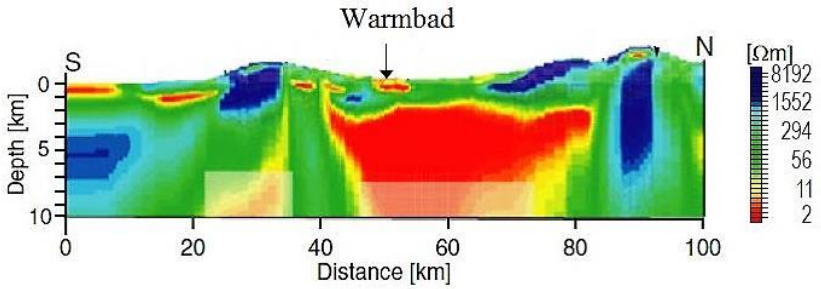

Figure 2-9: Conductivity features of MT 2 (from Weckmann et al. 2012). See Figure 1-1 for the location of this magnetotelluric survey.

In addition to uncovering deep saline groundwater that has migrated to shallower depths in Warmbad, MT research in South Africa has also revealed a continuous layer representing the carbonaceous and pyritiferous black shales of the Whitehill Formation (Weckmann et al. 2007; Branch et al. 2007; Branch 2013) in Jansenville (Figure 2-10). This highly conductive layer is the main target for the anticipated shale gas development and is surrounded by less conductive zones that likely represent saline groundwater as well (Figure 2-10).

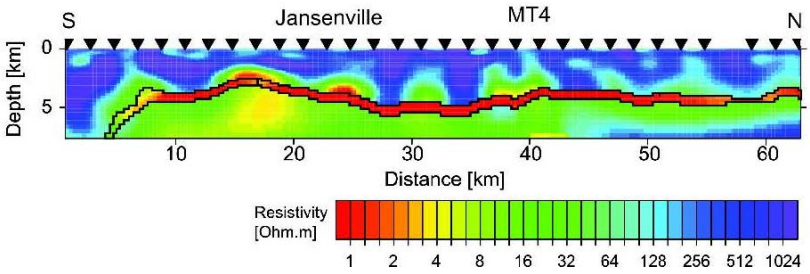

Figure 2-10: Conductivity features of MT4 (from Branch 2013). Highly conductive zones (yellow and red) revealed in the MT models are caused by the carbon-rich sequences of the Whitehill Formation. Low resistivity zones may also be saline water reservoirs.

Evidence for reservoir connectivity in thermal springs (i.e. hot springs conducting deep groundwater) has also been implicated in South Africa using stable and radioactive isotopes (e.g. Diamond & Harris 2000; Swana 2016). The sections below discuss the application of such isotopes in groundwater studies to study reservoir connectivity and other important aspects.

2.6. Deuterium and Oxygen-18 (δ^2H and $\delta^{18}O$) – Stable Water Isotopes

Soddy (1913) defined isotopes as atoms of the same element having the same atomic number but different atomic masses. Hydrogen has three naturally occurring isotopes: ^1H (protium), ^2H (deuterium) and ^3H (tritium). Protium and Deuterium are both stable and tritium is unstable. Oxygen has three naturally occurring isotopes namely, ^{16}O, ^{17}O and ^{18}O. Table 2-1 lists the natural abundances of both oxygen and hydrogen isotopes (Gauch 2012). The natural abundance of ^{16}O is high because it is a principal product of stellar evolution (Fowler et al. 1955).

Table 2-1 Natural abundances of oxygen and hydrogen isotopes (Mook 2000).

Oxygen		Hydrogen	
Isotope	Abundance (%)	Isotope	Abundance (%)
^{16}O	99.76	^{1}H	99.985
^{17}O	0.038	^{2}H	0.015
^{18}O	0.200	^{3}H*	$< 10^{-15}$

Lavoisier (1783) was the first to state that water is not an element but a compound made up of oxygen and hydrogen (H_2O). Nowadays, it is well known that the stable isotopes of oxygen and hydrogen combine to form nine different configurations of isotopically stable water molecules with atomic masses ranging from 18 to 22: $^{1}H_2{}^{16}O$ (18), $^{1}H^{2}H^{16}O$ (19), $^{2}H_2{}^{16}O$ (20), $^{1}H_2{}^{17}O$ (19), $^{1}H^{2}H^{17}O$ (20), $^{2}H_2{}^{17}O$ (21), $^{1}H_2{}^{18}O$ (20), $^{1}H^{2}H^{18}O$ (21), and $^{2}H_2{}^{18}O$ (22). Water molecules with the atomic masses 18 to 21 are the most abundant (Fetter 2001; Adelana 2005). ^{17}O is not naturally abundant (Table 2-1) and therefore its corresponding water molecule is not abundant. The most abundant isotopic water molecules are thus: $^{1}H_2{}^{16}O$; $^{2}H_2{}^{16}O$ and $^{1}H_2{}^{18}O$. Table 3 lists the characteristics of these water molecules.

Table 2-2 Characteristics of three types of water molecules (Hoefs 1997).

	$^{1}H_2{}^{16}O$	$^{2}H_2{}^{16}O$	$^{1}H_2{}^{18}O$
Density @ 20°C	0.997	1.1051	1.1106
Boiling point	100.0	101.42	100.14
Vapour pressure @ 100 °C	760	721.60	
Temperature density maximum	3.98	11.24	4.30

2.6.1. Fractionation of $\delta^{18}O$ and $\delta^{2}H$ during Precipitation

Fundamentally, groundwater recharge is derived from precipitation (rain or snow). It is therefore important to understand the isotopic evolution of precipitation in order to study groundwater recharge (McGuire & McDonnell 2007).

Precipitation occurs when water vapour passes the dew point[4]. As precipitation forms within the condensing cloud, equilibrium fractionation preferentially partitions heavy isotopes (^{18}O and ^{2}H) into the denser phase (rain or snow) and light isotopes (^{16}O and ^{1}H) into vapour. This is referred to as the rainout effect. It is attributed to Rayleigh distillation. Rayleigh distillation (Equation 2-1) states that the isotopic ratio in a diminishing reservoir of the reactant (vapour) is a function of its initial isotopic ratio, the remaining fraction of that reservoir and the equilibrium fractionation factor for the reaction (Clark & Fritz 1997). Figure 2-11 depicts the fractionation of $\delta^{18}O$ according to Rayleigh distillation (Clark & Fritz 2000). Note that the enrichment factor increases when temperature decreases (Appelo & Postma 2005 p. 37).

$$R = R_0 f^{\alpha-1} \qquad \text{Equation 2-1}$$

On Equation 2-1:

- R_0 is the initial isotopic ratio ($^{18}O/^{16}O$ or $^{2}H/^{1}H$)
- R is the ratio after a given proportion of the water vapour had reacted (i.e. “rained-out”)
- f is the residual vapour component in the cloud
- α is the equilibrium fractionation factor between liquid and water vapour at the prevailing “in-cloud” temperature

[4] The dew point is the temperature at which air is saturated with water vapour (Clark & Fritz 2000).

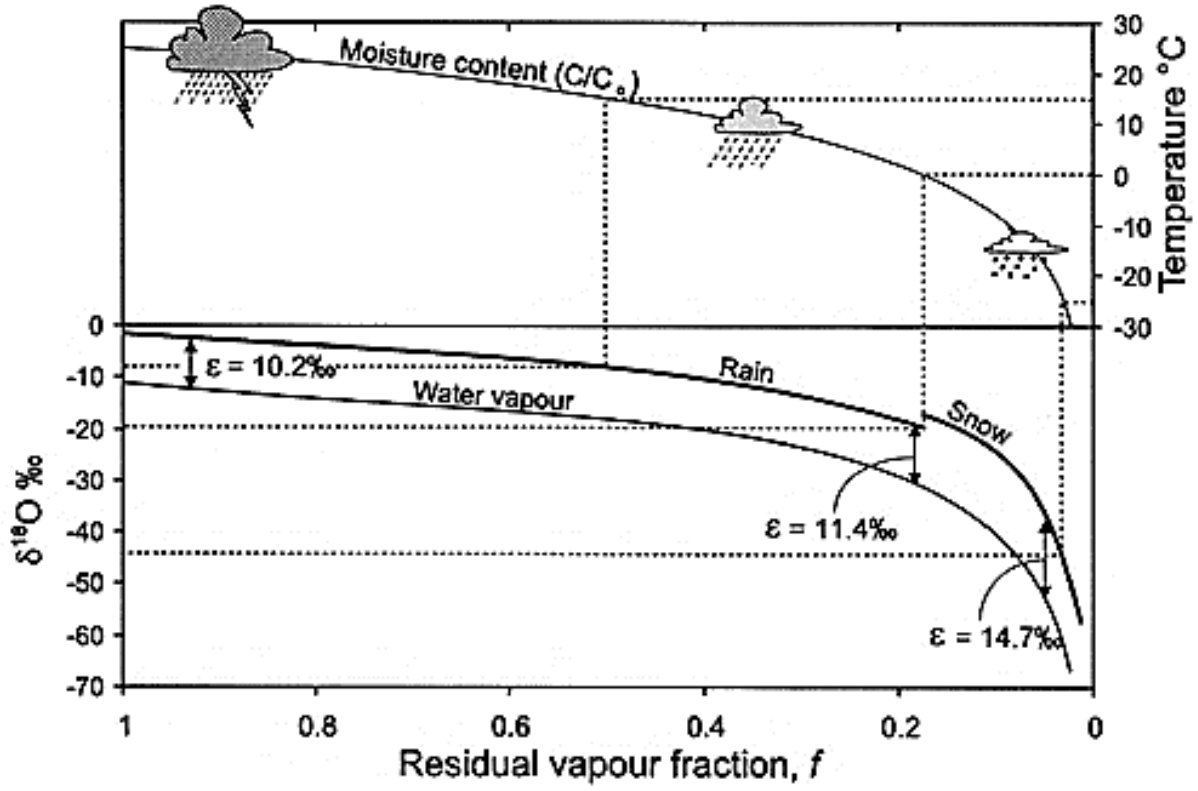

Figure 2-11: Change in the $\delta^{18}O$ content of rainfall according to a Rayleigh distillation, starting with $\delta^{18}O_{vapour}$ = -11‰, temperature = 25°C, and a final temperature of -30°C (from Clark & Fritz 2000 p. 48). Note that at 0 °C, fractionation between snow and water vapour replaces rain-vapour fractionation. The equilibrium fractionation factor (ε) increases with decreasing residual vapour. The vapour fraction remaining (f) has been calculated from the decrease in moisture carrying capacity (humidity) of air at lower temperatures, starting at 25 °C. Dashed lines link $\delta^{18}O$ of precipitation with temperature of condensation.

Vogel & van Urk (1975) noted that the $\delta^{18}O$ (‰) content of precipitation in the semi-arid regions of southern Africa is extremely variable. In the same publication it was also noted that the $\delta^{18}O$ concentration (‰) in groundwater from the same region is remarkably consistent and generally more depleted in the heavier isotope (^{18}O) than the precipitation values. This is also noted in West et al. (2014). Here, $\delta^{18}O$ and $\delta^{2}H$ concentrations measured in tap water are more varied and generally more enriched than $\delta^{18}O$ and $\delta^{2}H$ concentrations measured in groundwater (Figure 2-12).

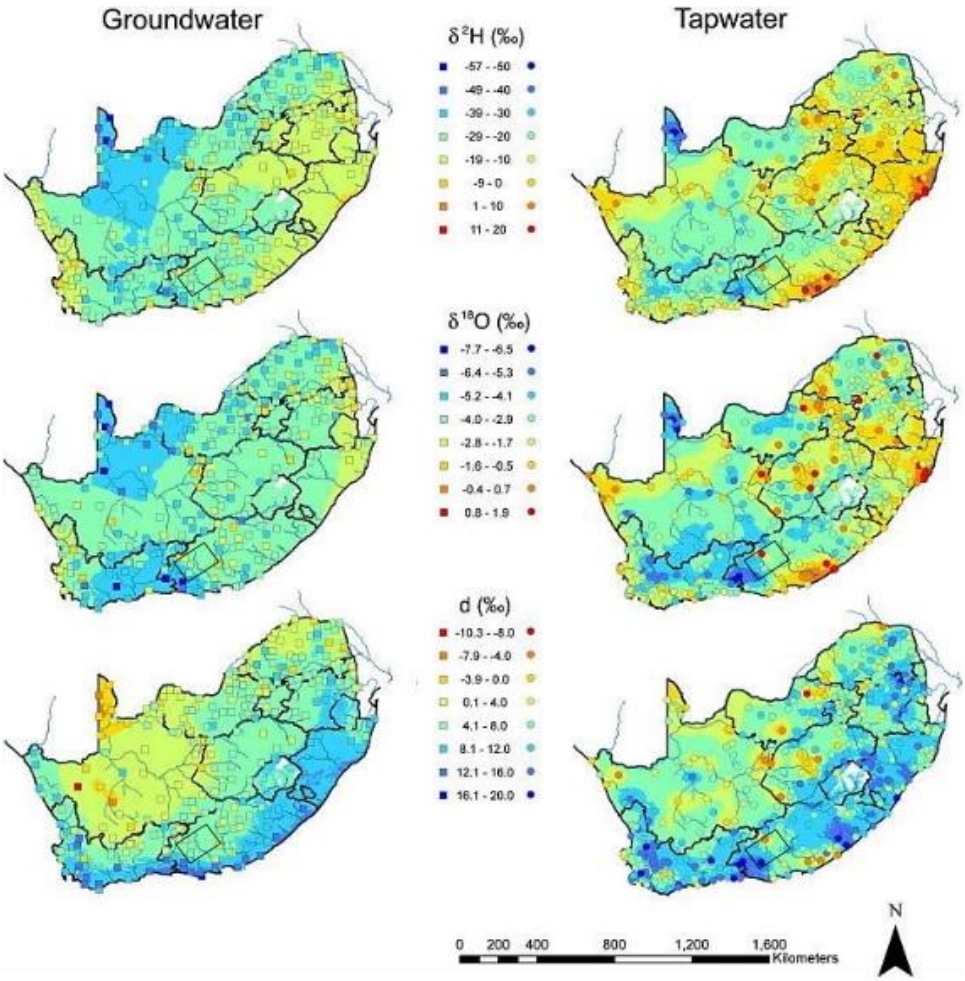

Figure 2-12: Measured δ^2H and $\delta^{18}O$ for tapwater sampled in South Africa overlaid on a modelled isoscape based on a geostatistical model. Also shown are d-excess values (modified from West et al. 2014). Note the demarcation of the study area (black rectangle).

Slight groundwater isotopic variations were noted in Diamond & Harris (2000). Here, the $\delta^{18}O$ and δ^2H of thermal springs in Western Cape decrease with increasing distance from the west coast of South Africa. This is in part related to the continental effect. The section below discusses the continental effect and other geographic and temporal effects affecting the isotopic composition of precipitation and groundwater.

2.6.2. Geographic and Temporal Effects Affecting the Isotopic Composition of Precipitation

Dansgaard (1964) established a linear relationship between surface air temperatures and stable water isotopes ($\delta^{18}O$ (Equation 2-2) and $\delta^{2}H$ (Equation 2-3)):

$$\delta^{18}O = 0.69T_{annual} - 13.6\ ‰ \qquad \text{Equation 2-2}$$

$$\delta^{2}H = 5.6T_{annual} - 100\ ‰ \qquad \text{Equation 2-3}$$

This relationship between temperature and water isotopes ($\delta^{18}O$ and $\delta^{2}H$) is the basis for the geographic and temporal effects (latitude, continental, seasonal and amount effects) affecting the isotopic composition of precipitation (McGuire & McDonnell 2007). Also, groundwater recharged during different climatic conditions than present can exhibit different ^{18}O and ^{2}H signatures. This implies that the isotopic composition of precipitation could have been different from the present one, due to the correlation between stable water isotope ratios ($\delta^{18}O$ and $\delta^{2}H$) and temperature (Aggarwal 2013). As such, Miller et al. (2015) and Murray et al. (2015) identified that old groundwater likely from deep aquifers in the Karoo Basin, has different and more depleted $\delta^{18}O$ and $\delta^{2}H$ signatures than modern groundwater likely from shallow aquifers (Table 1-1)

Latitude Effect

The latitude effect explains a phenomenon where, as air masses move away from the equator towards the poles, condensation temperatures decrease leading to precipitation depleted in heavy isotopes (^{18}O and ^{2}H) at the poles (Figure 2-13) (Adelana 2005; McGuire & McDonnell 2007).

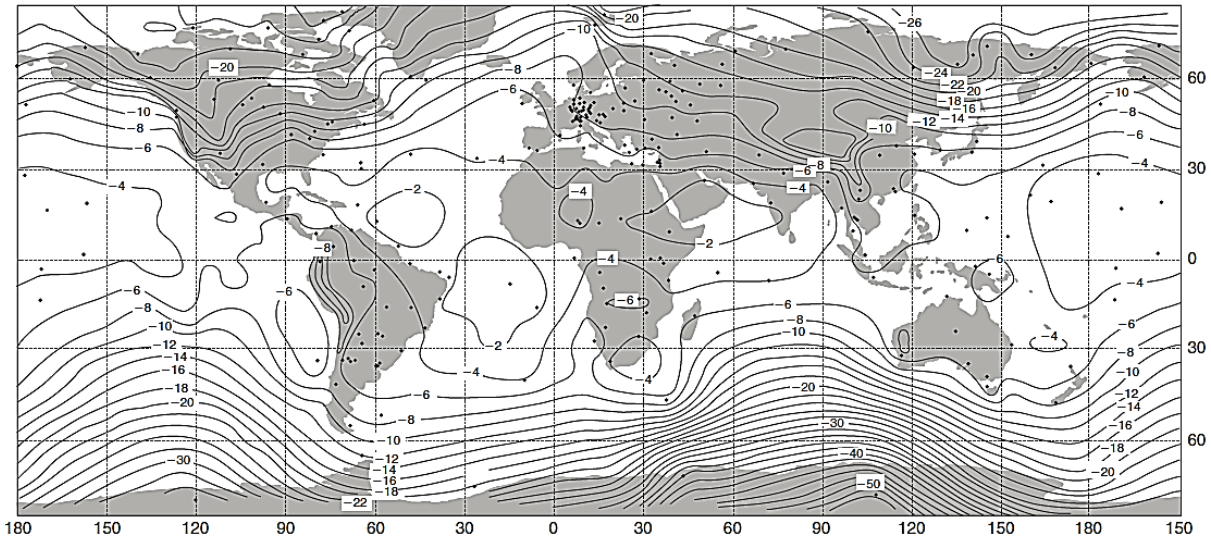

Figure 2-13: Mean $\delta^{18}O$ distribution in precipitation for stations with at least 24 months of records (from Clark & Fritz 1997 p.66). This is based on IAEA (International Atomic Energy Agency) world meteorological precipitation monitoring data summarized by (Rozanski et al. 1993).

Continental Effect

The continental effect describes the overall depletion of heavy isotopes in precipitation as air masses follow a trajectory from the isotopically enriched ocean to typically temperate climates inland. This effect is attributed to progressive rainout. It is correlated with the temperature gradient and depends on topography and climate (Dansgaard 1964; McGuire & McDonnell 2007).

Elevation or Altitude Effect

The elevation effect describes the depletion of heavy isotopes in precipitation with increasing altitude (Vogel & van Urk 1975). This is caused by the general decrease of cloud temperatures with elevation. In turn this leads to progressive condensation and thus more fractionation, a combined effect resulting in higher rainfall depleted in heavier isotopes on the windward side (McGuire & McDonnell 2007). An example of the altitude effect is observed in the Jonkershoek Valley, Stellenbosch (Table 2-3). Here, bulk monthly rainfall collected at a range of altitudes yielded an altitude effect of approximately 0.32 ‰ ^{18}O per 100 m ($R^2 = 0.801$) (Midgley & Scott 1994).

Table 2-3 Variation in ^{18}O with altitude in the Jonkershoek Valley. Values are for bulked monthly rainfall for May 1993 (Midgley & Scott 1994).

Altitude (m)	^{18}O
409	-5.7
579	-5.6
655	-6.9
898	-7.3
937	-8.4
1219	-8.1
1234	-8.2

Seasonal Effect

Because the isotopic composition of inland precipitation is removed from the moderating influence of the ocean, it is instead characterised by strong local temperature variations. For example, rain in winter is isotopically depleted compared to rain in summer due to the decrease in temperature (McGuire & McDonnell 2007). Figure 2-14 shows signs of the seasonal effect on rainwater collected in Cape Town Airport (Harris et al. 2010).

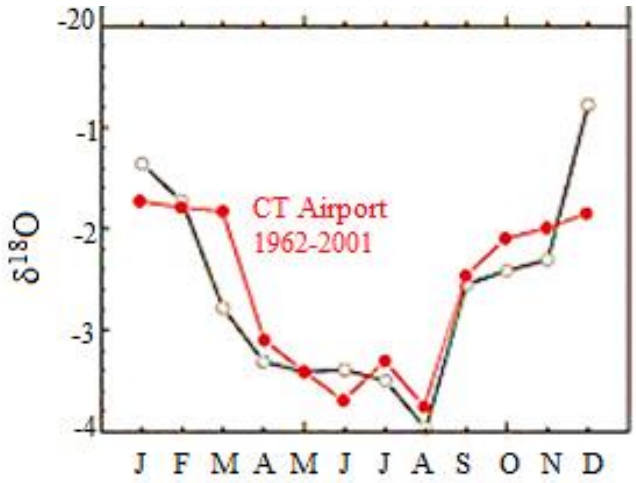

Figure 2-14: Plot of weighted average annual $\delta^{18}O$ for the University of Cape Town (UCT) (marked with black line) and Cape Town International Airport (marked with red line) vs. month (Harris et al. 2010).

Amount Effect

The amount effect describes the dependence of $\delta^{18}O$ and $\delta^{2}H$ concentration on the amount of rainfall. According to this effect, heavier rain or prolonged rainstorms result in depleted $\delta^{18}O$ and $\delta^{2}H$ values. The amount effect is largely attributed to progressive condensation and variations in the intensity of rain (Adelana 2005). Figure 2-15 depicts the amount effect on precipitation sampled at six locations in northern Kwa-Zulu Natal. Here, the three most isotopically depleted samples represent three extreme rainfall years (1990-1992) in that area (Meyer et al. 2001).

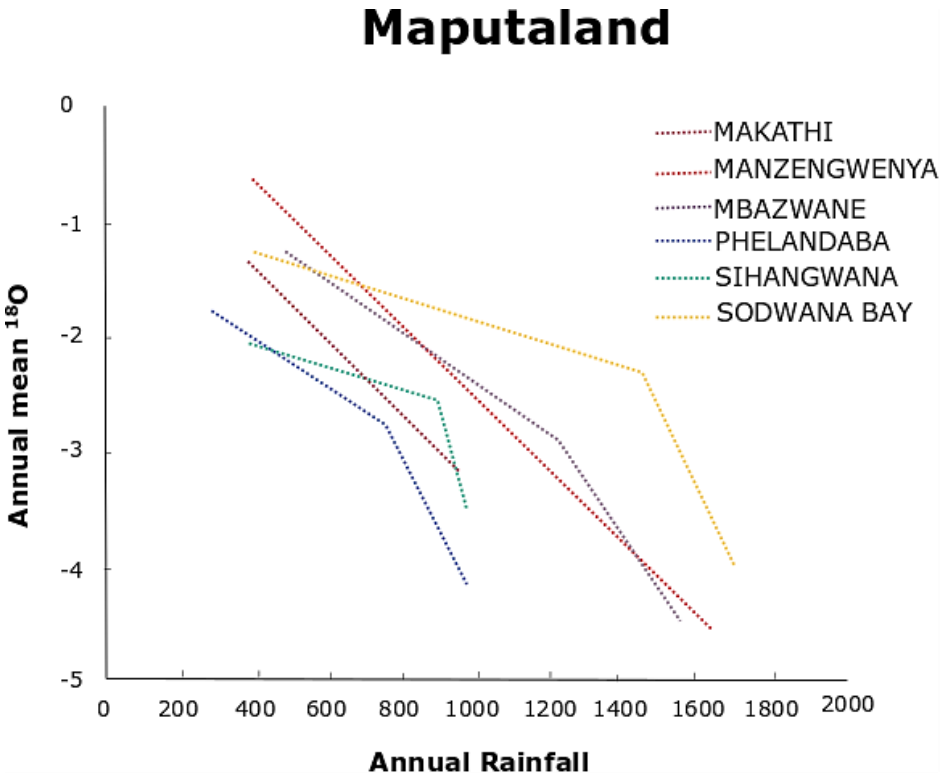

Figure 2-15: Relation between rainfall amount and annual $\delta^{18}O$ in rain for six stations over three years in northern Kwa-Zulu Natal (from Meyer et al. 2001).

In addition to the abovementioned effects, much can be learned about groundwater recharge and groundwater salinization from $\delta^{2}H$ and $\delta^{18}O$ in groundwater. This is achieved through plotting $\delta^{2}H$ concentrations against $\delta^{18}O$ for groundwater and precipitation and comparing this to the Global Meteoric Water Line (GMWL) and salinity indicators such as EC (Nakwafila 2015). The GMWL is discussed below.

2.6.3. The Global Meteoric Water Line

Craig (1961) identified a linear relationship between $\delta^{18}O$ and $\delta^{2}H$ for global meteoric waters (Equation 2-4). This linear relationship is referred to as the Global Meteoric Water Line (GMWL) and is considered an adequate fit for global meteoric waters except for waters in closed basins in which evaporation is a dominant factor governing the isotopic relationship (Figure 2-16).

$$\delta^2 H = 8\delta^{18} O + 10 \qquad \text{Equation 2-4}$$

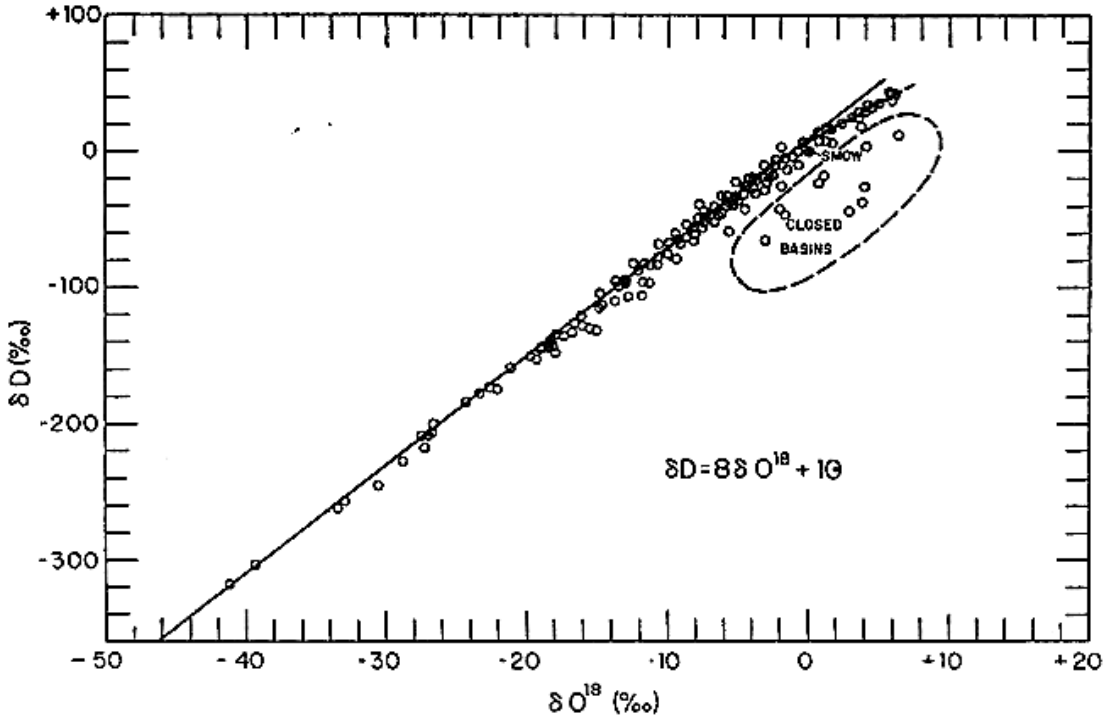

Figure 2-16: $\delta^{2}H$ (expressed here as δD) and $\delta^{18}O$ variations in rivers, lakes, rain, and snow, expressed as per mil enrichments relative to SMOW (Standard Mean Ocean Water) (from Craig 1961). Points which fit the ellipse of the dashed line at the upper end of the curve are data from rivers and lakes in East Africa.

On Equation 2-4, the slope value of 8 represents the rate of change between $\delta^{18}O$ and $\delta^{2}H$. It is closely related to the isotopic fractionation of the two isotopes and thus the rate of evaporation. Because the flux of moisture from the oceans and its return through rainout and runoff is, on

an annual basis and global scale close to dynamic equilibrium (Gat 1996), the slope of the GMWL represents equilibrium fractionation. The y-intercept (y = 10) represents the d-excess (deuterium excess). D-excess is a measure of the relative ^{18}O and ^{2}H contained in water and is correlated with physical atmospheric conditions such as humidity, air temperature and sea surface temperature. D-excess can be used to trace the oceanic source area of precipitation and the mixing of air masses from different sources, in particular, recycled air moisture (Froehlich et al. 2002). In South Africa, d-excess values in groundwater and tap water are high along the coast due to the high humidity from the Indian and Atlantic Oceans (Figure 2-12).

2.6.4. Deviations of Local Meteoric Water Lines (LMWL) from the Global Meteoric Water Line (GMWL)

A regression of $\delta^{18}O$ and $\delta^{2}H$ for local precipitation produces a Local Meteoric Water Line (LMWL) for that specific area. The regional Meteoric Water Line (MWL) for Southern Africa is determined from a regression of rainfall data collected in De Aar and Dewetsdorp by Kirchner et al. (1991). The line that defines the ^{18}O vs. ^{2}H relationship for this rainfall data is shown on Equation 2-5. Here, we see that the line has a smaller gradient and y-intercept compared to the GMWL.

$$\delta^2 H = 7.45\delta^{18}O + 12.14 \qquad \text{Equation 2-5}$$

LMWLs may deviate from the GMWL due to processes such as enhanced moisture content modification (changes the d-excess) and secondary evaporation (changes the slope) (Figure 2-17). Therefore, the orientation of a LMWL relative to the GMWL may change if recharge waters underwent secondary evaporation at surface during or before recharging into the groundwater system. The point where a LMWL intersects the GMWL represents the isotopic composition of the unevaporated meteoric water in a certain area (Craig 1961; Adelana 2005; Kim & Lee 2011). The approximate mean isotopic concentration of the rainwater from which groundwater in Bedford was derived was reconstructed by projecting the groundwater relationship of the sampled groundwater back to the SA regional MWL (Sami 1992). Bedford is ~140 km from the study area and the LMWL that was used in Bedford is used in this study.

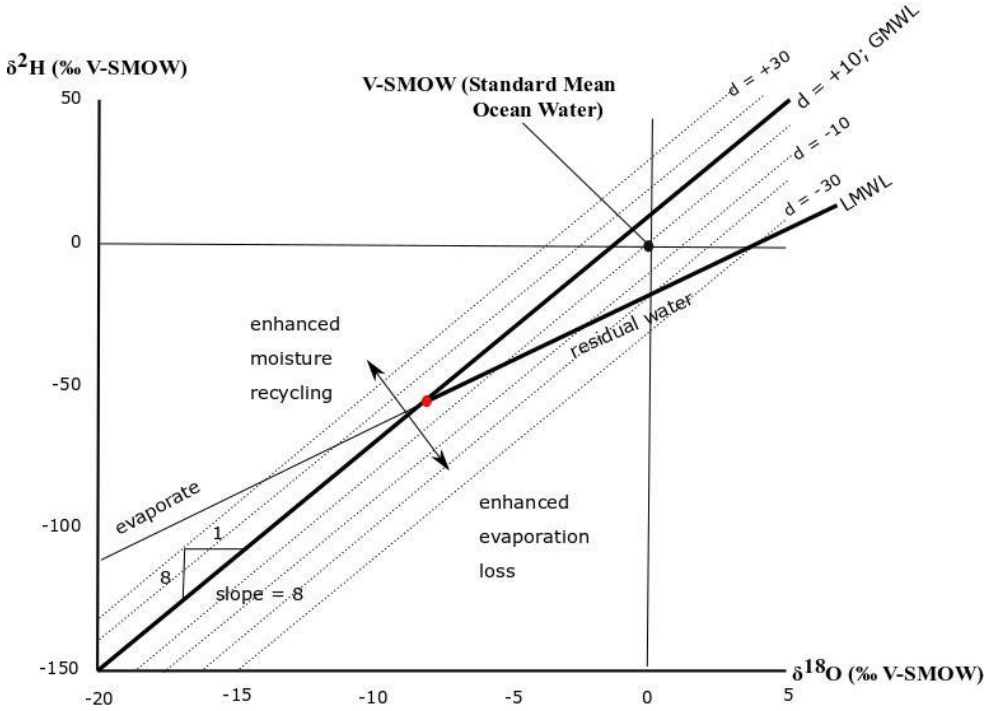

Figure 2-17: Schematic plot of $\delta^{18}O$ versus $\delta^{2}H$ showing the GMWL (d = 10, slope = 8) of Craig 1961, LMWL (slope <8), ocean water (SMOW) and relative changes in the d-excess (d). D-excess in precipitation increases in response to enhanced moisture recycling as a result of increased evaporate content. D-excess is reduced in the case where water is lost by evaporation (modified from Froehlich et al. 2002). Also shown is the position where the GMWL intersects a respective LMWL (with a different slope-red dot); this position signifies the isotopic composition of the original unevaporated meteoric water of respective evaporated water.

Secondary evaporation leads to kinetic fractionation (Stewart 1975). Kinetic fractionation is explained on Figure 2-18. Here, the boundary layer represents a thin atmospheric layer over the liquid water interface with virtually 100 % humidity. The transition zone (which lies directly above the boundary layer) has less humidity (<100 %) and is thus where secondary evaporation manifests. This secondary evaporation leads to kinetic fractionation through net diffusion which is a unidirectional process that depletes the boundary layer and the well mixed water column in the more diffusive isotopes ($^{1}H_{2}{}^{16}O$) (Sami 1992; Clark & Fritz 2000). Kinetic fractionation usually occurs in dry regions where evaporation rates are high, and results in lower LMWL gradients, for example, the line that defines the LMWL for southern Africa (Equation 2-5) deviates from the GMWL because southern Africa is largely semi-arid (Snyman 1998).

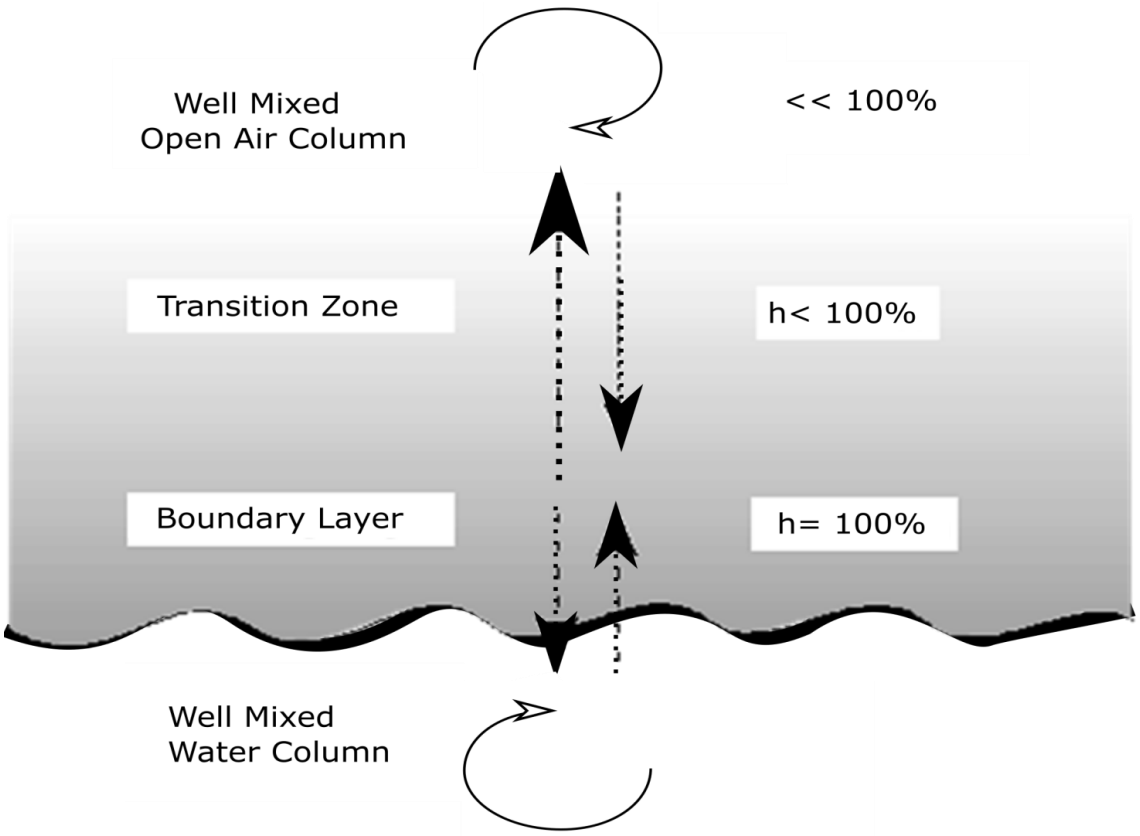

Figure 2-18: Model for kinetic fractionation over a water body (h represents humidity) (from Clark & Fritz 2000). Arrows indicate relative fluxes of water between the mixed water column and the boundary layer, and between the boundary layer and the well mixed air column. Differences in the rate of diffusion of ^{18}O to ^{16}O and ^{2}H to ^{1}H impart a kinetic isotope depletion in the overlying air column.

2.7. Tritium (^{3}H) – Unstable/Radioactive Hydrogen Isotope

Tritium is a radioactive hydrogen isotope (with a half-life of 12.33 years) that was discovered by physicists Ernest Rutherford, Marcus Oliphant and Paul Harteck in 1934 when they bombarded deuterium with high-energy deuterons (nuclei of deuterium atoms) (Lucas & Unterweger 2000; Pourimani & Aghamohammadi 2014). However, the primary production of tritium (which takes place in the upper atmosphere) was discovered in the late 1940's by Libby (1946). The section below discusses this natural production of tritium and the incorporation of tritium into the hydrological cycle.

2.7.1. Natural production of ^{3}H in the Upper Limits of the Critical Zone

Tritium, much like ^{14}C, is naturally produced in the upper atmosphere through the reaction of cosmic rays and neutrons with gases such as nitrogen, oxygen and argon (Figure 26) (Casaletto et al. 1962; Libby 1946). In the atmosphere, tritium oxidises to tritium oxide (T_2O) and takes part in the water cycle (Aggarwal et al. 2013). Also, similarly to radiocarbon, atmospheric tritium concentrations increased during the Atomic Age (Mazor 2003). The increase of tritium concentration in the atmosphere and its significance in labelling natural waters is discussed in the section below.

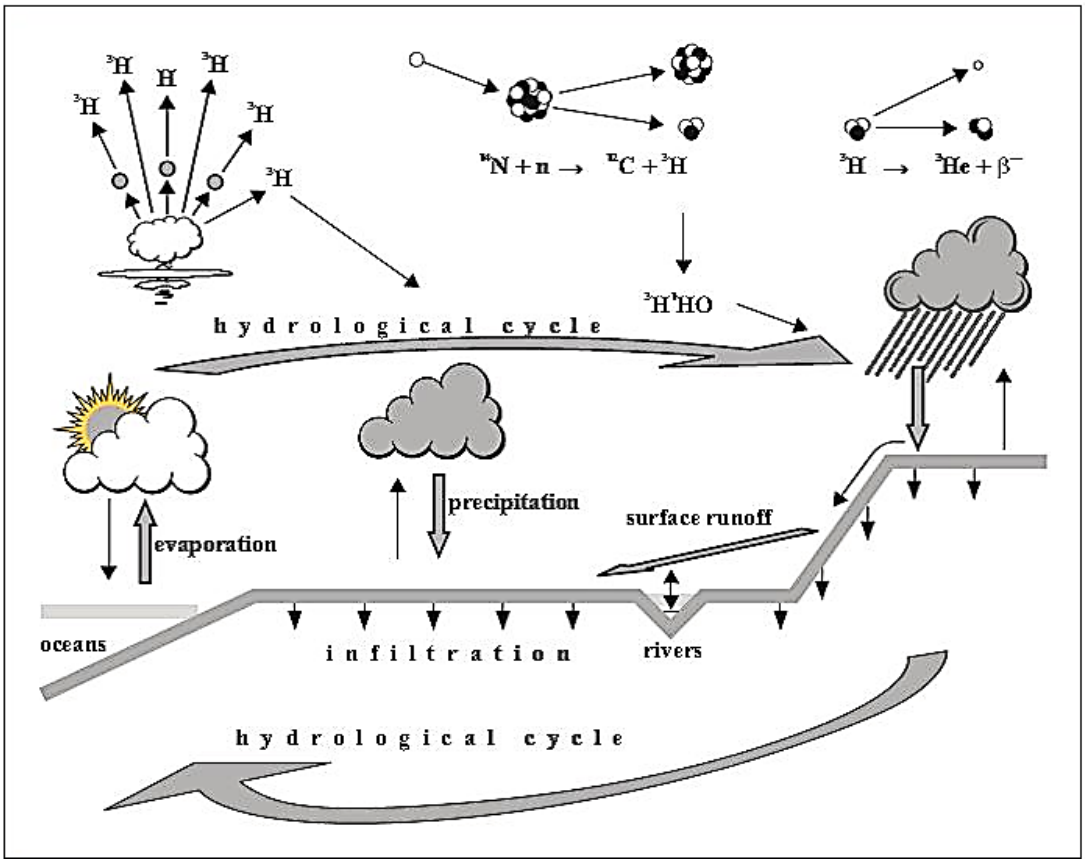

Figure 2-19: Origin and Distribution of tritium (from (ECOMETRIX Incorporated in association with Rowan Williams Davies & Irwin Incorporated 2009). Tritium is produced in the upper atmosphere by reaction of cosmic rays and neutrons with gases. Also shown on the Figure is that, tritium decays to helium-3 (^{3}He) by beta decay.

2.7.2. Nuclear Weapons Testing Impact on Atmospheric ^{3}H Concentrations

In South Africa, atmospheric tritium levels peaked (~ 40 TU) in the early 1960s due to atmospheric nuclear weapons testing in the Southern Hemisphere (Figure 2-20). Present-day atmospheric tritium concentrations are between 2 to 3 TU (Talma & van Wyk 2013). Similarly to ^{14}C, the distinct rises in atmospheric tritium in the 1950s-1960s (see section 2.8.2) provide a means of determining when moisture percolates through the soil to recharge groundwater (Vogel et al. 1974). In the Southern Hemisphere, groundwater that was recharged before 1950 has tritium concentrations of less than 1 TU while groundwater recharged after 1950 has tritium concentrations between 1 and 4 TU. Groundwater containing more than 4 TU is probably contaminated with artificial tritium (e.g. in landfill sites) (Butler 1998 p. 25; Miller et al. 2015; Murray et al. 2015 p. 16).

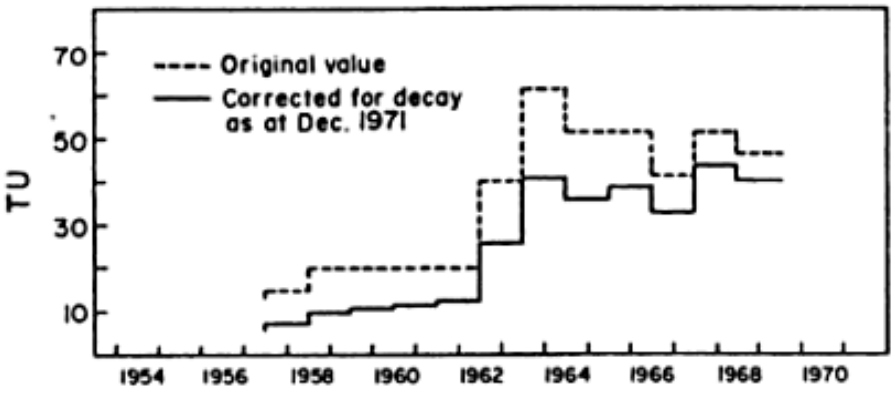

Figure 2-20: Estimated tritium content of precipitation in Pretoria (Mazor 2003).

2.7.3. Groundwater Age Calculations Using ^{3}H

Tritium enters the hydrological cycle by mixing with atmospheric water vapour and subsequently precipitation (see section 2.7.1). When water infiltrates into the ground, ^{3}H decays according to beta decay (Figure 2-19). This decaying ability forms the basis for tritium groundwater age calculations. The relatively small half-life of tritium (12.33 years) allows for the calculation of groundwater ages up to only 100 years. Tritium groundwater ages are calculated using Equation 2-6 (Schlosser et al. 1988). Unlike ^{14}C, tritium forms part of the water molecule and so does not experience significant changes other than decay in groundwater (Vogel et al. 1974; Atkinson et al. 2014).

$$\tau = T_{1/2} / \ln 2 \times \ln\left(1 + \frac{He^3}{H^3}\right)$$ Equation 2-6

On Equation 2-6:

τ is $\frac{tritium}{He^3}$ age in years

$T_{1/2}$ is the half-life of tritium

^3He is the helium concentration

^3H is the concentration of tritium in the sample

2.8. Radiocarbon (^{14}C) – Unstable/Radioactive Carbon Isotope

Carbon has three naturally occurring isotopes, of which two are stable and one is unstable (^{14}C). On the earth's surface, the abundance of natural ^{14}C (also known as radiocarbon) relative to the two stable naturally occurring carbon isotopes is ^{12}C: ^{13}C: ^{14}C = 98.9 %: 1.1 %: 1.2 × 10-10% (Smith 1972).

The existence of ^{14}C was first discovered by F.N.D Kurie at Yale University in 1934 (Key 2001). Thereafter, ^{14}C was discovered in atmospheric CO_2 by Willard F. Libby in 1946 (Libby et al. 1949). Libby et al. (1949) determined the half-life of ^{14}C to be 5568 years and developed radiocarbon dating of organic carbon of biological origin (Key 2001; Plummer & Glynn 2013). This transformed research in a number of fields, including archaeology and quaternary geology/climatology by establishing ages and chronologies of events that have emerged over the past 45 000 years (Plummer & Glynn 2013). In the 1960s, the half-life of ^{14}C was revised. Three different laboratories agreed that the half-life of ^{14}C is 5730 ± 40 years (Godwin 1962; Key 2001). However, according to (Chiu et al. 2007) the modern half-life of ^{14}C may be underestimated by approximately 300 years.

2.8.1. Natural production of ^{14}C in the Upper Limits of the Critical Zone

The natural production of ^{14}C occurs in the upper atmosphere (at approximately 12 km above the earth's surface between the stratosphere and troposphere) (Figure 2-21). Here, neutrons

with energies between 5 to 10 MeV are produced by cosmic rays. These neutrons in turn gain thermal energies by colliding with air molecules (Hussain 1991) and are subsequently captured by nitrogen. The highest ^{14}C production is at mid-latitudes. The northern hemisphere contains 4.5% more radiocarbon than the southern hemisphere because of the faster absorption of radiocarbon in the sea which covers 40% more area in the southern hemisphere than in the northern hemisphere (Hussain 1991; Hua 2016).

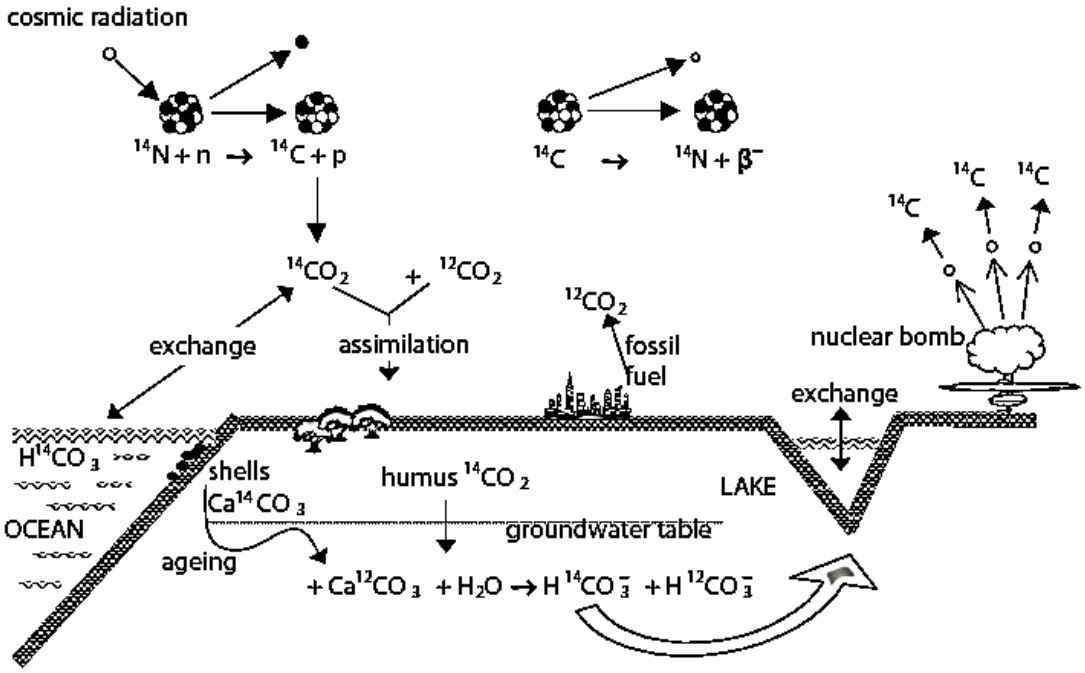

Figure 2-21: Origin and distribution of ^{14}C in nature (from Mook 2000 p.75). After production, ^{14}C oxidizes to ^{14}CO and then $^{14}CO_2$. $^{14}CO_2$ is absorbed by plants during photosynthesis and becomes assimilated into the Earth's biological and hydrological cycles (Hussain 1991; Mook 2000 p. 75). In the CZ, when ^{14}C is out of equilibrium with the atmosphere, it decays to nitrogen and produces a beta particle with a maximum energy of 156 keV (Engelkemeir et al. 1949; Godwin 1962). The figure also shows how the nuclear bomb detonations of the late 1940's until the 1960's increased the concentration of atmospheric ^{14}C.

2.8.2. Nuclear Weapons Testing Impact on Atmospheric ^{14}C Concentrations

Ruben & Kamen (1941) were the first to produce artificial ^{14}C when they bombarded graphite in a cyclotron. This was done in an attempt to produce a radioactive carbon isotope that could be used as a tracer in biological systems (Plummer & Glynn 2013). Similarly to ^{3}H (section 2.7.2), artificial ^{14}C was also produced and liberated into the atmosphere during atmospheric nuclear bomb detonations in the Atomic Age[5] (Praˇvaˇlie 2014). Before that, natural variations in the atmospheric concentration of ^{14}C were attributed to changes in the Earth's magnetic field, variability in solar activity (Barbetti 1980 p. 199) and changes in the carbon cycle (Graven 2015).

On the 16th of July 1945, the USA carried out the first atmospheric atomic bomb test (known as the Trinity Test) (Key 2001). Between 1945 and 1963, many countries followed suit conducting atmospheric, underground and underwater nuclear tests (Katz 2008). Nearly 90% of all nuclear tests were conducted in the northern hemisphere specifically by the USA, USSR (Union of Soviet Socialist Republics) and China. Only 10% of tests were carried out in the southern hemisphere by countries such as France and the United Kingdom (Praˇvaˇlie 2014). Figure 2-22 shows the temporal fluctuations of nuclear tests conducted in the atmosphere by the five nuclear powers from 1945 to 1980.

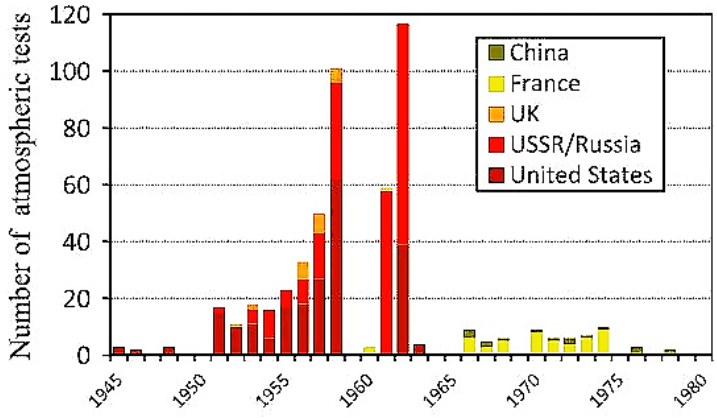

Figure 2-22: Temporal fluctuations of nuclear tests conducted in the atmosphere by the five nuclear powers during 1945 to 1980 (Praˇvaˇlie 2014).

[5] The Atomic Age, also known as the Atomic Era, is the period of history following the detonation of the first nuclear ("atomic") bomb, Trinity, on July 16, 1945, during World War II (Praˇvaˇlie 2014; Key 2001).

As a result of atmospheric nuclear weapons testing, artificially produced thermal neutrons from bomb detonations interacted with atmospheric ^{14}N to generate more atmospheric ^{14}C. This led to a 65% increase in atmospheric radiocarbon concentrations above pre-bomb concentrations in the southern hemisphere (Figure 2-23) (Vogel 1971; Hussain 1991; Vogel et al. 2002).

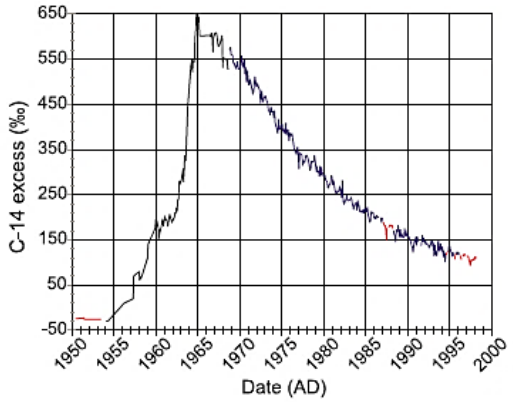

Figure 2-23: The elevated ^{14}C levels in mid-southern latitudes caused by testing nuclear weapons in the atmosphere. The measurements were mainly made on CO_2 collected at the CSIR (Council for Scientific and Industrial Research) on the eastern side of Pretoria. The data are expressed as parts per thousand (‰) above the standardised (unpolluted) value for 1950. Regional and local pollution by fossil fuel consumption is mainly responsible for the depressed values during the winter months (from Vogel et al. 2002).

In 1963, many of the then nuclear states, signed the Limited Test Ban Treaty (LTBT). The LTBT (also referred to as the Partial Ban Treaty) had a remarkable impact in limiting radioactive isotopes in the atmosphere as it banned nuclear tests in all global environments, except for the underground (Praˇvaˇlie 2014). France and China never signed the LTBT but stopped atmospheric bomb testing in 1974 and 1980, respectively (Figure 2-22) (United States of America Department of State[6]). It is worth noting that between 1960 and 1964, France conducted atmospheric nuclear bomb tests in the Sahara desert, Africa (Director of Central Intelligence 1964). Ever since atmospheric nuclear tests ceased, the concentration of ^{14}C in the atmosphere decreased. Present day atmospheric ^{14}C values in the southern hemisphere are between 100 to 110 pMC (percent Modern Carbon) (Clark 2015 p.193).

[6] United States of America. Department of State. Limited Test Ban Treaty available at: https://www.state.gov/t/isn/4797.htm

Atmospheric nuclear tests promoted an unnatural assimilation of ^{14}C and ^{3}H into the hydrological cycle during the Atomic Age (see sections 2.7.2). This process is relevant for groundwater dating (see section below) as it labelled the age of the atmosphere and eventually hydrologic cycle with ^{14}C and ^{3}H concentrations between consecutive years since the bomb testing period. This process thus offers the possibility of estimating if groundwater was recharged before or after 1950 (Hua 2016). It is stated in Murray et al. (2015 p.12) that groundwater with ^{14}C concentrations greater than 85 pMC represents groundwater that was recharged after 1955.

2.8.3. Groundwater Age Calculations Using ^{14}C

The application of ^{14}C to directly date groundwater was first developed by Münnich (1957). The technique essentially determines the time that has elapsed since groundwater was recharged by measuring the decrease of ^{14}C in DIC (Dissolved Inorganic Carbon). Groundwater ages assist in determining the natural groundwater flow. This can in turn help with calibrating numerical mass-transport models (Geyh 2000; Sanford 2011). Also, groundwater ages assist with identifying old groundwater likely from deep aquifers that has migrated to shallow aquifers (e.g. Miller et al. 2015). Thus, groundwater age is an essential consideration in any palaeohydrologic and geohydraulic study (Geyh 2000).

When DIC in groundwater is out of equilibrium with the atmosphere (e.g. when it enters the groundwater system) the ^{14}C contained within the DIC decays. This physical process is the basis of the age determination of groundwater. The large half-life (5730 ± 30 years) of ^{14}C allows for the determination of groundwater ages up to ca. 40 000 years calculated using Equation 6 (Plummer & Glynn 2013 p.35; Atkinson et al. 2014).

$$t_{(years)} = \frac{5730}{\ln 2} \times \ln \frac{A_0}{A} \qquad \text{Equation 2-7}$$

On Equation 2-7:

5730 is the half-life of ^{14}C

A_0 is the initial ^{14}C content (pMC value) after adjustment for geochemical reactions without radioactive decay

A is the measured ^{14}C content (pMC) in the sample

Although the application of radiocarbon to date groundwater has been refined over the years (in terms of sample collection, analysis and application), calculated ^{14}C groundwater ages, still cannot be converted to real calendar ages (e.g. through dendrochronology like other biological radiocarbon "datable" materials). This is due to the complexity of aquifers: isotope decay is not the only geochemical process that lowers the concentration of ^{14}C in DIC. Carbonate dissolution can dilute the concentration of ^{14}C in DIC because "carbonates, generally having been deposited millions of years ago, are practically ^{14}C-free" (Vogel & Ehhalt 1963 p. 386). This influences the initial ^{14}C content in DIC. The initial ^{14}C content refers to the ^{14}C content of groundwater that occurs following groundwater recharge and isolation of the recharge water from the modern ^{14}C reservoir of unsaturated zone CO_2 (Plummer & Glynn 2013 p. 80). $\delta^{13}C$ measured in groundwater assists with determining the initial ^{14}C in groundwater and with thus groundwater radiocarbon age corrections (see section below).

2.9. Carbon-13 ($\delta^{13}C$) – Stable Carbon Isotope

$\delta^{13}C$ denotes the ratio of the two stable carbon isotopes: ^{12}C and ^{13}C. $\delta^{13}C$ is a useful tool for tracing the transfer of carbon in ecosystems because different components in the terrestrial environment have distinct $\delta^{13}C$ values (Figure 2-24) (e.g. Button 1991; Ostle et al. 2000; Carbone & Trumbore 2007). DIC in groundwater may come from various components of the terrestrial environment such as, atmospheric CO_2, pedogenic carbonates, CO_2 generated from the decay of C4, C3 or CAM plants. The origin of DIC in groundwater can be determined from the value of $\delta^{13}C$ in groundwater ($\delta^{13}C_{DIC}$). The value of $\delta^{13}C_{DIC}$ in turn plays an important role in groundwater studies as it can be used to reconstruct groundwater recharge environments. This assists in studying the evolution of groundwater and in quantifying water-rock interactions for the correction of ^{14}C groundwater ages (Vogel & Ehhalt 1963; Trumbore et al. 1992; Geyh 2000; Fetter 2001; Clark 2015). The sections below discuss how $\delta^{13}C$ enters the groundwater system and how using its evolution assists with tracing the evolution of groundwater.

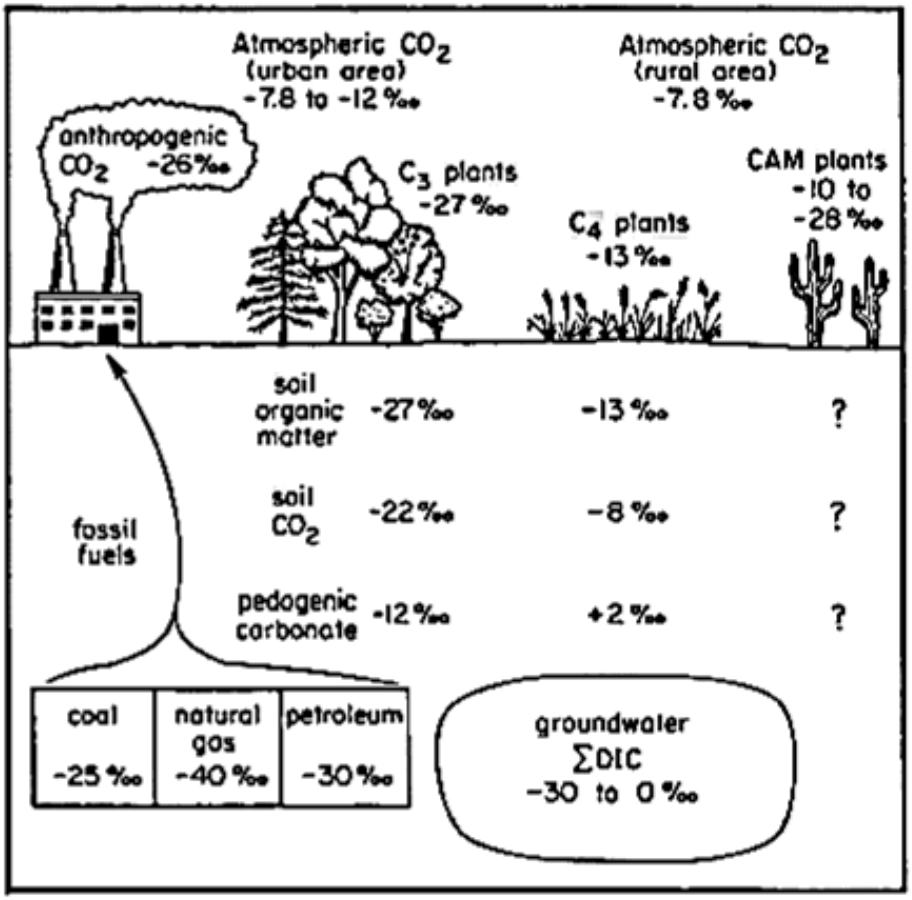

Figure 2-24: Stable Carbon isotope ratios of major components of terrestrial ecosystems (from Button 1991 p.175).

2.9.1. Dissolution of Soil-Respired $CO_{2(g)}$ or Soil CO_2 to form Dissolved Inorganic Carbon (DIC) in Groundwater

On Figure 2-24 it is shown that C3 plants have $\delta^{13}C$ values of approximately -27 ‰ and that C4 plants have $\delta^{13}C$ values of approximately -13 ‰. The isotopic composition of soil-respired $CO_{2(g)}$ generated from the decay of C3 plants eventually becomes modified to approximately -23 to -20 ‰ (an enrichment of ~ 4.4 ‰) during fractionation through diffusion. This enrichment is due to the necessary increment of $\delta^{13}CO_2$ during the outward diffusion of $^{12}CO_{2(g)}$ (more diffusive) and $^{13}CO_{2(g)}$ (less diffusive) from the soil to lower atmospheric partial pressures. In order to obtain fluxes into the atmosphere which balance the production of both $^{12}CO_{2(g)}$ and $^{13}CO_{2(g)}$ from the soil, the $\delta^{13}CO_{2(g)}$ must increase by 4.4 ‰ (Cerling et al. 1991). In arid regions (conducive to growing C4 plants), the soil-respired $\delta^{13}CO_{2(g)}$ usually increases

to approximately -7 ‰ (Figure 2-24). This is due to the already low partial pressures of soil CO_2 (P (atm) < $10^{-2.7}$) in such regions (Van der Kemp et al. 2000).

Soil-respired $CO_{2(g)}$ can be hydrated and react with carbonate species (such as $CO_{2(aq)}$, HCO_3^-, CO_3^2 or $CaCO_{3(aq)}$) to form DIC in groundwater. During such reactions, the resultant $\delta^{13}C_{DIC}$ is a function of enrichment factors (Table 2-4) between soil-respired $CO_{2(g)}$ and the carbonate species (weighted by their relative abundance) (Appelo & Postma 2005 p.218; Clark 2015 p.188).

Table 2-4 Enrichment of ^{13}C in carbonate species with respect to $CO_{2(g)}$ and $\delta^{13}C$ in species in equilibrium with a given $\delta^{13}C$ of $CO_{2(g)}$ (Appelo & Postma 2005 p. 218).

Species	‰ enrichment	$\delta^{13}C$ of species	
i	$\varepsilon^{13}C_{i/CO2(g)}$	$\delta^{13}C_{CO2(g)}$ = -7‰ (C4 plants)	$\delta^{13}C_{CO2(g)}$ = -23‰ (C3 plants)
$CO_{2(aq)}$	-1	-8	-24
HCO_3^-	9	2	-14
CO_3^{2-}	8	1	-15
$CaCO_3$	11	4	-12

The resultant DIC can form under open or closed system conditions in either carbonate or silicate aquifers. Carbonate dissolution in open system conditions describes the formation of DIC from recharge waters in contact with abundant soil-respired $CO_{2(g)}$. The soil-respired $CO_{2(g)}$ in such conditions can quickly dissolve in water to form either $CO_{2(aq)}$ or HCO_3^- depending on the extent of hydration of soil-respired $CO_{2(g)}$: further hydration results in the formation of HCO_3^-. Clark (2015 p. 188) showed that groundwater with pH values less than 6.4 at 10 °C in open system conditions has DIC composed mainly of $CO_{2(aq)}$, therefore its $\delta^{13}C_{DIC}$ will be close to soil-respired $\delta^{13}C_{soil}$ (because $CO_{2(aq)}$ has an enrichment factor of -1 ‰ when reacting with soil $CO_{2(g)}$). Larger pH values indicate that DIC is dominated by HCO_3^-. The $\delta^{13}C_{DIC}$ in this case will be $\delta^{13}C_{soil}$ + 10 ‰ (because the enrichment factor of HCO_3^- is 9 ‰ + 1 ‰ when reacting with $CO_{2(aq)}$). This is shown on Figure 2-25 here, an increase in pH

corresponds to an increase in HCO_3^- and $\delta^{13}C_{DIC}$. This pH control on $\delta^{13}C_{DIC}$ in groundwater in open system conditions distinguishes groundwater evolving under open system conditions from groundwater evolving under closed system conditions in carbonate or silicate aquifers. Adams et al. (2011) encountered groundwater dominated by HCO_3^- in topographically higher/steeper areas where surface ponding does not occur in Sutherland (~400 km west of study area).

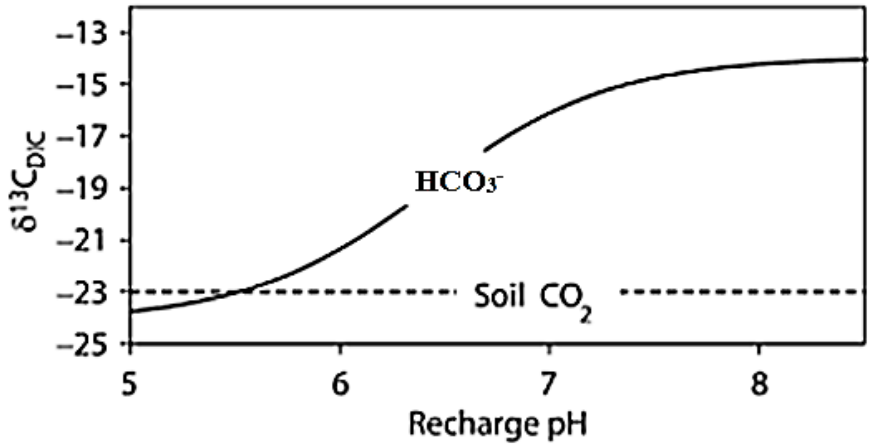

Figure 2-25: Effect of recharge pH on the $\delta^{13}C$ of dissolved inorganic carbon (DIC) in equilibrium with soil CO_2 (open system conditions). Calculated for case where $\delta^{13}C$ of soil CO_2 is -23 ‰ at 15 °C (modified from Clark 2015 p. 188).

Closed system conditions describe groundwater conditions where recharge waters are not entirely or completely in contact with soil-respired $CO_{2(g)}$ (unlike open system conditions) (Merkel & Planer-Friedrich 2008 p.145). In such conditions, DIC is derived in roughly equal proportions from soil $CO_{2(aq)}$ and $CaCO_3$ ($\delta^{13}C$ ~ 0‰). Therefore, groundwater dissolving calcite under closed system conditions in temperate climates will have a $\delta^{13}C_{DIC}$ of ~ -12 ‰ (half of $\delta^{13}C$ ~ -24 ‰ in $H_2CO_3^*$ which is mostly $CO_{2(aq)}$) (Vogel & Ehhalt 1963 p. 388; Appelo & Postma 2005 p.219).

2.9.2. $\delta^{13}C_{DIC}$ and Carbonate Weathering

$\delta^{13}C_{DIC}$ values change during open and closed system weathering of carbonates. This phenomenon serves as a guideline for evaluating whether further reactions have taken place in

the subsurface (Appelo & Postma 2005). Clark (2015) shows that the final DIC in carbonate aquifers has $\delta^{13}C$ between -10 ‰ to -13 ‰ (if soil CO_2 is $\delta^{13}C$ between -20 to -23 ‰) whether it is evolving under open or closed system conditions. This ambiguity is one of the reasons as to why carbonate aquifers are known for having a complicated geochemistry. Unfortunately carbonates may occur in silicate aquifers (within fractures, or as carbonate grains, cobbles or cement). Therefore this effect may be observed even in silicate aquifers as well (Clark 2015; Clark & Fritz 1997).

Groundwater in open system conditions evolving in carbonate aquifers reach calcite saturation at nearly neutral pH (between 6.5 and 7.5). Therefore, the major ion contributing to DIC is HCO_3^-:

$$CO_2 + H_2O \leftrightarrow HCO_3^- + H^+ \qquad \text{Equation 2-8}$$

If $\delta^{13}C_{soil}$ in such an aquifer is -20 ‰, the fractionation process progresses as:

$$\delta^{13}C_{CO_2} + \varepsilon^{13}C_{HCO_3^- - CO_2} \rightarrow \delta^{13}C_{DIC} \qquad \text{Equation 2-9}$$

$$-20‰ + 10‰ \rightarrow -10‰$$

Unfortunately, this result is similar the one reached when calcite dissolution in carbonate aquifers occurs under closed system conditions where exchange with soil CO_2 is limited. In these situations, the initial $\delta^{13}C_{DIC}$ value will increase as ^{13}C-enriched DIC (H_2CO_3) is gained from the bedrock:

$$H_2CO_3 + CaCO_3 \rightarrow Ca^{2+} + 2HCO_3^- \qquad \text{Equation 2-10}$$

Thus the final $\delta^{13}C_{DIC}$ becomes half of $\delta^{13}C_{CO_2}$ due to ^{13}C mixing with $\delta^{13}C_{CaCO_3}$ (0 ‰):

$$\delta^{13}C_{CO_2} + \delta^{13}C_{CaCO_3} \rightarrow \delta^{13}HCO_3^- \qquad \text{Equation 2-11}$$

$$-20‰ + 0‰ \rightarrow -10‰$$

2.9.3. Evolution of $^{13}C_{DIC}$ in Silicate Aquifers

The evolution of $\delta^{13}C_{DIC}$ in silicate aquifers is less complicated (provided that there are no carbonates within the aquifer) because the only source of carbon within the aquifer is soil $CO_{2(g)}$ (Vogel & Ehhalt 1963 p. 384; Clark 2015 p.191). In open system conditions, the only control on the change in the $\delta^{13}C_{DIC}$ value is pH. When the groundwater enters closed system conditions, the $\delta^{13}C_{DIC}$ value does not change even as the pH increases (Figure 2-26). Also, if carbonates occur within a silicate aquifer, they tend to dilute the ^{14}C concentrations because carbonates (e.g. limestone), having been deposited millions of years ago, essentially have no ^{14}C (Vogel & Ehhalt 1963). The section below discusses the correction of ^{14}C ages for carbonate dissolution. Also discussed is ways on how to account for the nuclear bomb effect when calculating ^{14}C ages.

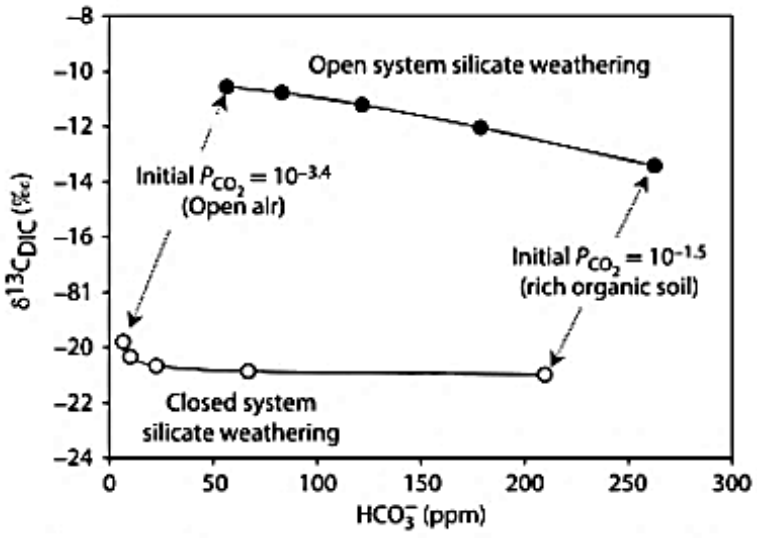

Figure 2-26: $\delta^{13}C$ of dissolved inorganic carbon during open and closed system silicate weathering, for $\delta^{13}C$ of soil CO_2 of -20 ‰ and at 10 °C (Clark 2015 p.191).

2.9.4. ^{14}C Age Corrections Using $\delta^{13}C_{DIC}$ Signatures

When calculating the radiocarbon age of groundwater, the initial ^{14}C concentration (A_0) in the recharge area must be determined. As mentioned earlier, the initial ^{14}C concentration in DIC can be diluted or lowered by carbonate dissolution. Measuring $\delta^{13}C_{DIC}$ in groundwater quantifies the extent of this carbonate dissolution. This assists in adjusting ^{14}C content of groundwater from the ^{14}C content in the soil zone to determine the initial ^{14}C concentration in groundwater.

Various hydrologists (e.g. Fontes & Garnier 1979; Ingerson & Pearson 1964; Kalin 1999 etc.) have developed models that account for some of the more important carbonate dissolution reactions that occur in groundwater. In South Africa, Harris et al. (1997), using $\delta^{13}C$ signatures in DIC and carbonates, identified Precambrian carbonate rocks to be a suitable source of CO_2 for gas exhalations at Bongwan, KwaZulu-Natal.

Although the mentioned models are based on assumptions regarding chemical and isotopic fractionation reactions, they at least cater to specific reactions that may lead to the dilution of ^{14}C. The output of carbonate dilution models is an initial ^{14}C value that has been adjusted for carbonate dissolution (Plummer & Glynn 2013 p.39-48). The Pearson Model (Ingerson & Pearson 1964) is arguably one of the most simple traditional A_0 adjustment methods. It accounts for carbonate dissolution in groundwater by using isotope mass balance relations for ^{13}C and ^{14}C:

$$A_{0Pearson} = \frac{(A_g - A_c)(\delta_{DIC} - \delta_c)}{(\delta_g - \delta_c)} + A_c \qquad \text{Equation 2-12}$$

Where:

A	is the ^{14}C pMC value
δ	is the $\delta^{13}C$
DIC	Dissolved Inorganic Carbon
g	Soil-respired CO_2
c	carbonate mineral(s)

Rearranging Equation 2-12 yields an equation to calculate the dilution factor (refered to as the q value). The dilution factor varies between 0-1 (1 is equivalent to no carbonate dilution):

$$\frac{A_{0Pearson} - A_c}{A_g - A_c} = \frac{\delta_{DIC} - \delta_c}{\delta_g - \delta_c} = q\ (dilution\ factor) \qquad \text{Equation 2-13}$$

Assuming that A_0 ~ 100 pMC (approximately current atmospheric ^{14}C concentration in the southern hemisphere) before adjustment and incorporating the dilution factor (Equation 2-13), the conventional groundwater ^{14}C age equation (Equation 2-7) becomes:

$$Calculated\ Age\ (years) = -8033 \times \ln \frac{14C_{measured}}{q \times 100} \qquad \text{Equation 2-14}$$

A final step when calculating groundwater ages is to subtract the excess ^{14}C from bomb detonations in the 1950s (Mook & van der Plicht 1999). Considering that the groundwater samples for this project where collected in 2016 (and early 2017), the final step is thus:

$$Corrected\ Age\ (years) = Calculated\ Age + (2016 - 1950) \qquad \text{Equation 2-15}$$

3. Study Area

The first two chapters of this thesis introduced the topic and gave a background on the application of isotopes in the hydrological cycle. It was shown that, using stable water isotopes, groundwater recharge mechanisms can be studied. Stable carbon isotope ($\delta^{13}C$) can be used to trace the evolution of DIC in groundwater. Unstable hydrogen and carbon isotopes (^{3}H and ^{14}C, respectively) can be used to determine the residence time of groundwater. In the sections below various aspects of the study area are discussed. These include the geology and geohydrology as an understanding of these aspects constitutes an important role in defining the aquifer(s) in the study area.

3.1. Geology of the Study Area

The study area (~14 671.5 km^2) is situated in the south-central part of the Karoo Basin (23.577 to 26.315 °E and -33.113 to -31.703 °S). This area falls within the Eastern Cape Province of South Africa and identified region for shale gas development and the AEON-ESSRI baseline projects. The landscape of the study area is dominated by sub-horizontal sandstones and siltstones of the Beaufort Group (Adelaide Subgroup) that are intruded by abundant dolerite sills and dykes in its northern sector (Figure 3-1). Sediments of the Cape Supergroup encompass a small portion in the south-western part of the study area. Here, the Cape Supergroup sediments are thrust within the Cape Mountains (Booth & Shone 2002) (Figure 3-2). Thrust faults and folded bedding planes have been shown to be conduits for the transport of hot fluid flow to shallower depths within the Cape Mountains and the flanking Beaufort Group sediments in the southern part of the Karoo Basin during the formation of the Cape Fold Belt ~252 Ma (Egle 1996; Craddock et al. 2007).

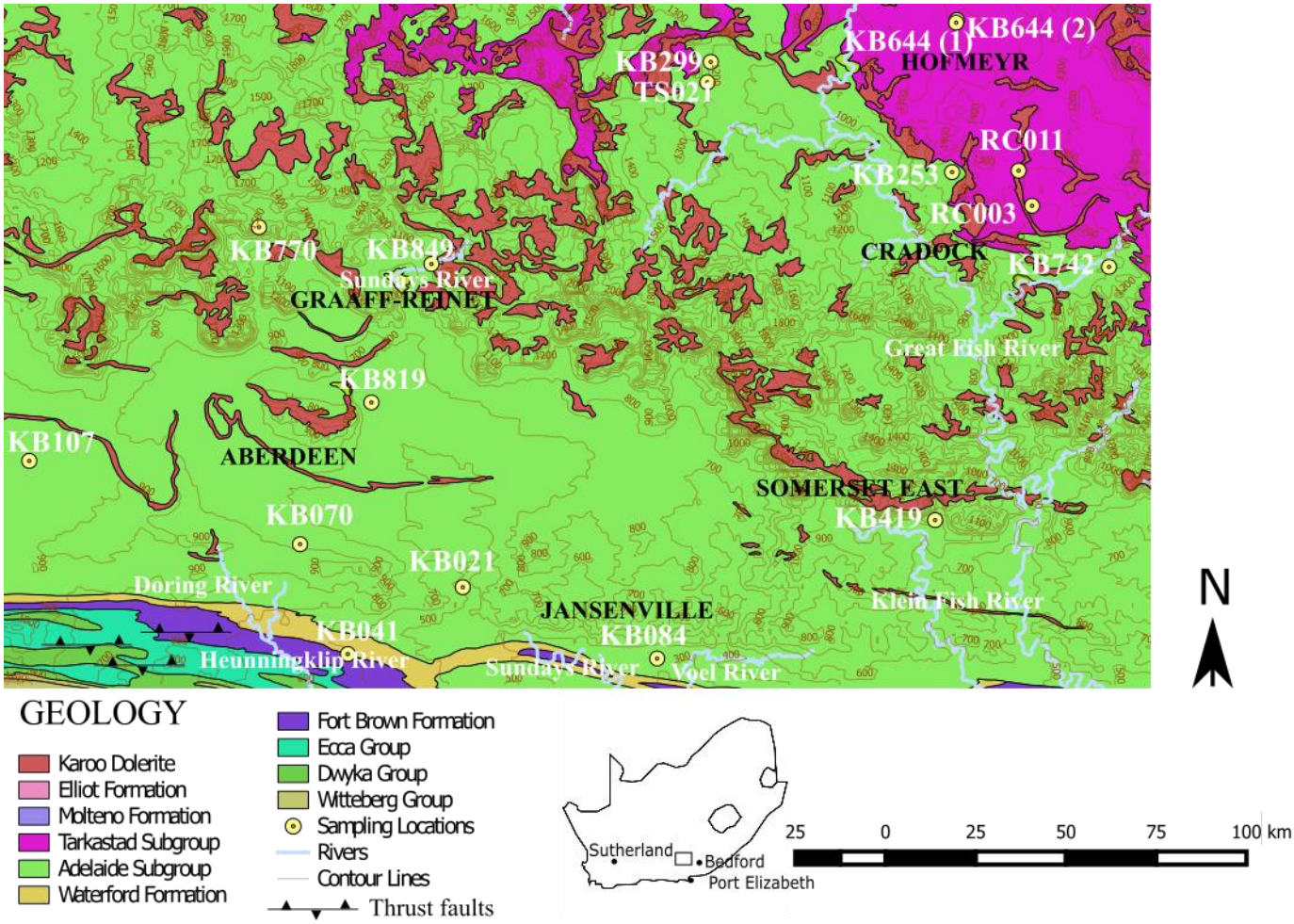

Figure 3-1: Simplified geological map of the study area, which is located in the south-central part of the Main Karoo Basin in the Eastern Cape Province of South Africa. Dense contour lines in the southern part of the study area mark the general edge of the Great Escarpment, which signifies an increase in elevation (> 2 km) generally from the southern part to the northern part of the study area. After the deformation of the Cape Groups during the formation of the Cape Mountains the lower Karoo Basin sequences were deformed especially in the southern part. This deformation is shown by the presence of thrust faults in the study area.

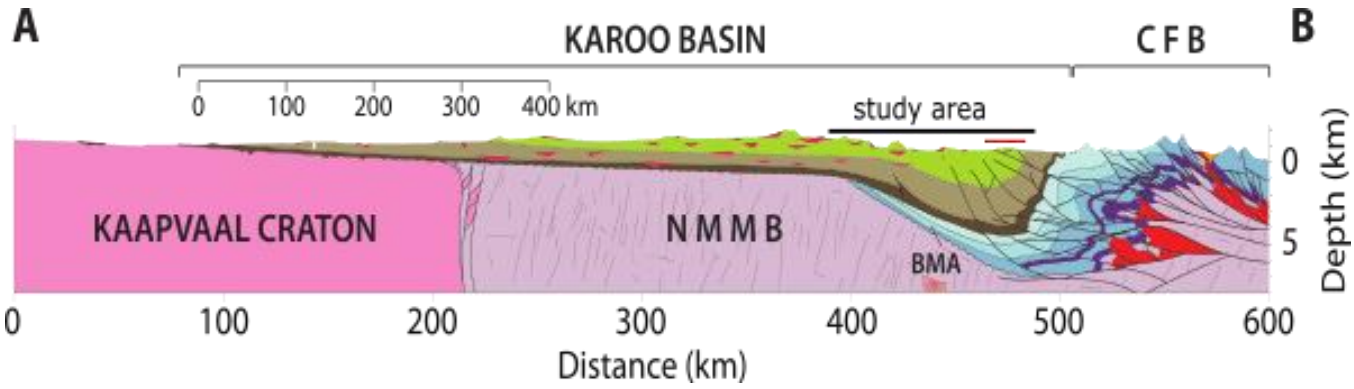

Figure 3-2: N-S geological cross section of the Karoo Basin. See Figure 1-1 for a line representing the position of this cross section in SA and for the legend. NMMB stands for Namaqua Natal Mobile Belt. The red line symbolises the area where relatively older groundwater was collected for this study (see section 6.1).

Within the interior of southwest Gondwana, deposition in the Karoo Basin followed that of the Cape Supergroup during the Carboniferous (~350 Ma). It continued until the break-up between the East and the West of Gondwana in the Middle Jurassic (~183 Ma) and the eruption of the Karoo Large Igneous Province. The basin covers approximately 620 000 km^2 of South Africa and comprises three to six km thick sedimentary rocks collectively known as the Karoo Supergroup (Linol & de Wit 2016). Along the southern margin, where the basin borders the Cape Mountains, the rock sequences are often duplicated along thrusts and folds due to the formation of the Cape Mountains (Figure 3-1). To the north, the Karoo Supergroup is extensively intruded by dolerite sills and capped by basalts of the Drakensberg Group (Linol et al. 2016). The stratigraphy and the subsurface geology of the study area is best described using borehole core descriptions of Soekor boreholes, such as CR 1/68 (Figure 3-3), which was drilled near Cradock. Cradock is one of the small towns that fall within the study area of this research project.

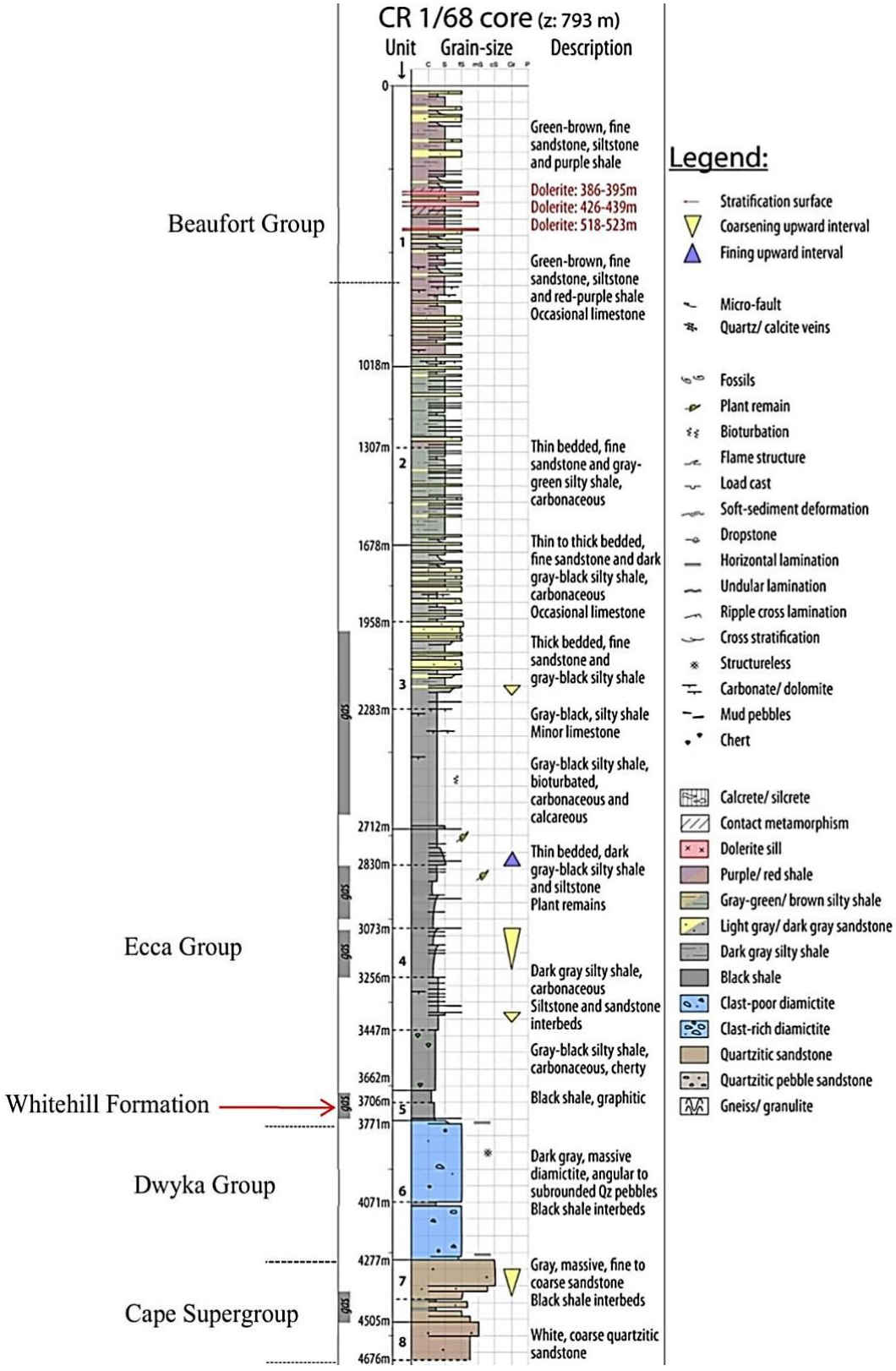

Figure 3-3: Typical example of Soekor borehole data: description of CR 1/68 deep borehole drilled near Cradock (modified from Linol & de Wit 2016). Also shown is the depth of the Whitehill Formation (~290-280 Ma), which is targeted for shale gas development (see section 2.4). The Beaufort Group constitutes most Karoo shallow aquifers (KGEG 2013).

The Dwyka Group forms the basal part of the Karoo Supergroup, deposited from the Late Carboniferous to the Early Permian (~290 Ma) by successive glacial and deglaciation processes (Schulz et al. 2016 and references therein). The depositional environment of the Dwyka Group is interpreted as wide subglacial valleys and lakes carved by an Antarctic-like ice cap. During deposition, a thick (~800 m) sequence of diamictites and rhythmites accumulated in the southern part of the Karoo Basin while striated pavements formed much of the northern margin (Visser 1987). Subordinate mudrock and black shale are also recognised within the group (Thomas et al. 1990).

The overlying Ecca Group was deposited during the Permian, following rapid deglaciation across southern Africa (~290 Ma). This rapid ice-cap disintergration was initiated by the movement of the South Pole across Gondwana toward Antarctica. The deglaciation in turn gave way to the slow deposition of fine-grained, carbonaceous shales of the lower Ecca Group which comprise the Prince Albert, Whitehill and Collingham Formations (Linol and de Wit 2016). These, especially the organic-rich shales of the Whitehill Formation are the main target for shale gas development in the Karoo Basin (Geel et al. 2013; Geel et al. 2015 Black et al. 2016; Chere et al. 2017).

Above, the sedimentary rocks of the Beaufort Group were deposited from mid-Permian (~266 Ma) to mid-Triassic (~250 Ma) during the amalgamation of Gondwana into the Pangea mega-continent. This resulted in large-scale intra-continental deformation and lithosphere buckling providing space for widespread deposition of thick continental sequences (Linol & de Wit 2016). This group consists mostly of red-purple shales, mudstones, siltstones and cross-bedded sandstone (Smith & Botha-Brink 2014; Rubidge et al. 2016), interpreted to be deposited by meandering river systems (Linol & de Wit 2016). The Group was subdivided into the Lower Adelaide Subgroup and the Upper Tarkastad Subgroup in the eastern section of the Karoo Basin, east of longitude 24 °E by Johnson (1966) on the basis of mudstone coloration. The mudstones of the Adelaide Subgroup are massively bedded, ranging in colour between green, blue-grey and brown (Smith 1980). The Tarkastad Subgroup is characterised by abundant red mudstones (Selley 1997 p.299).

The uppermost Molteno, Elliot and Clarens Formations were deposited before the eruption of the overlying Drakensberg basalts and the intrusion of dolerite sills and dykes (~ 182 Ma) (Duncan et al. 1997). The Molteno Formation is the oldest of these siliciclastic formations. This formation was deposited by perennial low-sinousity braided streams (Turner 1983). It is

dominated by coarse sandstones, interbedded with grey shales (du Toit 1954). The overlying Elliot Formation was deposited during increasingly arid conditions in alluvial flood plains that were interacting with fluvial and aeolian processes. This formation is dominated by red-bed successions of mudstones, siltstones and immature, fine- to medium-grained sandstones (Bordy & Eriksson 2015). The Clarens Formation is considered a climatically controlled fluvioaeolian to aeolian lithostratigraphic interval (Holzförster 2007). It is dominated by massive units interbedded with sandstones (Bordy 2008).

3.2. Geohydrology of the Study Area

Approximately down to 1018 m (and possibly deeper), the study area is underlain by the Beaufort Group (Figure 3-3). According to Woodford & Chevallier (2002), the Beaufort Group hosts multi-layered and multi-porous aquifers of variable thickness. Contact planes between two different sedimentary layers in this group may cause a discontinuity in the hydraulic properties of composite aquifers.

It is evident from the previous section that, the Karoo Supergroup is dominated by silicate rocks. On section 2.9.3 it is shown that the dissolution of silicate minerals in an aquifer without carbonates renders groundwater with $\delta^{13}C_{DIC}$ signatures between -14 to -11 ‰ in open systems and -20 to -21 ‰ in closed systems. However $\delta^{13}C_{DIC}$ of groundwater measured in the Karoo may be more enriched than the standard (e.g $\delta^{13}C_{DIC}$ ~ -26 to 4.7 ‰ in Swana (2016)). The enrichment of $\delta^{13}C_{DIC}$ values in Karoo groundwater may be due to the occurrence of carbonates (e.g. in the Whitehill Formation). These carbonates have more enriched $\delta^{13}C$ signatures (according to de Wit (2016), $\delta^{13}C_{carb}$ are approximately -2 ‰ for the Whitehill Formation). In addition, according to Swana (2016), methanogenesis in the Karoo may also have a role to play in the enrichment of groundwater $\delta^{13}C_{DIC}$.

Research on deep aquifers is limited but indicates possible deep groundwater circulation and migration (Weckmann et al. 2012; KGEG 2013; Swana 2016). Old groundwater detected at shallower depths within the study area may be groundwater that has migrated from aquifers of the Dwyka or Ecca Groups. Woodford & Chevallier (2002) postulate that the Dwyka Group is likely to contain saline groundwater because some investigators (e.g. Johnson et al. 1997) infer a marine setting for the deposition of the diamictites in the Dwyka Group. However, de Wit (2016) postulates that marine fossils only occur in some parts of the Karoo Basin (particularly in southern Namibia), therefore, the deposition of the Dwyka Group (and Lower Ecca

formations) may have taken place in terrestrial settings as evidenced by the abundance of terrestrial fossils found within these units. However, the terrestrial depositional environment may have been connected to marine waters that may have continuously infiltrated the southern Karoo Basin (Schulz et al. 2016; de Wit 2016; Chere et al. 2017). This infiltration could be the cause for the occurrence of saline groundwater within most Lower Karoo formations.

3.3. Vegetation of the Study Area

The study area can be described as a summer-rainfall region that is dominated by the Nama-Karoo Biome (Figure 3-4) (Kane 2009). The Nama-Karoo biome covers approximately 248 273 km^2 of South Africa and characterises an area covered by a lime-rich weakly developed soil type with mostly C4-type grasses and dwarf shrub-land vegetation (Mucina et al. 2006; Dupont et al. 2013; South African Department of Environmental Affairs 2015). A study done by Vogel et al. (1978) found C4 plants in South Africa to have $\delta^{13}C$ values between -12 and -13 ‰ (Erasmus et al. 2016). Groundwater researchers (e.g. Verhagen et al. 2009; Swana 2016) do not consider the $\delta^{13}C$ of soil-respired $CO_2(g)$, which should be -7 to -8.6 ‰ for C4 plants (see section 2.9.1), perhaps because isotopic fractionation due to diffusion is negligible in the Karoo Basin (e.g. Ramnarine et al. 2012). Instead, the $\delta^{13}C$ of the plant tissue itself is considered.

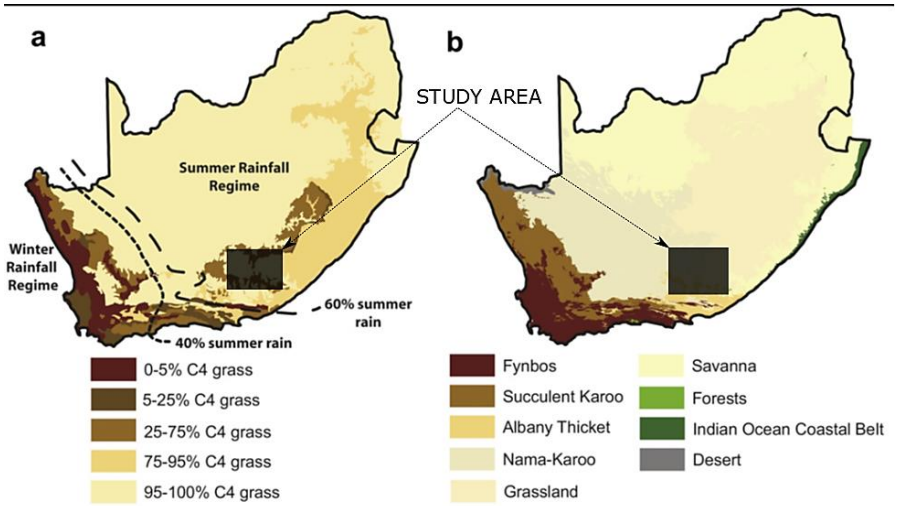

Figure 3-4: Vegetation of the study area a) the distribution of C4 grasses as a percentage of all grasses in South Africa (Vogel et al. 1978) b) distribution of vegetation biomes in South Africa (Mucina et al. 2006).

The abundant C4 plants within the study area (Figure 3-4) are naturally water efficient, nitrogen efficient and well adapted to undisturbed land like there was before the arrival of European settlers in South Africa (Mucina et al. 2006). An influx of agriculture after European settlers arrived (ca. 1652) introduced alien species which were mostly C3 plants through the removal of indegenous C4 vegetation (Milton 2004). Additionally, in the future, the vegetation within the study area and South Africa as a whole may contain even more C3-type vegetation because it has been projected that an increase in atmospheric CO_2 (likely caused by anthropogenic practises) will improve the nitrogen-use efficiency of C3 plants, giving them an even greater advantage over C4 grasses in South Africa (Milton 2004). The increase in C3 plants species in South Africa since the arrival of European settlers and the projected increase of C3 plant species in the future demonstrate the significant impact anthropogenic practises have across the CZ. The section below discusses the population within the study area and its access to water resources as this determines land use practises and thus how people further influence the CZ.

3.4. Population and Access to Water Resources

The estimated total population within the study area is 126 622 (Table 3-1). Of the major towns, Cradock has the largest population and Hofmeyr has the lowest. The most densely populated town is Aberdeen. The largest group in the study area is black. The number of households with access to piped water inside their dwelling or yard or within 200 m from the yard increased by 10.2% from 18 963 households in 2011 to 20 893 households in 2016 (South African Census[7] 2016). Water consumption is projected to increase within the study area due to the projected population growth rate of at least 6.6% per year in the Eastern Cape (Eastern Cape Socio Economic Consultative Council (ECSC) 2016). Also, similarly to the rest of the country, the study area has experienced drought over the past couple of years. This has resulted in decreasing dam levels, for example in 2017 Nqweba dam in Graaff-Reinet was only at 11.4% of its capacity. Keke (2006) postulates that, in times of drought, groundwater provides a reliable source of water if properly managed.

[7] South African census data http://www.statssa.gov.za/?page_id=6283

Table 3-1 Demographics of the study area[7].

Town	Estimated Total Population	Population Density (per km^2)	Black Population (%)	Coloured Population (%)	White Population (%)
Jansenville	5 612	230	42.9	48.7	7.8
Aberdeen	7 162	470	19	73	6.7
Somerset East	18 825	260	58.8	32.2	7.2
Graaff-Reinet	35 672	180	28.2	62.2	8.7
Cradock	36 671	290	61.8	25.4	11.8
Middelburg	19 000	420	49.21	43.9	6.2
Hofmeyr	3 680	217	80.3	15.8	3.2
Total	126 622	2 067	48.60	34.14	7.38

Groundwater consumers within the study area usually drill for groundwater at the contact between dolerite intrusions and sedimentary rocks because these areas act as linear zones of relatively higher permeability which in turn act as conduits for groundwater flow within aquifers (Murray et al. 2012). However, below the great escarpment and where dolerite intrusions are uncommon successful boreholes are usually sited on fold-axes and antithetic fracture systems (Woodford & Chevallier 2002 p. 136) or rivers.

3.5. Land Use within the Study Area

As mentioned earlier, the study area falls within the Nama-Karoo biome (see section 3.3). According to the Department of Environmental Affairs (2015), only 0.8% of the Nama-Karoo is protected under formal jurisdictional protection. Land uses within the biome are dominated by agriculture in the form of extensive grazing and wildlife management (SANBI South African National Biodiversity Institute[8]). Both small and large stock production takes place

[8] http://pza.sanbi.org/vegetation/nama-karoo-biome

here, while other significant land uses include mining and various forms of tourism, ecotourism and allied livelihood activities (SANBI).

Towns within the study area have their unique dynamics and attractions. One Graaff-Reinet main attractions is the Valley of Desolation (Figure 3-5). The Valley of Desolation is situated to the immediate south of the Great Escarpment and is fringed by dolerite pillars with columnar joints. Such joints may act as preferential pathways for groundwater and are usually a target for groundwater exploration below the escarpment (Woodford & Chevallier 2002). Elsewhere in the Karoo preferential pathways bringing groundwater to shallow depths may be connected to deep groundwater reservoirs (>300 m). This thesis is focused on documenting these area(s) using isotopes. The following chapter discusses the methods that were used to achieve this goal.

Figure 3-5: The Valley of Desolation in Graaff-Reinet (from https://www.graaffreinet.co.za/listing/valley_of_desolation). The Valley of Desolation is situated south of the Great Escarpment and is flanked by columnar joints in dolerite sills.

4. Methodology

The methodology of this project involves three phases. Phase 1 was conducting a hydrocensus (water census). The hydrocensus began in November 2014 with four postgraduate students. The team built good relationships with the land owners and residents in each town visited. Phase 2 relates to groundwater sampling. After the hydrocensus a groundwater team started collecting samples for the bigger AEON-ESSRI groundwater project. This was followed by sampling groundwater for this project. Phase 3 involved isotope analysis at the Environmental Isotope Laboratory of iThemba Laboratories in Johannesburg.

4.1. Hydrocensus

The Department of Water Affairs (2004) defines a hydrocensus as a task that involves gathering information on water features, water supply sources and sources of potential water pollution in a particular site or area. The hydrocensus for this study and the AEON-ESSRI baseline projects involved visiting groundwater sites, recording GPS coordinates, elevation, date/time, marking site descriptions and measuring/recording the dimensions of the borehole equipment used to abstract groundwater (e.g. casing height, casing and pipe diameters) (Figure 4-1). The outputs of the conducted hydrocensus are presented here in the form of hydrocensus maps (Figure 5-1 to Figure 5-3) and electrical conductivity profiles (Figure 5-4 to Figure 5-17).

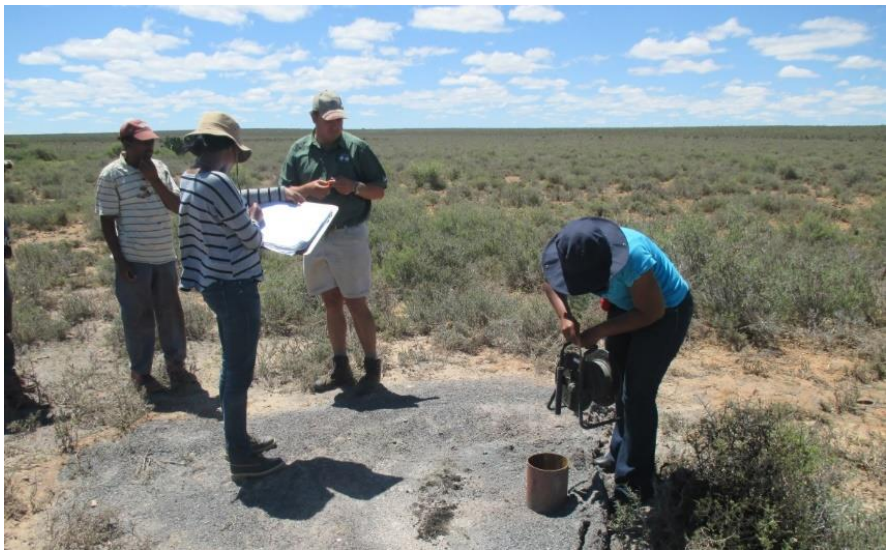

Figure 4-1: Photo of AEON-team conducting a hydrocensus in the Karoo (the author of this thesis is capturing hydrocensus data on the clipboard in this photo).

During the hydrocensus, if the borehole was operational at the time of the visit, the type of borehole equipment (e.g. wind pump or electrical pump), water use and electrical conductivity measurements were recorded. However, if the borehole was open and without any water extraction equipment (i.e. a pump), water-level measurements, borehole depth measurements, electrical conductivity profiling and slug tests were performed. In addition, a photo of the borehole or water body, along with additional comments and/or farm manager's contact details were recorded for future reference. The hydrocensus data was archived, and serves as a data pool with suitable sites for various AEON-ESSRI baseline groundwater projects.

4.1.1. Electrical Conductivity (EC)

Electrical Conductivity (EC) (measured in µS/m) is the ability of a material to carry the flow of an electric current. EC can be used as a proxy for water chemistry and hydrologic processes (Moore et al. 2008). Electrical conductivity was measured using a Model 107 TLC (Temperature Level Conductivity) Meter (Figure 4-2) which consists of a 19 mm diameter probe attached to a millimetre-marked Solinst PVDF (Polyvinylidene fluoride) flat tape mounted on a reel. Water was collected from each site in a 500 ml plastic bottle. The probe was submerged in water. When the probe makes contact with the water it "beeps" and displays the EC and temperature readings on a small Liquid Crystal Display (LCD) screen.

Figure 4-2: Model 107 TLC (Solinst[9]).

[9] All groundwater sampling products from Solinst are labelled with (Solinst) hereon. Solinst products are available at: http://www.geowater.co.za/groundwater.html.

4.1.2. Electrical Conductivity Profiling

EC profiling was performed to determine vertical locations of transmissive zones (water strikes) for groundwater sampling (see Figure 5-4 to Figure 5-17 for EC profiles). During earlier stages of the project, electrical conductivity profiling was conducted using the Model 107 TLC Meter (Figure 4-2). To profile each borehole, it was lowered down and pulled back up slowly while recording the EC and temperature at every meter. This proved tedious Therefore, the TLC Meter was later replaced with a LTC (Level Temperature Conductivity) Levelogger Junior Edge Model 3001 (Figure 4-3). This links with a data logger, pressure transducer, temperature and electrical conductivity sensors within a 22 x 190 mm 4-electrode platinum coating to automatically record and store electrical conductivity profile data until retrieval. To lower the probe down each borehole, it was attached to a tag line. Solinst 4.1.1 computer software was used every morning and every evening to prepare for deployment and to download the data.

Figure 4-3: Levelogger Junior Edge Model 3001 (Solinst).

4.1.3. Falling-Head Slug Test

Falling head slug tests were conducted to determine borehole yields within the study area (see Figure 5-3 for a map with interpolated borehole yields across the study area). A falling-head slug test is a low cost aquifer test whereby the water level of a borehole is rapidly changed or shrugged. The time it takes for the water level to return back to static water level is measured to determine hydraulic conductivity and borehole yield. The apparatus used for slugging

included a LT (Level Temperature) Levelogger Junior Edge probe (this looks identical to the Levelogger Junior Edge Model 3001 shown on Figure 4-3 but has different functions), a water-weighted 1.5 m long cylinder (the "slug", used to disturb the water level) and a tag line. The procedure (Figure 4-4) starts with lowering the LT probe line 2-3 ms below the static water-level and holding the weighted cylinder just above the static water-level. This is followed by quickly dropping the weighted cylinder and leaving it inside the borehole for approximately 5 minutes. Rapidly dropping the weighted cylinder raises the water level and leaving it inside the borehole for 5 minutes allows for the water level to revert back to static (Fabbri et al. 2012; Ola et al. 2016). These changes in water level are measured by the probe. The level and temperature data is then downloaded from the probe, and the rate at which the water-level reverts back to static is calculated using a flow characteristic programme.

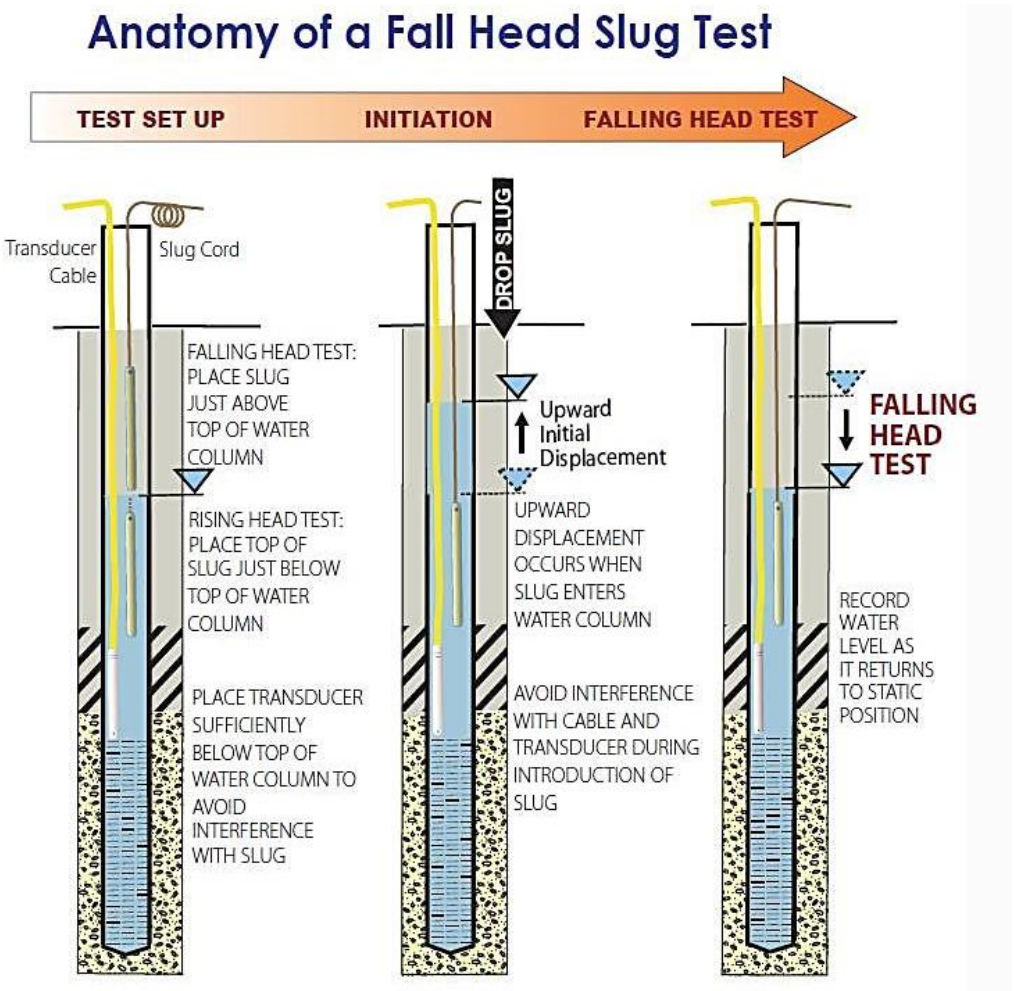

Figure 4-4: Schematic figure of a falling-head slug test (from http://www.midwestgeo.com/fieldtools/supporting-files/h(o)_slug_information.pdf).

4.2. Groundwater Sampling

A total of 17 boreholes were selected at different geographical locations from the hydrocensus data for sampling. Water samples were collected using a 12 Volt Low Flow Pump (Figure 4-5) with a Power Booster III Controller (Figure 4-6). The Power Booster was connected to the field vehicle's battery for power (Figure 4-7). Temperature, pH (measured with an Adwa AD11/AD12 pH meter) and EC of the water were monitored while purging the borehole. A representative sample was collected once the monitored parameters stabilised (15-20 min).

Figure 4-5: 12 Volt Low Flow Pump.

Figure 4-6: Power Booster III Controller (Solinst).

Figure 4-7: Power Booster III Controller connected to a car battery.

All isotope samples were collected in plastic bottles that were rinsed thoroughly with deionised water. $\delta^{18}O$ and $\delta^{2}H$ samples were collected in 500 ml plastic bottles. ^{3}H samples were collected in 1L bottles. ^{14}C and $\delta^{13}C$ samples were collected following the drum precipitation experiment. The objective of conducting a drum precipitation experiment is to obtain enough carbon (minimum 2g) for a radiocarbon measurement. This was achieved by precipitating DIC at a minimum of 2 meq/l (e.g. ~150 mg/l HCO_3) from 50 L of sample water per borehole.

After purging each borehole, a few litres (<5 L) of sample water were mixed with approximately 200 g of $BaCl_2$ in order to precipitate DIC as $BaCO_3$ (Hussain 1991). The drum was then rinsed well with sample water and filled. While filling, approximately three drops of a previously prepared phenolphthalein (an indicator) solution were added to the sample water along with approximately 200 ml of cleaned NaOH solution and the prepared $BaCO_3$ solution.

The water turned pink after adding the NaOH solution (Figure 4-8) and a cloud of precipitate formed when the $BaCl_2$ solution was added (Figure 4-9). The drum was then screwed shut and placed at the back of the vehicle. Precipitation continued and formed a visible layer below the draining stopcock while driving. Above the precipitate was a clear supernant. All but 2 L of the supernant was discarded. The precipitate was reserved in a 2 L container where it further compacted. After further compaction, the precipitation was transferred to a 1 L bottle and topped with the reserved supernant. Atmospheric exposure was limited for the alkaline by working quickly and making sure that the alkaline sample is closed and stored away from direct sunlight at every step during the experiment as advised by the laboratory manager (Mike Butler).

Figure 4-8: The sample water turns pink after the addition of NaOH.

Figure 4-9: Precipitate starting to form.

4.3. Laboratory Analysis

Groundwater alkalinity was measured at Innoventon Laboratory in Port Elizabeth using the standard alkalinity measurement through titration. 50 to 100 ml of each groundwater sample was placed in a 250 ml beaker and this was placed onto a stir plate (with a bar magnet in the flask). The initial pH of the sample was measured. If the sample pH was below 8.3, several drops of bromocresol green pH indicator were added. If the colour of the solution turned blue, the sample was titrated with 0.02 N H_2SO_4 or HCl until the colour changed to yellow (pH 4.5). The total volume of acid used for the titration was recorded. If above 8.3, the initial pH of the sample was measured. If the sample pH was above 8.3, several drops of phenolphthalein indicator were added. If the colour of the solution turned pink, the sample was titrated with

0.02 N H_2SO_4 or HCl until the colour changed from pink to clear (pH 8.3). The volume of acid used for the titration was then recorded. Then the titration procedure for samples with pH below 8.3 was followed. The Phenolphthalein Alkalinity and Total Alkalinity were calculated using Equation 4-1 and Equation 4-2, respectively (Snoeyik & Jenkins 1980).

$$= Amount\ of\ acid\ used\ to\ reach\ pH\ 8.3\ (ml) \times Normality of\ acid\left(\frac{eq}{L}\right) \times \frac{100000\left(\frac{mgCaCO_2}{eq}\right)}{sample\ volume\ (ml)} \qquad \text{Equation 4-1}$$

$$= Amount\ of\ acid\ used\ to\ reach\ pH\ 4.5\ (ml) \times Normality of\ acid\left(\frac{eq}{L}\right) \times \frac{50000\left(\frac{mgCaCO_2}{eq}\right)}{sample\ volume\ (ml)} \qquad \text{Equation 4-2}$$

Where:

$$Normality = Molarity\left(\frac{moles}{L}\right) \times the\ number\ of\ hydrogen\ exchanged\ in\ a\ reaction\ (\frac{eq}{moles})$$

All isotope analyses were performed in the laboratory of Environmental Isotope Group (EIG) of iThemba Laboratories in Johannesburg. The following is an account of the laboratory isotope analysis procedure. A first batch of 4 water samples were analysed in November 2016 and a second batch of 13 samples were analysed in February 2017. The equipment used for stable isotope analysis for the first batch of water samples consisted of a Thermo Delta V mass spectrometer connected to a Gasbench (Penna et al. 2010). This equipment requires sample preparation that involves sample water equilibration with H_2 and CO_2. Equilibration time for each water sample with hydrogen lasts about 40 minutes and twenty hours for CO_2. Using this technique, the analytical precision was estimated at 0.2 ‰ for O and 0.8 ‰ for H. Stable isotopes in the second batch of water samples were measured using a Los Gatos Research

(LGR) Liquid Water Isotope Analyser (Berman et al. 2013; Wassenaar et al. 2016). The LGR Liquid Water Analyser does not require equilibration sample preparation. The analytical precision using the LGR Liquid Water Analyser equipment is estimated at 0.5 ‰ for O and 1.5 ‰ for H. Laboratory standards, calibrated against international reference materials, were analysed with each batch of samples. $\delta^{2}H$ and $\delta^{18}O$ are reported relative to SMOW (Standard Mean Ocean Water) and $\delta^{13}C$ is reported relative to PDB (Pee Dee Belemnite). Analytical results are reported in the common delta-notation:

$$\delta\ (‰) = \left(\frac{R_{sample}}{R_{standard}} - 1\right) \times 1000 \qquad \text{Equation 4-3}$$

Where:

δ	is the final isotopic ratio
R_{sample}	is the isotopic ratio of the sample
$R_{standard}$	is the isotopic ratio of the standard

Water samples for tritium analyses were first distilled and subsequently enriched by electrolysis. The electrolysis cells consist of two concentric metal tubes (Figure 4-10) that are insulated from each other. The outer anode, which is also the container, is made of stainless steel. The inner cathode comprises mild steel.

Figure 4-10: Electrolytic cells.

Approximately 500 ml of the water sample, having first been distilled and containing sodium hydroxide, was introduced into the cell. A direct current of 10–20 Ampere was then passed through the cell. After several days, the electrolyte volume was reduced to approximately 20 ml. The samples were then prepared for counting by directly distilling the enriched water sample from the highly concentrated electrolyte. 10 ml of the distilled water sample was mixed with 11 ml Ultima Gold and placed in a vial in a Hewlett Packard Liquid Scintillation Analyser (Figure 4-11). Here, the samples were counted for 2 to 3 cycles of four hours each. Detection limits were 0.2 TU for the enriched samples.

Figure 4-11: Tri-Carb 9770TR/5L Hewlett Packard Liquid Scintillation Analyser.

For radiocarbon analysis, CO_2 was generated by acidification of the field precipitate with phosphoric acid (H_3PO_4):

$$3BaCO_{3(s)} + 2H_3PO_{4(aq)} \rightarrow Ba_3(PO_4)_{2(s)} + 3CO_{2(g)} + 3H_2O_l \qquad \text{Equation 4-4}$$

The CO_2 sample gas was transferred from the production/purification line into a 1 L Pyrex flask, the pressure (610 mmHg max.) was measured on a manometer and isolated. 10 ml of Carbosorb®E was pipetted into a standard 20 ml low-K glass counting vial that is attached to the system through a vacuum-tight, flexible connection. Air was removed by opening the vial briefly. The CO_2 sample was then transferred quantitatively from the measuring volume by freezing with liquid N_2 into a small trap which forms part of a low-volume (~60 ml) section of

the system. The trap is pumped to vacuum to remove residual non-condensable gas. The small volume section is isolated, and then the tap to the vial is opened. CO_2 is allowed to sublimate whilst the vial was shaken by hand (note the this connection is flexible). When conducting this experiment, the rate of CO_2 absorption usually balanced its release from the trap through ambient (~25°C) warming at pressures around 300-400 torr.

Uncooled, the rate of absorption under such conditions causes the temperature of the Carbosorb® in the vial to rise to 70 °C. In the experiments, this did not seem to have any effect on the counting characteristics. However, the NH_4 released by the Carbosorb forms a gas "blanket" over its surface, through which the CO_2 has to diffuse. When the vial is kept cool in a water bath, the equilibrium pressure reduced to approximately 40 torr, implying more complete CO_2 absorption, due to lower NH_4 pressures above the Carbosorb® surface.

The counting vial is removed from the vacuum system and 10 ml Permafluor ®E+ is added. The vial is capped tightly and the 'cocktail' was shaken well before counting. Figure 4-12 shows the ^{14}C 'cocktail' and CO_2 samples.

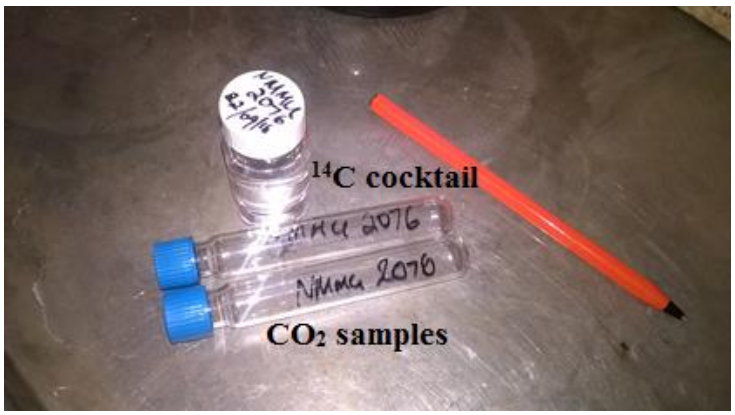

Figure 4-12: Samples prepared from field precipitate.

Because of a considerable overlap between the pulse height spectrum of ^{14}C and the spectrum of ^{222}Rn, samples for radiocarbon analysis must be stored for about three weeks to allow ^{222}Rn ($t_{1/2}$ = 3.85 days) to decay to below significant levels. The prepared sample 'cocktails' are therefore placed immediately in the cooled and darkened sample changing chamber of a Hewlett Packard TriCarb liquid scintillation spectrometer. After the ^{222}Rn intensity has sufficiently declined, the water samples are counted four times following four hours after each count. ^{14}C results are expressed in percent modern carbon (pMC).

5. Results

5.1. Hydrocensus Maps and Electrical Conductivity Profiles

The hydrocensus results, which yielded preliminary results for this project include electrical conductivity readings, borehole yields, and groundwater level readings for groundwater sampled for the bigger AEON baseline studies. Figure 5-1 to Figure 5-3 show interpolated EC, water level and borehole yield hydrocensus results, respectively. Also, during the hydrocensus phase of the project, vertical locations of transmissive zones (water strikes) were determined using EC to profile each open borehole (Figure 5-4 to Figure 5-17). Note that the EC measurements are reported in mS/m on the EC profiles to align with the depth measurements (m) (1 mS/m = 10 µS/cm). Water strikes are identified as a "spike (sharp decrease/increase)" in EC. Some boreholes had distinct water strikes (e.g KB041= 20 m and 50 m (Figure 5-5); KB084 = 50 m (Figure 5-7); KB419 = 58 (Figure 5-11); KB819 = 31 (Figure 5-14); KB849 = 40 m (Figure 5-15); RC011 = 20 m (Figure 5-16) and RC003 = 20 m (Figure 5-17)). However, the rest of the profiled boreholes had no distinct water strikes. The bottom of the borehole for such boreholes was typically identified as the water strike because borehole drillers in the Karoo usually stop drilling once the water strike is reached. When possible (≤60 m because the groundwater sampling pump reaches a limit at 60 m), groundwater samples for this project were collected at the water strike.

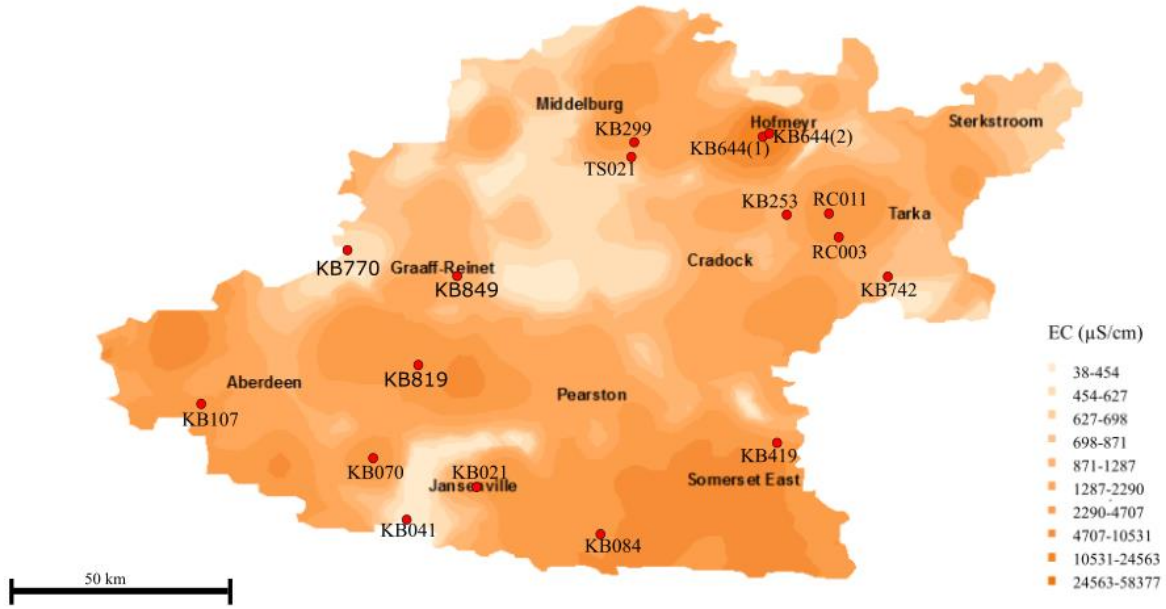

Figure 5-1: Interpolated (using Kriging on ArcGIS) EC (µS/cm) map. Also shown on the map are groundwater sampling locations for this thesis (red labelled circles).

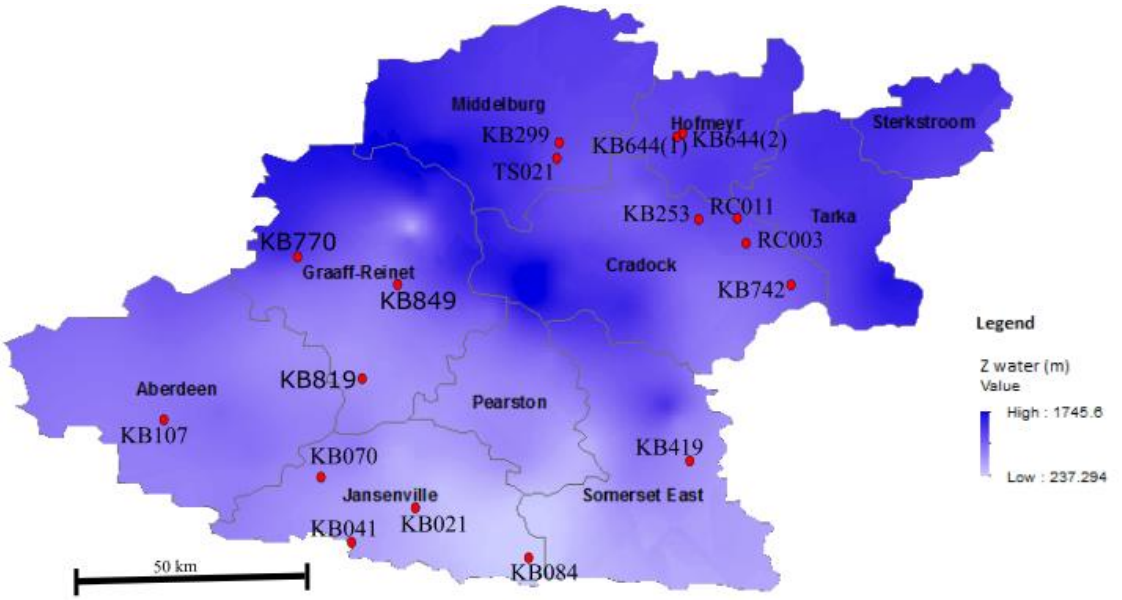

Figure 5-2: Interpolated (using Kriging on ArcGIS) Water Level (masl) Map. Also shown on the map are groundwater sampling locations for this thesis (red labelled circles).

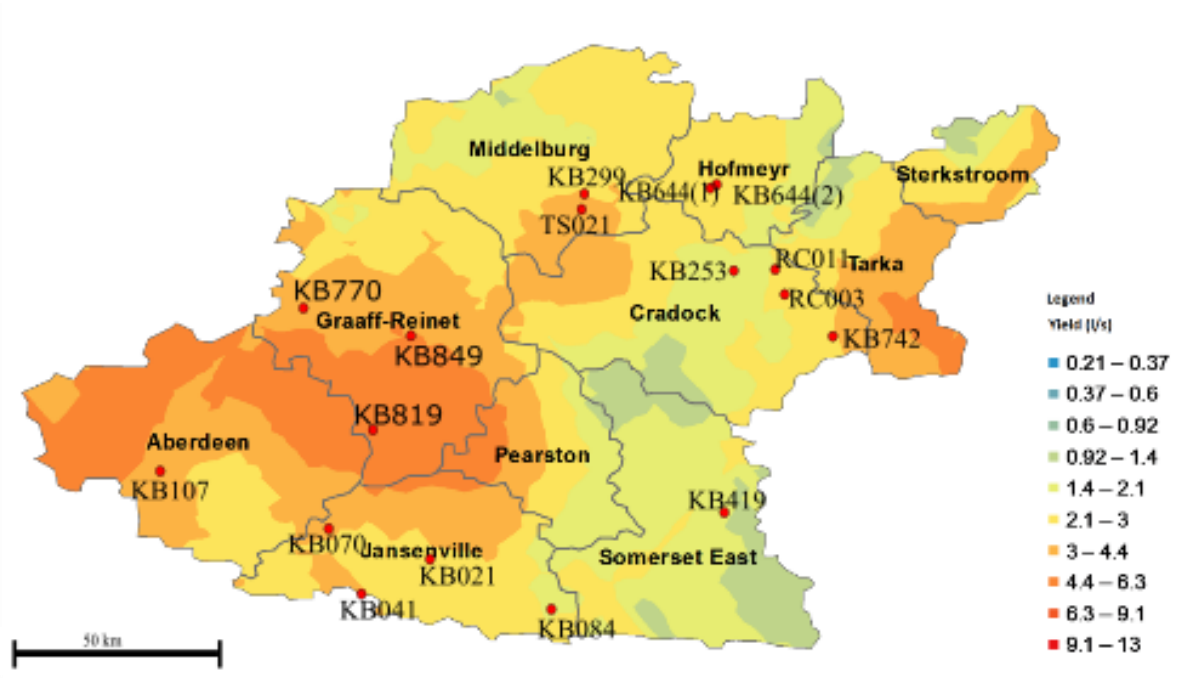

Figure 5-3: Interpolated (using Kriging on ArcGIS) yield (l/s). Also shown on the map are groundwater sampling locations for this thesis (red labelled circles).

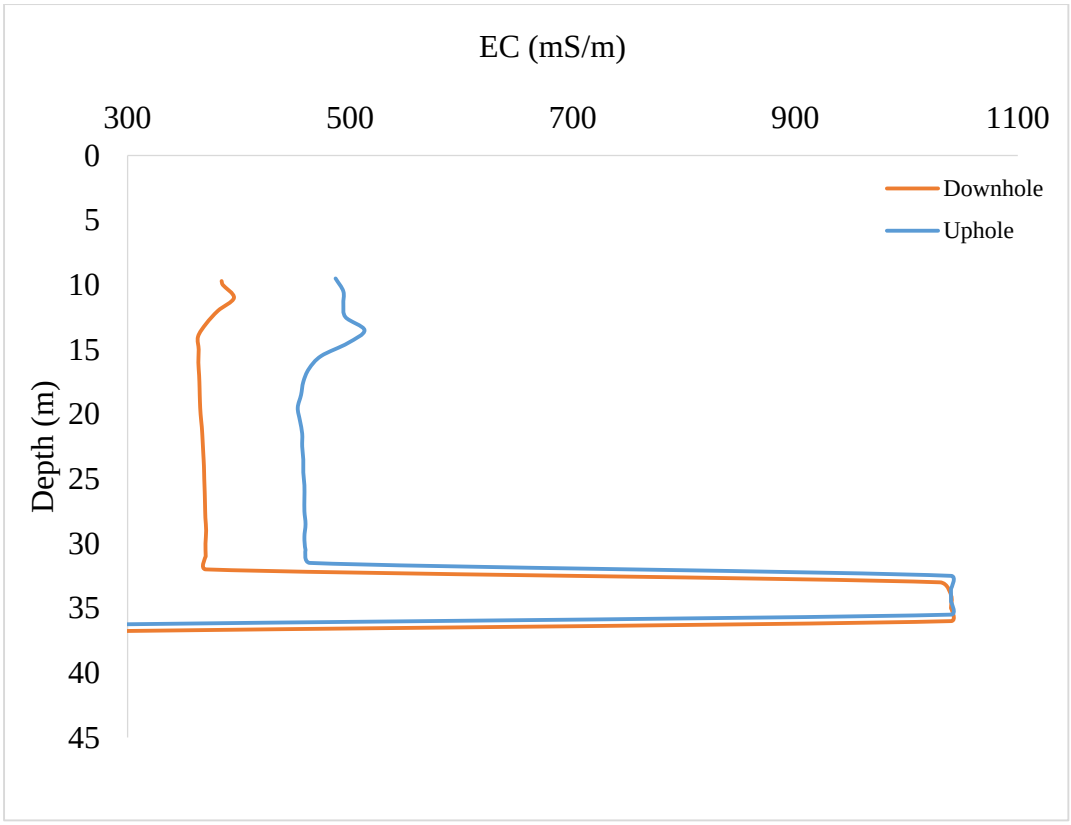

Figure 5-4: EC profile for KB021.

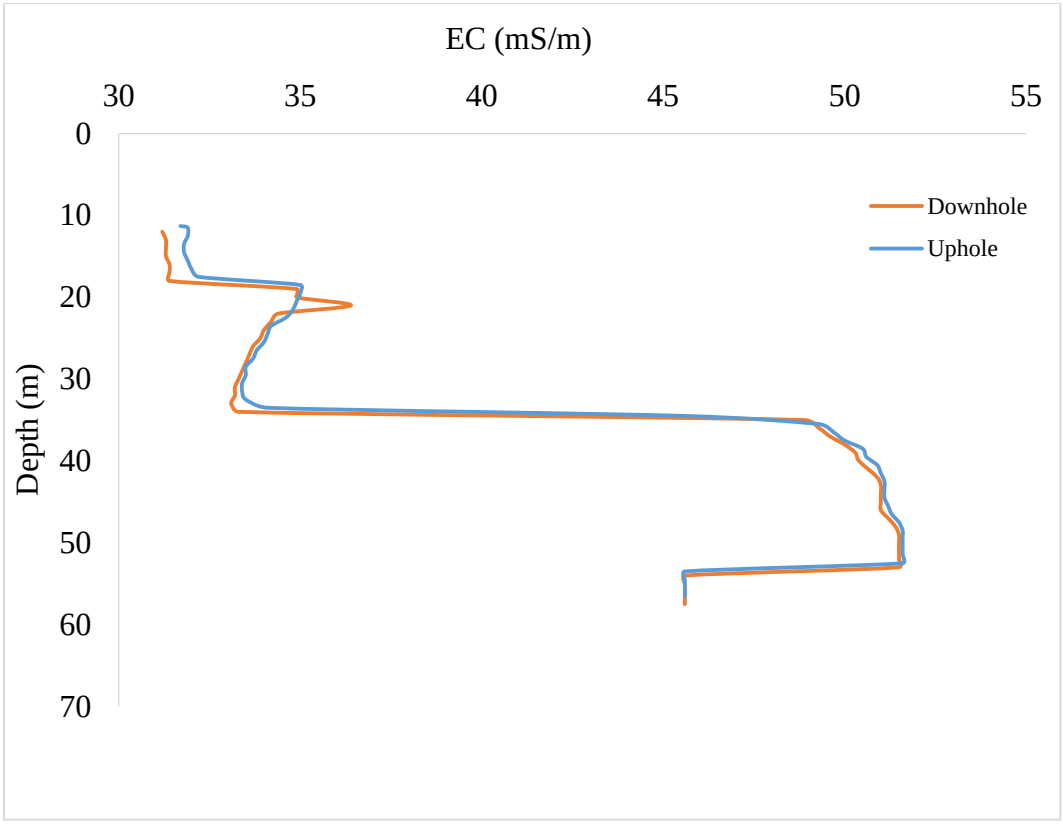

Figure 5-5: EC profile for KB041.

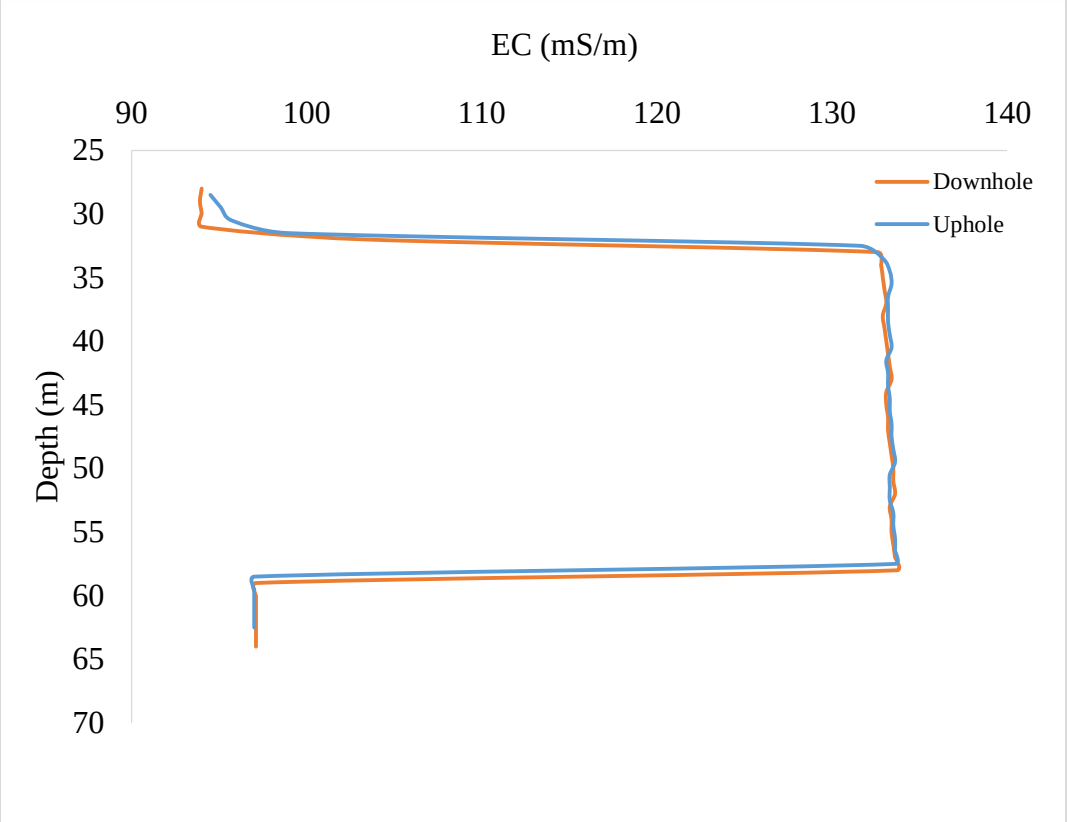

Figure 5-6: EC profile for KB070.

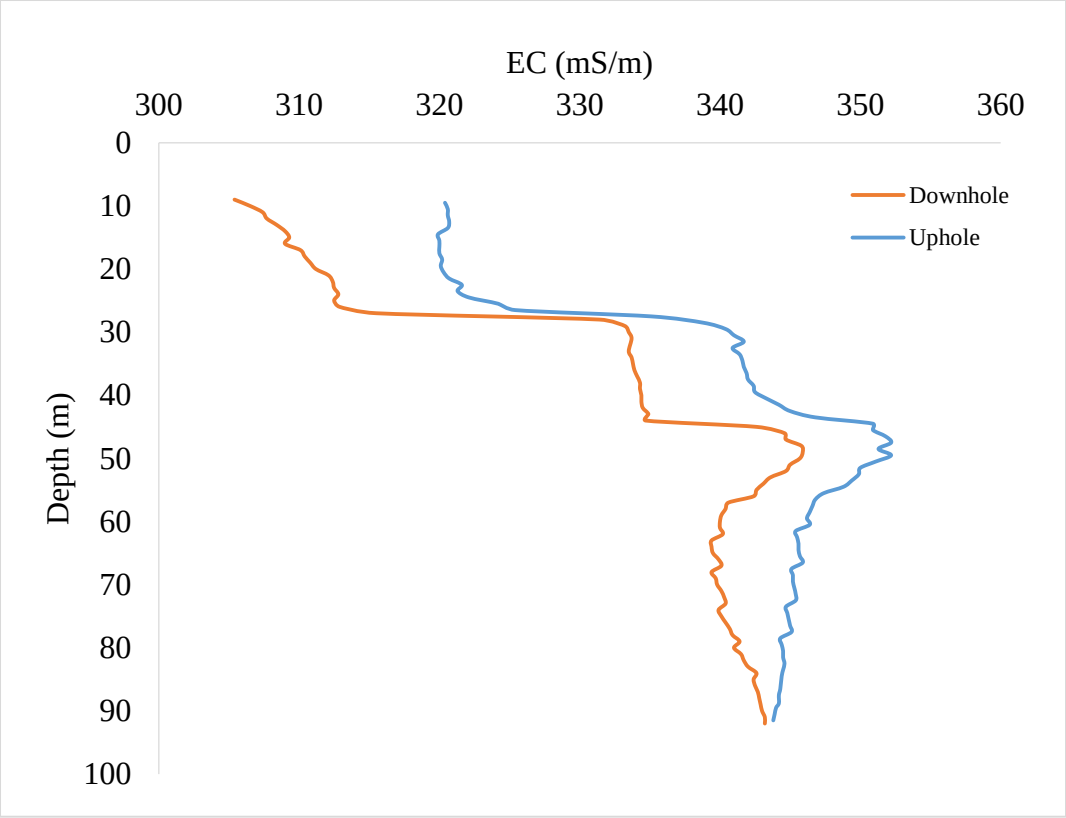

Figure 5-7: EC profile for KB084.

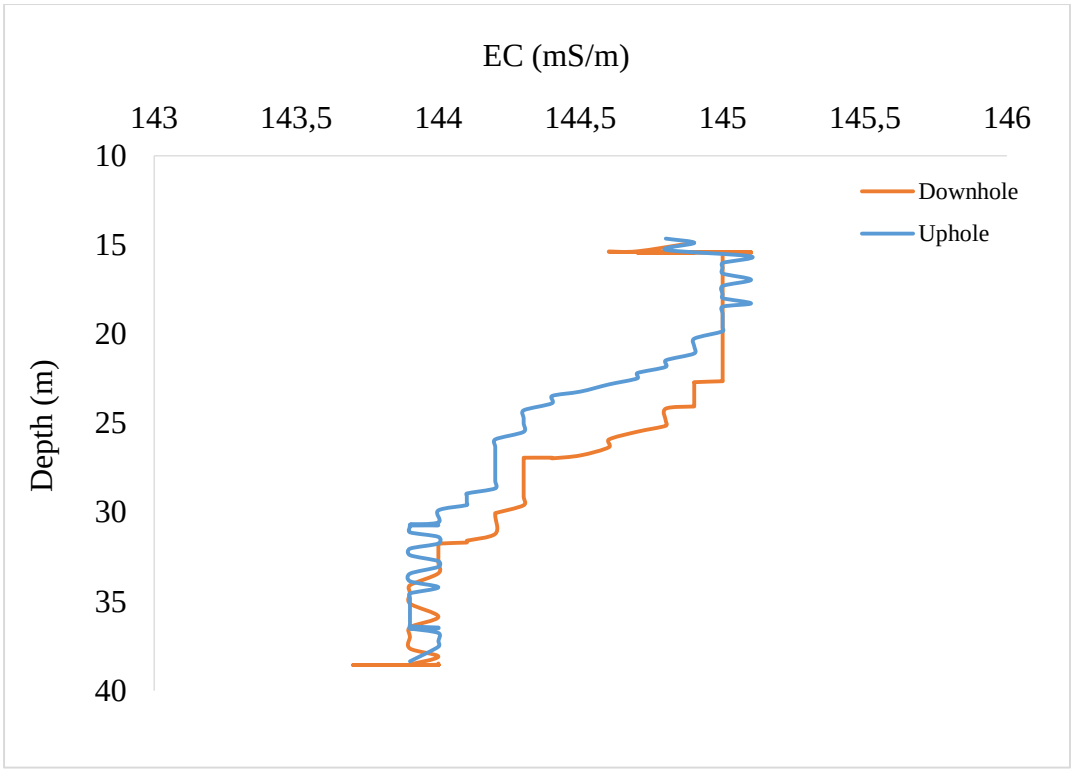

Figure 5-8: EC profile for KB107.

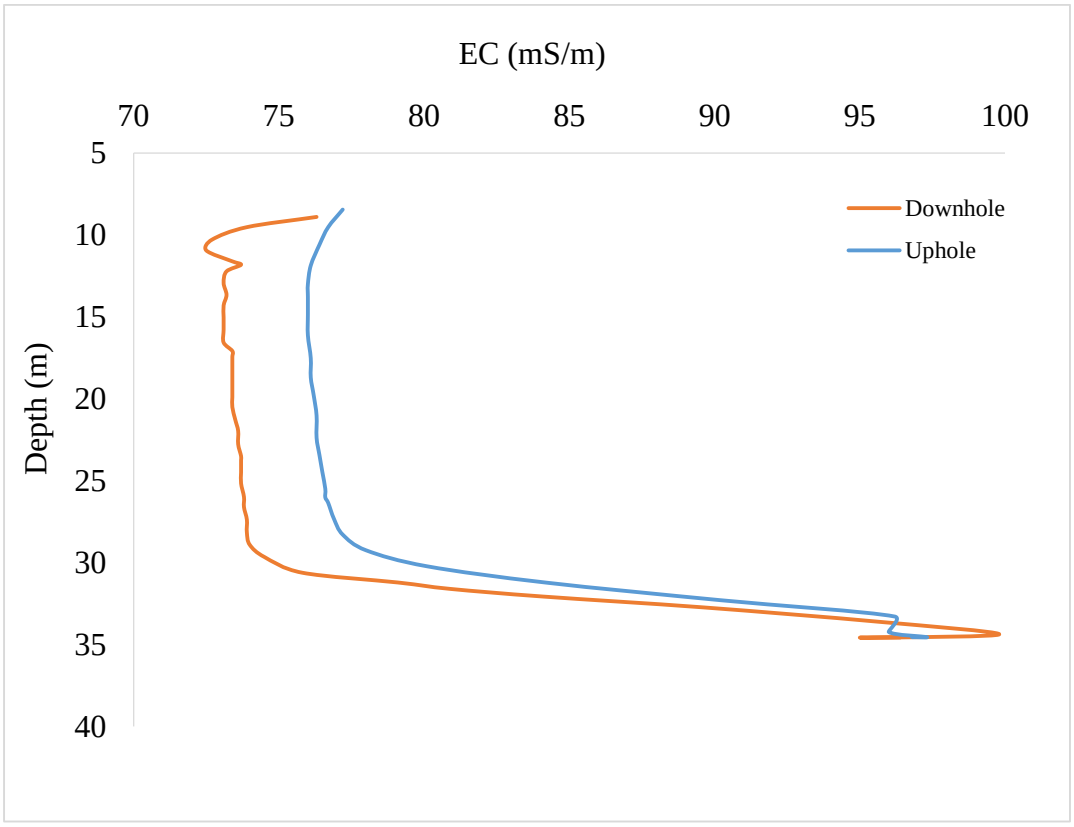

Figure 5-9: EC profile for KB253.

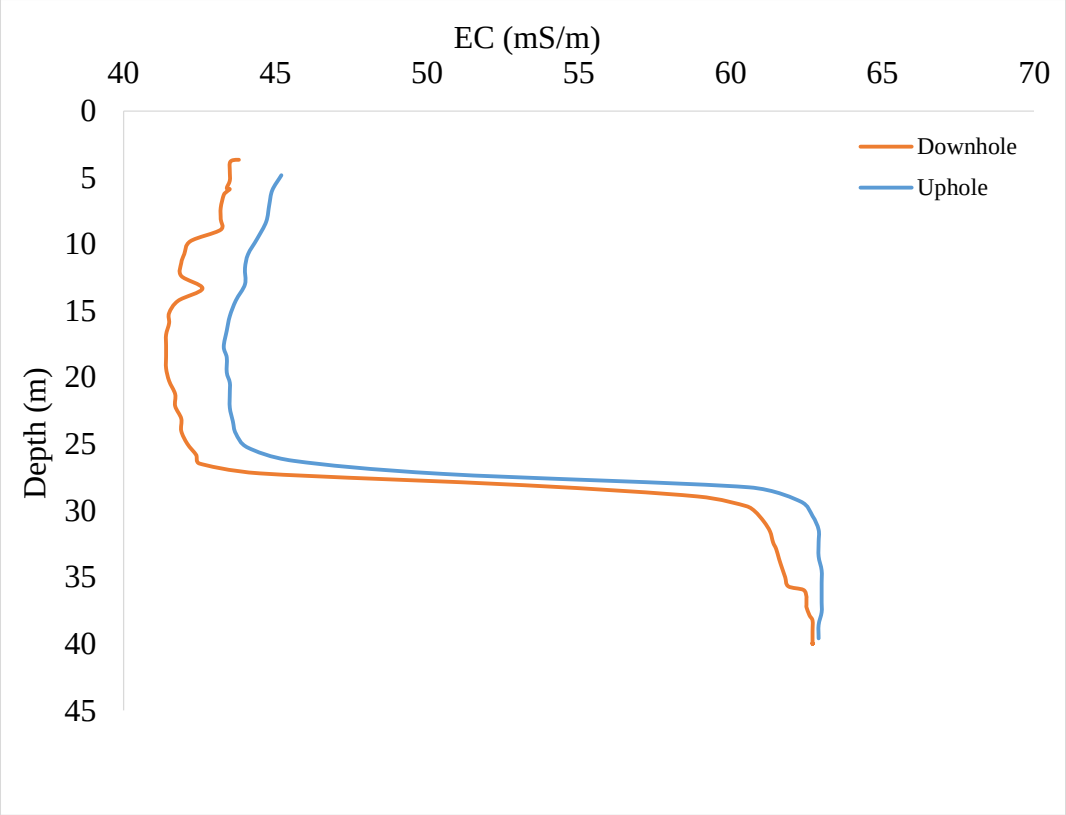

Figure 5-10: EC profile for KB299.

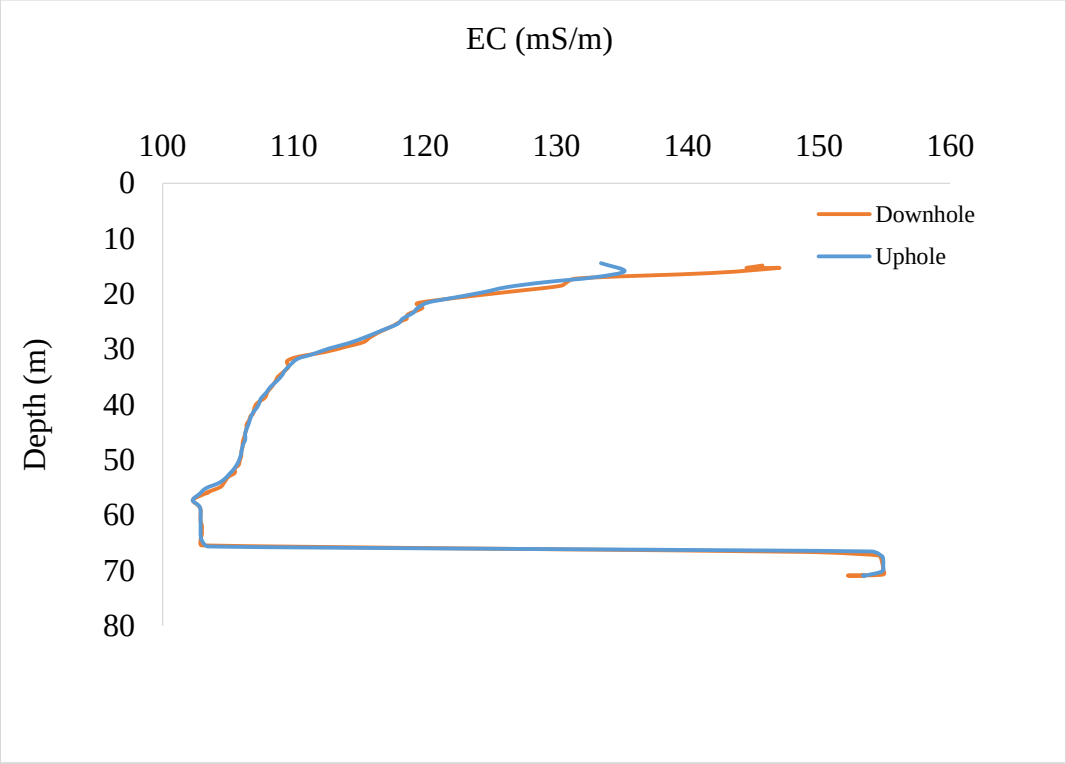

Figure 5-11: EC profile for KB419.

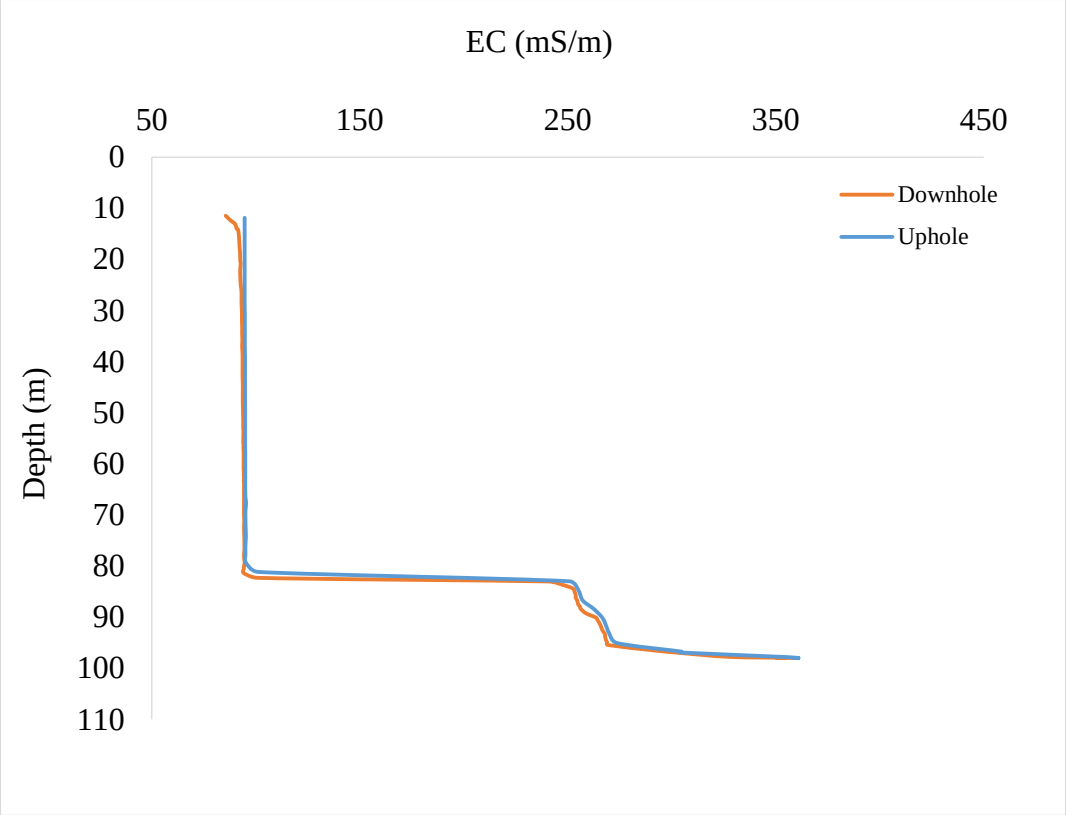

Figure 5-12: EC profile for KB644.

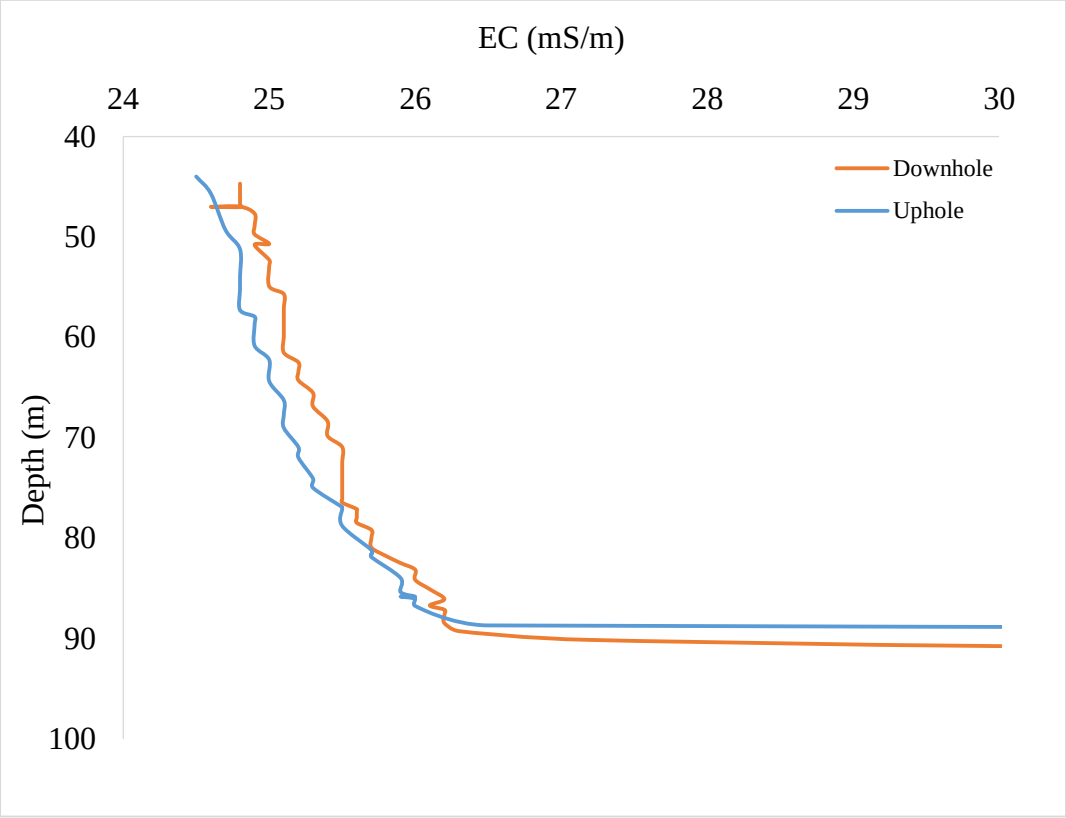

Figure 5-13: EC profile for KB770.

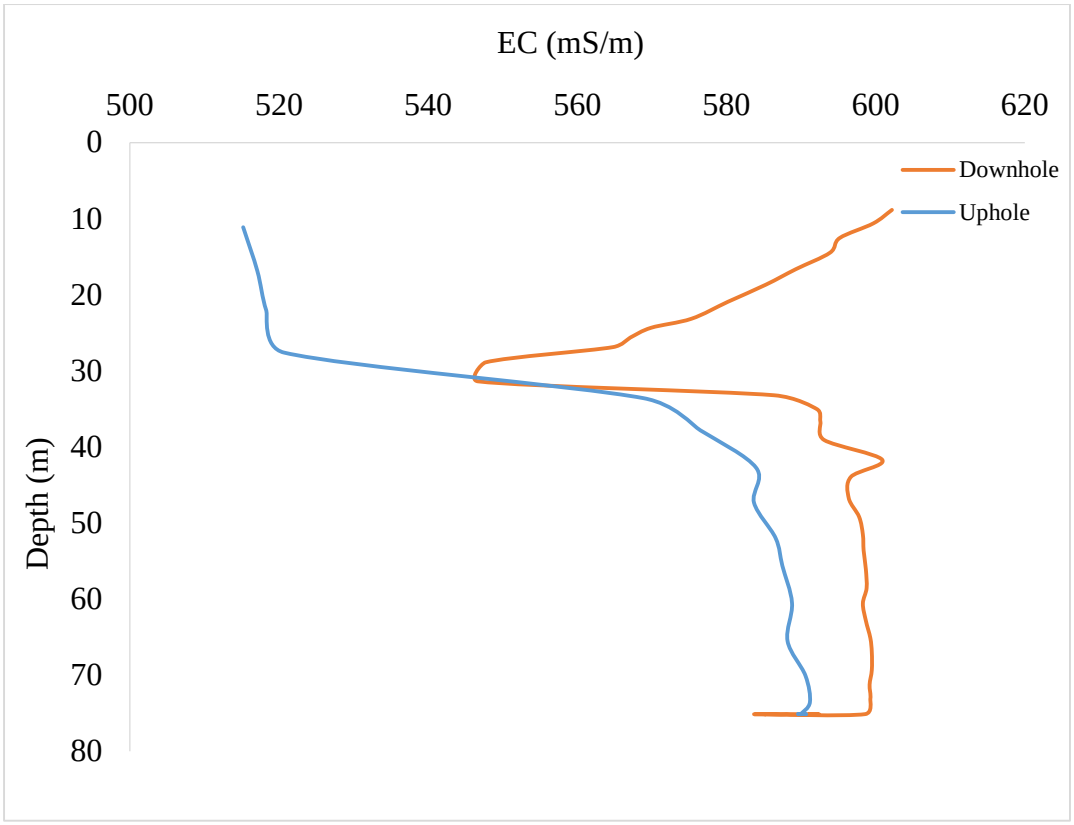

Figure 5-14: EC profile for KB819.

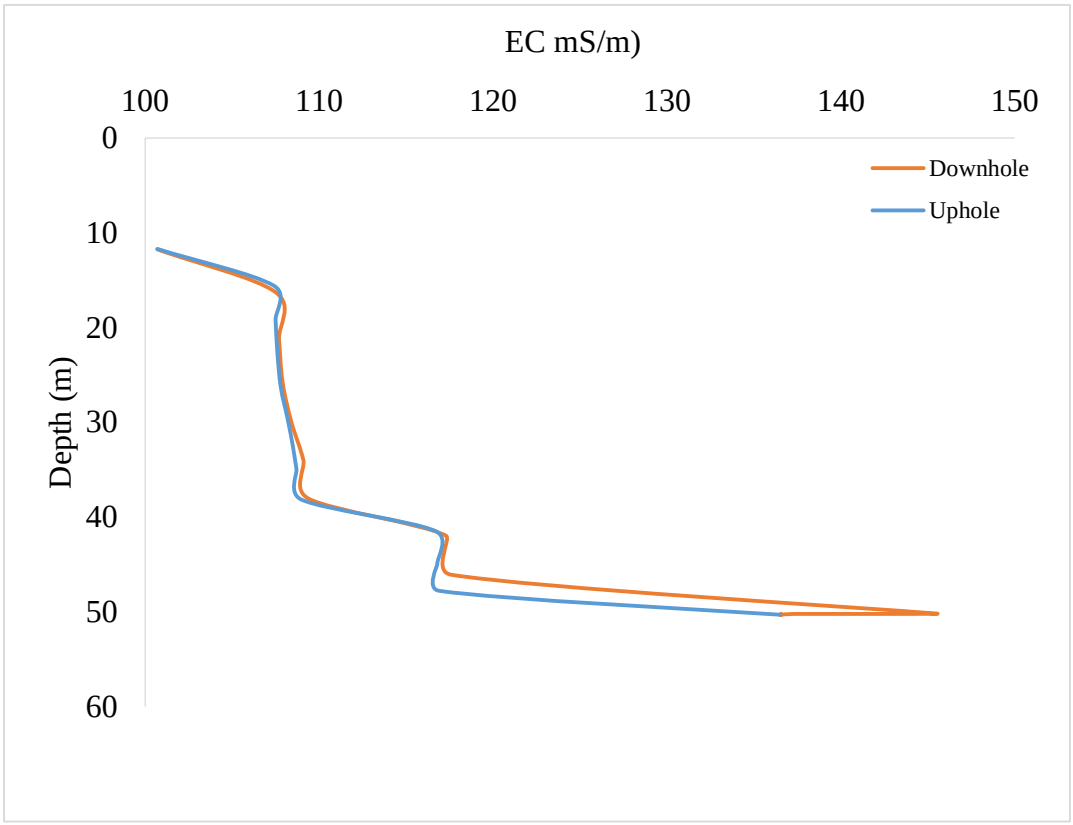

Figure 5-15: EC profile for KB849.

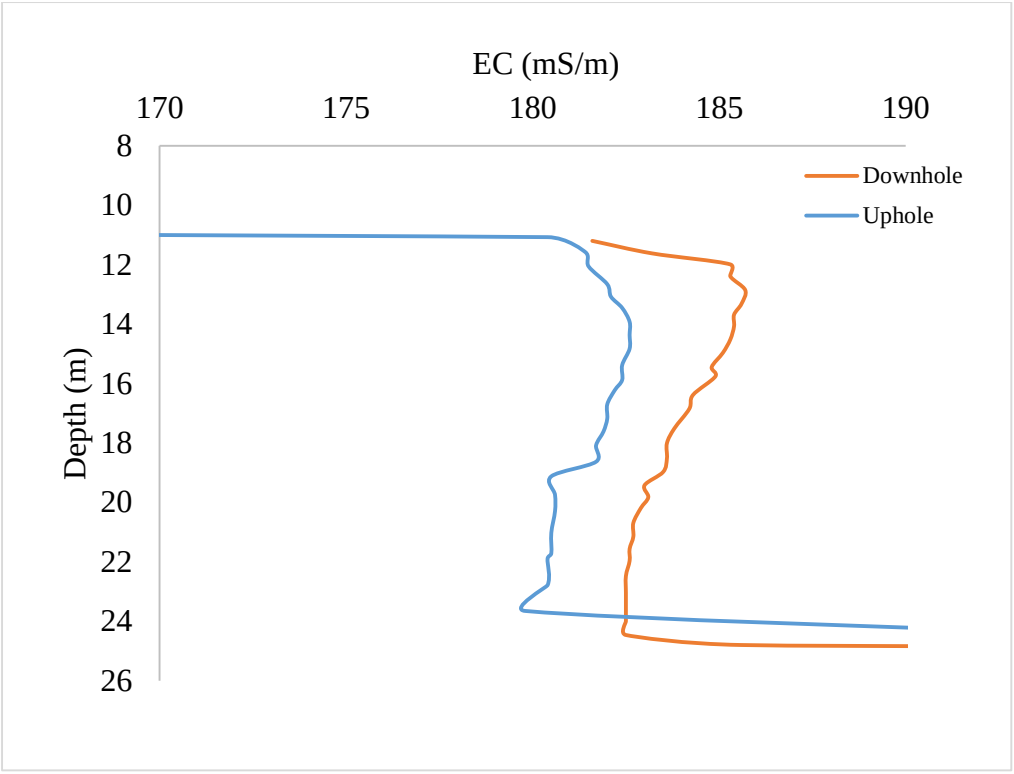

Figure 5-16: EC profile for RC011.

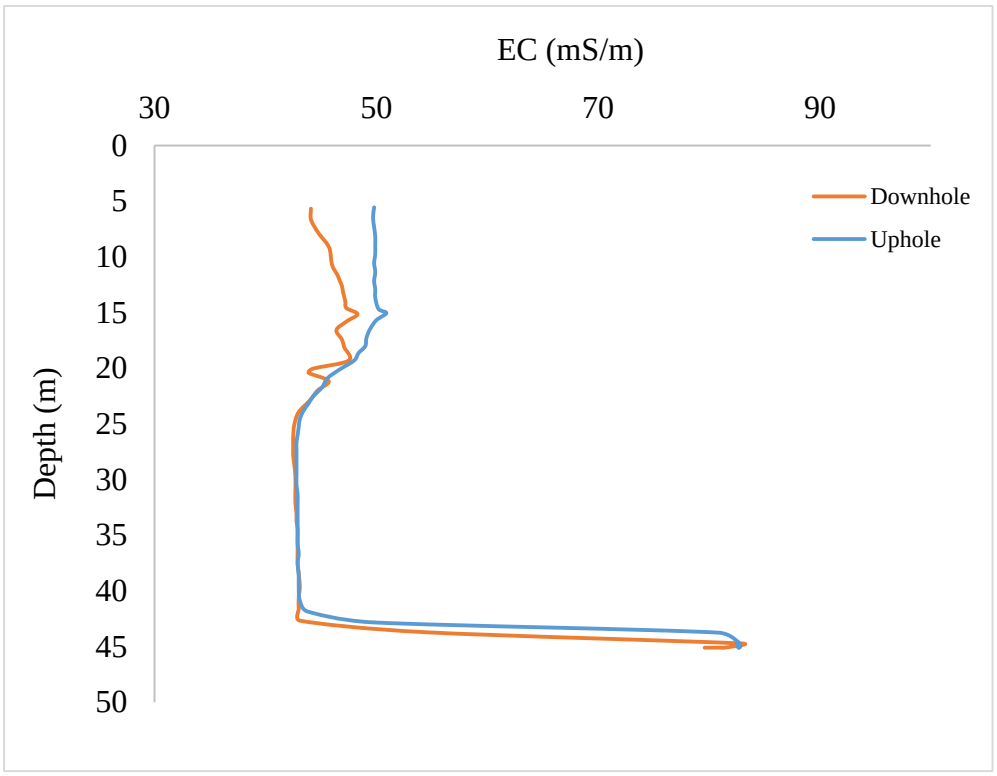

Figure 5-17: EC profile for RC003.

5.2. Laboratory and Field Results

The laboratory results include isotope ($\delta^{18}O$, $\delta^{2}H$, ^{3}H, $\delta^{13}C$ and ^{14}C) and alkalinity results from iThemba Laboratories and Innoventon Laboratory, respectively. Table 5-1 lists the general field parameters; these include results from the hydrocensus, water level measurements acquired during groundwater sampling and alkalinity results from Innoventon Laboratory. The uniformity (or lack thereof) of each data set was measured using the range, variance (σ^2) (Equation 5-1) and standard deviation[10]. Range is the difference between the highest and lowest number in a data-set. Variance is a measurement of the average degree to which each point differs from the mean in a data-set. Because the variance is squared it is not in the same unit of measurement as the original data-set. Therefore the standard deviation (σ) is calculated (Wright & London 2009 p.24-27). The standard deviation is the square-root of the variance.

$$\sigma^2 = \frac{\sum(X - \mu)^2}{N} \qquad \text{Equation 5-1}$$

Where:

X is the value of the ith element of the sample

μ is the value of the mean of the data-set

N is the sample size

[10] https://www.investopedia.com/ask/answers/021215/what-difference-between-standard-deviation-and-variance.asp and https://people.richland.edu/james/ictcm/2001/descriptive/helpvariance.html

Table 5-1 General Field Parameter Results

Sample Identification	Elevation m	Borehole Depth m	Water Level m	Sampling Depth mbgl	Temperature °C	EC µS/cm	pH	Sustainable Yield l/s	Total Alkalinity $mg.L^{-1}$	CO_3 Alkalinity $mg.L^{-1}$	HCO_3 Alkalinity $mg.L^{-1}$	Phenolpthalein Alkalinity $mg.L^{-1}$
KB021	457	39.5	8.5	35	19.9	3661	7.6	4.93	164.56	20.64	59.33	21.51
KB041	589	57.6	11.3	35	22.9	3983	7.23	0.2	225.8	13.46	96.52	14.03
KB070	763	64.6	27.5	45	19.3	1519	7.59	0.74	155.74			
KB084	318	91.6	8.77	50	22.5	3668	7.49	0.35	253.39	25.58	97.66	26.65
KB107	834	38.55		27	23.7	1307	7.75	1.49	437.1	22.2	192.49	22.94
KB253	1130	36.53	8.3	30	19.6	850	7.67	0.09	421.69	34.11	171.13	35.53
KB299	1145	41.84	3.62	27.5	18.3	414	8.08	0.84				
KB419	769	70.94	21.23	58	20	681	7.64	0.15	514.6	47.4	204.99	48.98
KB644(1)	1192	96.49	9.33	60	18.8	9169	7.29	0.2	439.58	76.2	138.8	78.74
KB644(2)	1192		10.44	60	19.5	7735	7.27					
KB742	960	41.06	7.86	33	21	1055	7.45	0.27	427.76	37.25	170.9	38.8
KB770	1404	102	6.45	60	22.8	674	7.85	0.05				
KB819	615	74.1	9.69	31	22.6	6183	7.27	1.49	333.8	22.03	134.42	23.84
KB849	817	48.59	10.63	40	24.3	1098	7.75	2.08	406.26	18.14	172.41	19.64
RC003	1094	45.09	5.27	20	19	715	7.87	1.49				
RC011	1240	24.84	10.7	20	19.2	2947	7.54	0.11				
TS021	1182	29.55	8.38	22	21	467	7.29	0.19				
Minimum	318	24.84	3.62	20	18.30	414	7.23	0.05	155.74	13.46	59.33	14.03
Maximum	1404	102,00	27.50	60	24.30	9169	8.08	4.93	514.60	76.20	204.99	78.74
Range	1086	77.16	23.88	40	6,0	8755	0.85	4.88	358.86	62.74	145.66	64.71
Mean	924	56.43	10.50	38.44	20.85	2713	7.75	0.92	343.66	31.70	143.66	33.07
Variance	89674	554.45	32.58	196.92	3.42	6897565	0.06	1.47	13978.18	312.35	2002.72	328.33
Standard Deviation	299	23.55	5.71	14.01	1.85	2626	0.24	1.21	118.23	17.67	44.75	18.12

Figure 5-18 is a stacked column bar graph that shows borehole depth, water level (mbgl) and sampling depth/water strikes for the sampled boreholes. Borehole depth varies between 24.84 and 102 mbgl (range = 77.16). The average borehole depth is 56.43 mbgl and the variance is 709.15. The standard deviation for the borehole depth dara-set is 26.63 mbgl (Table 5-1). The range and mean for the water level data-set is 23.88 mbgl and 10.50 mbgl respectively. The variance is 32.58 and the standard deviation is 5.71.

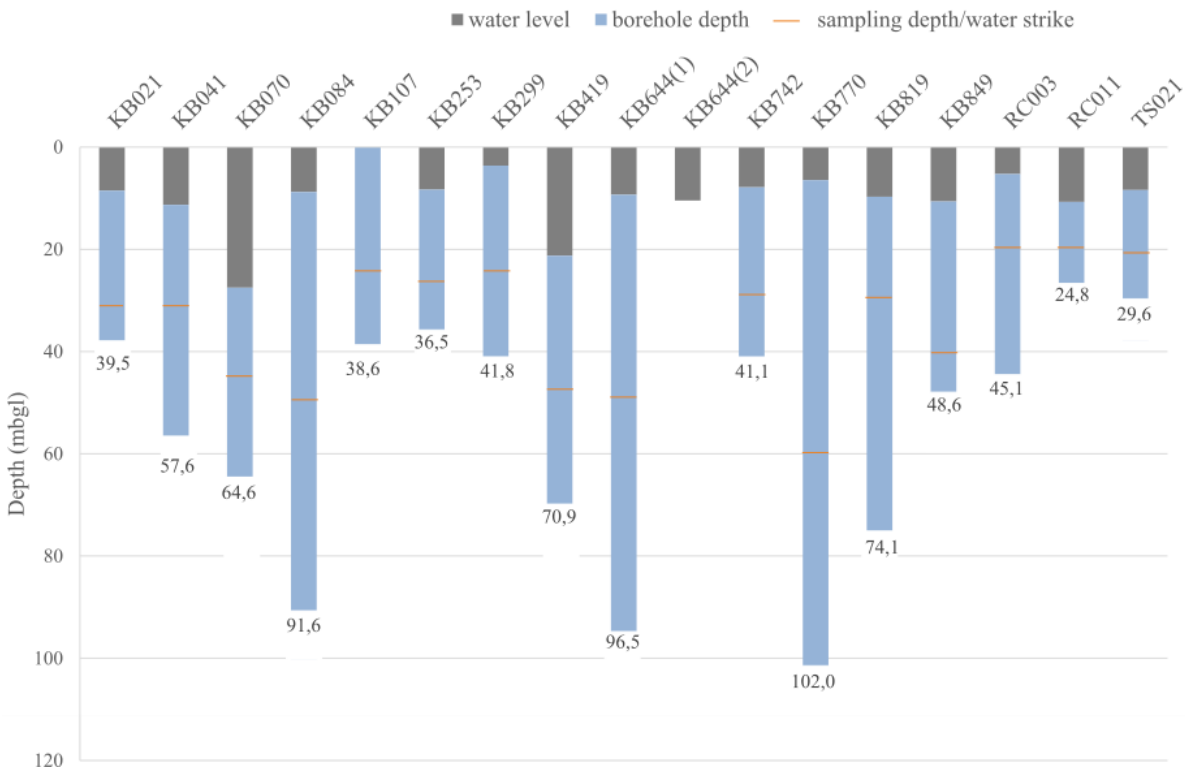

Figure 5-18: Water level, borehole depth (mbgl) and sampling depth/water strike bar graph for the sampled groundwater. Note that borehole KB107 had a pump at the time of groundwater sampling therefore the water level could not be measured. The groundwater for KB107 was collected from a tap that connects to the borehole and the borehole depth and water strike data was provided by the farm owner. Borehole KB644(2) had an obstruction and only the water level (mbgl) was measured.

In situ temperatures range from 18.3°C to 24.3°C with a range of 6°C. The average/mean temperature is 20.8°C. The temperature data-set is relatively uniform (Figure 5-19) and has the

third smallest variance (3.42) and standard deviation (1.85°C). The EC (µS/cm) data (Figure 5-20) is significantly variable compared to the temperature data (Figure 5-19) and ranges from 414 µS/cm to 9169 µS/cm. The average EC (µS/cm) is 2713.29 µS/cm. The variance of the data-set is 68 975 64.68 and the standard deviation is 2 626.32 µS/cm. The pH data-set is the most uniform data-set (Figure 5-21) with a variance of 0.06 and a standard deviation of 0.24. The average pH is 7.56. The lowest pH is 7.23. The highest pH is 8.08 (Table 5-1). The sustainable yields data-set is the second most uniform data-set with a variance of 1.47 and a standard deviation of 1.21 l/s. This data-set varies between 0.05 l/s and 4.93 l/s (Figure 5-22) and the average sustainable yield is 0.92 l/s. KB021 has the highest measured sustainable yield (4.93 l/s).

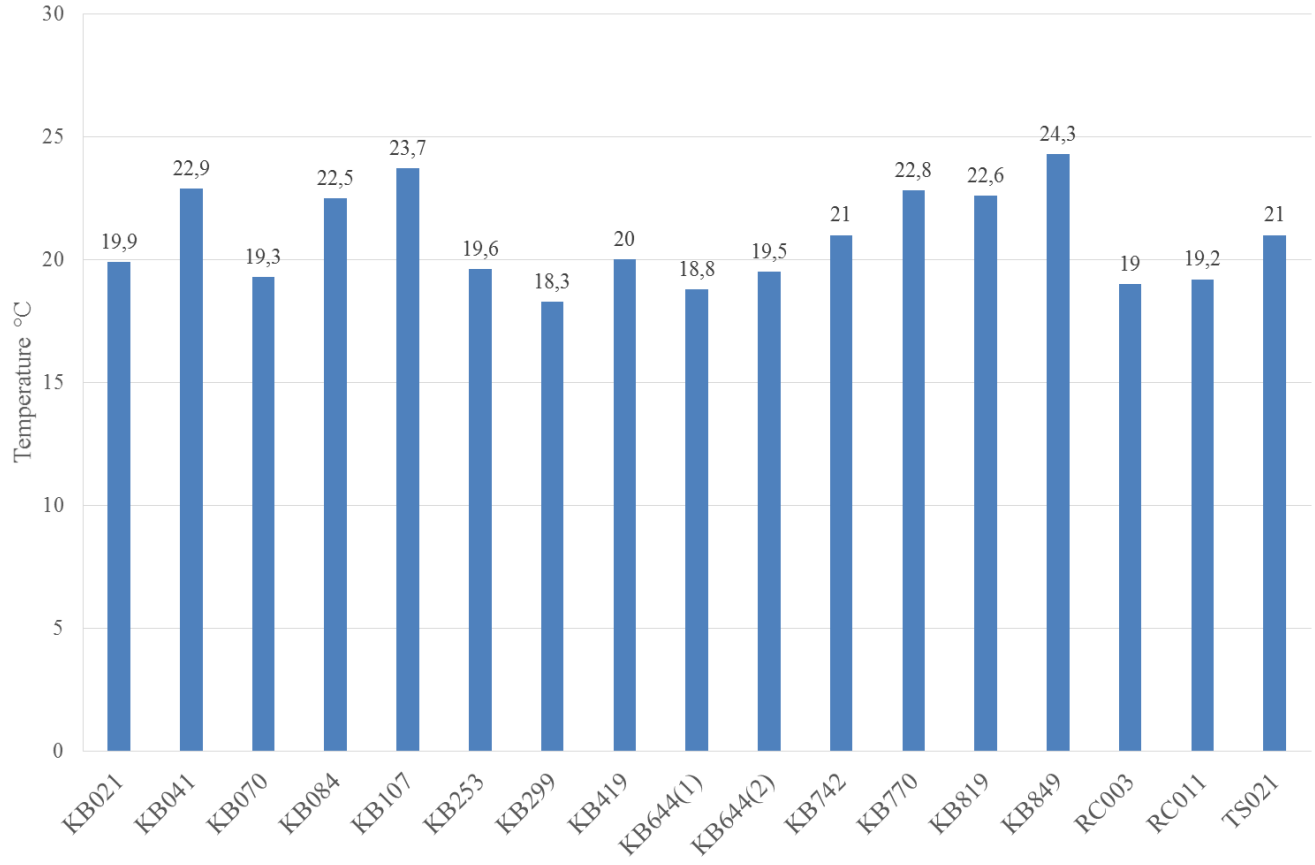

Figure 5-19: Temperature (°C) bar graph.

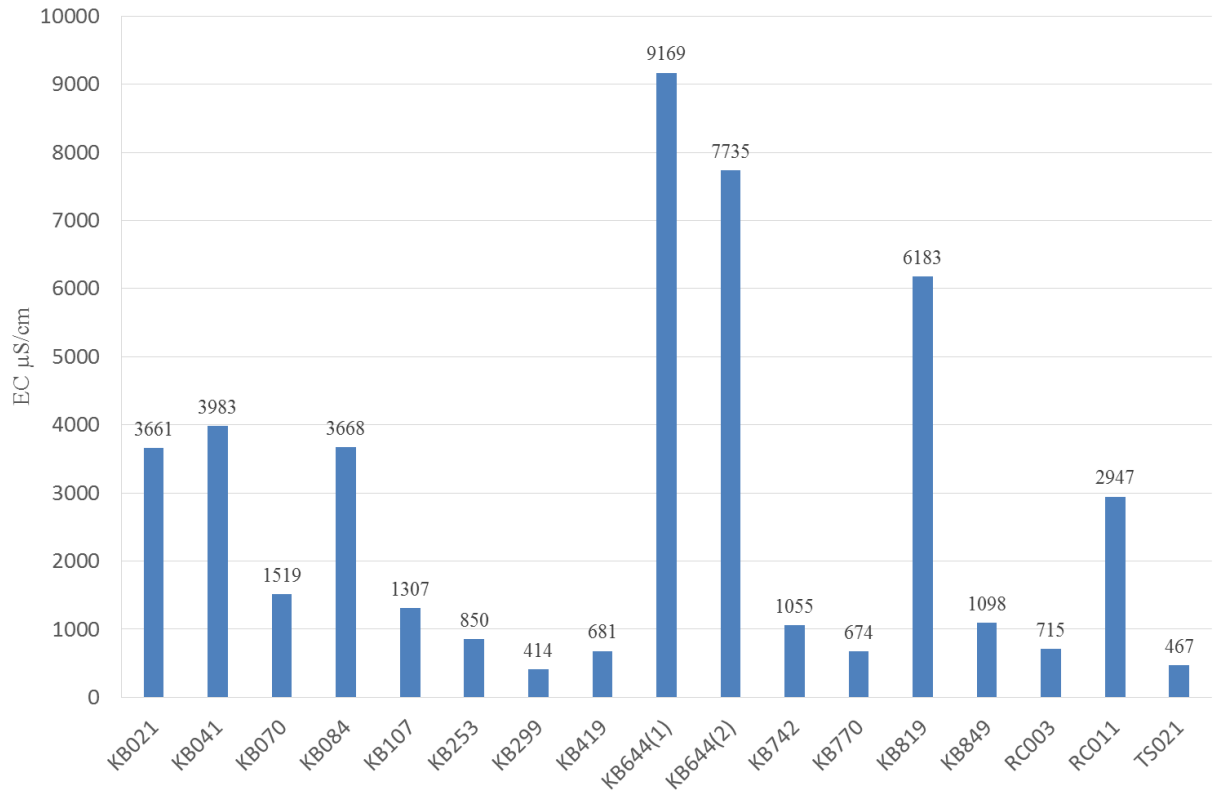

Figure 5-20: EC (µS/cm) bar graph.

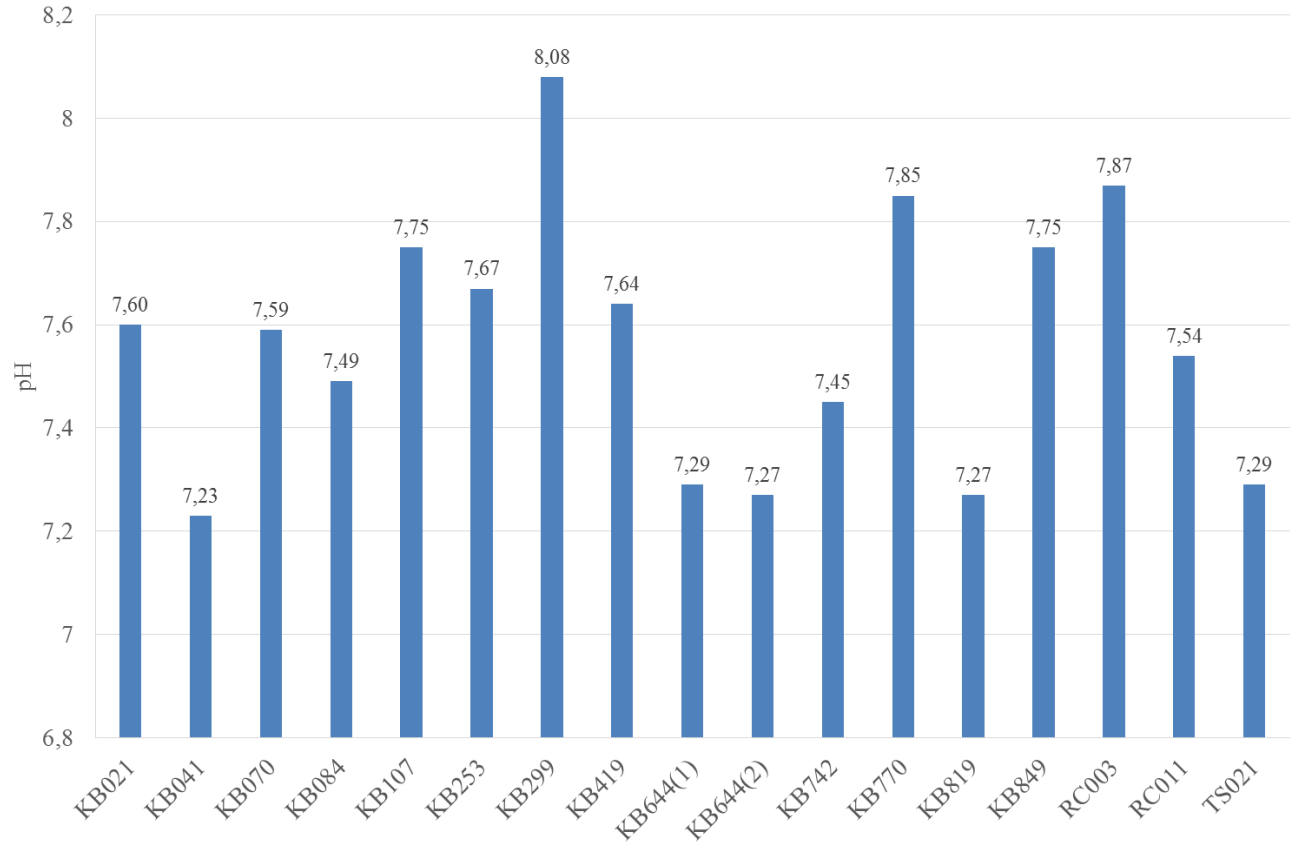

Figure 5-21: pH bar graph for the sampled groundwater.

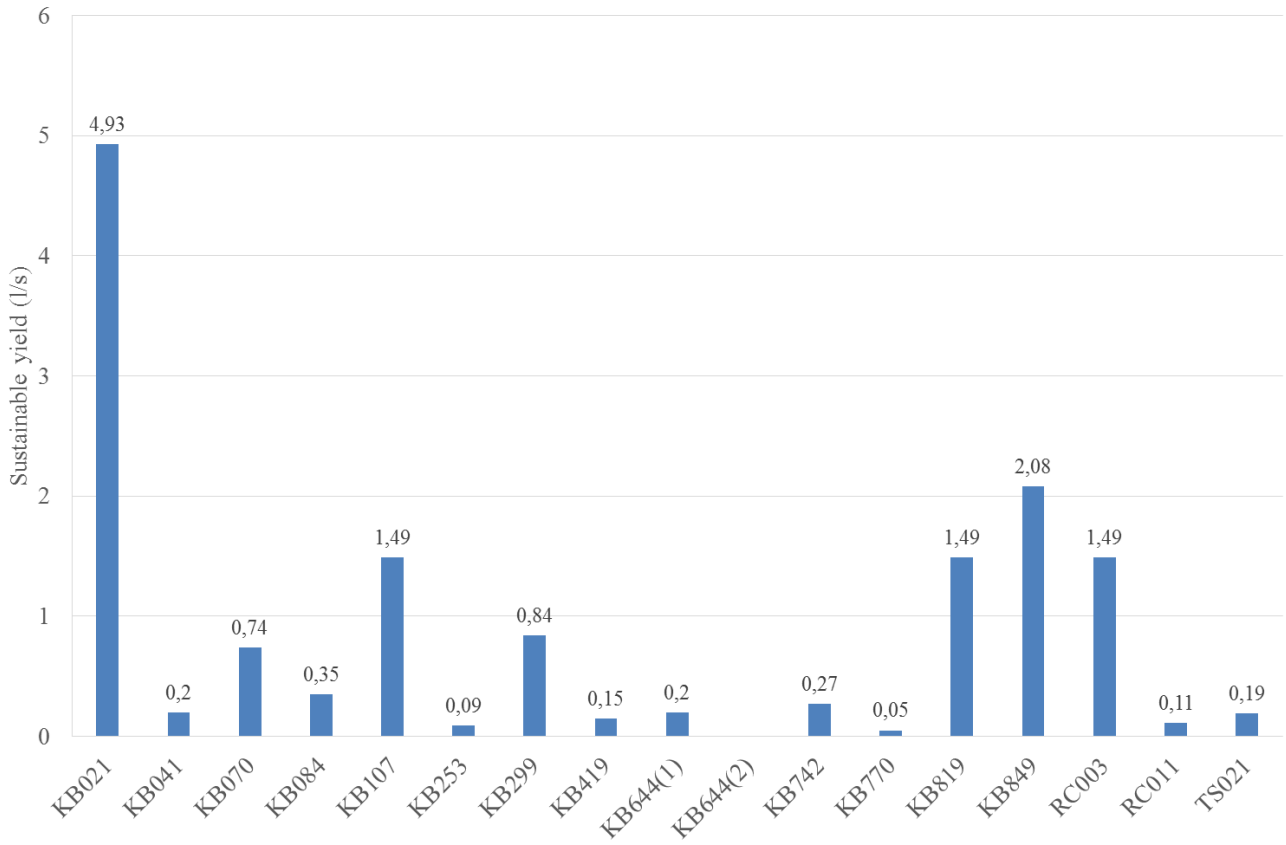

Figure 5-22: Sustainable yield bar graph for the sampled groundwater. Note that due to an obstruction on borehole KB644(2) the sustainable yield could not be measured on this borehole.

Of the 17 sampled boreholes 11 groundwater samples were tested for alkalinity. The total alkalinity (mg.L^{-1}) of these groundwater samples ranges from 155.74 to 514.60 mg.L^{-1} with an average of 343.66 mg.L^{-1} (Figure 5-23). The variance of the total alkalinity is 13 978.18 and the standard deviation is 118.23 mg.L^{-1}. The CO_3 alkalinity (mg.L^{-1}) of these groundwater samples ranges from 13.46 mg.L^{-1} to 76.20 mg.L^{-1} with an average of 31.70 mg.L^{-1}. The variance for the CO_3 alkalinity data-set is 312.35 and the standard deviation is 17.67 mg.L^{-1}. The HCO_3 alkanity (mg.L^{-1}) varies between 59.33 mg.L^{-1} and 204.99 mg.L^{-1}. The average HCO_3 alkalinity is 143.87 mg.L^{-1}. The variance for this data-set is 2002.72 and the standard deviation is 44.75. The lowest phenolphthalein alkalinity is 14.03 mg.L^{-1}. The highest phenolphthalein alkalinity is 78.74 mg.L^{-1} and the average phenolphthalein alkalinity is 33.07 mg.L^{-1} (Figure 5-24). The variance for the data-set is 328.33 and the standard deviation is 18.12 mg.L^{-1}.

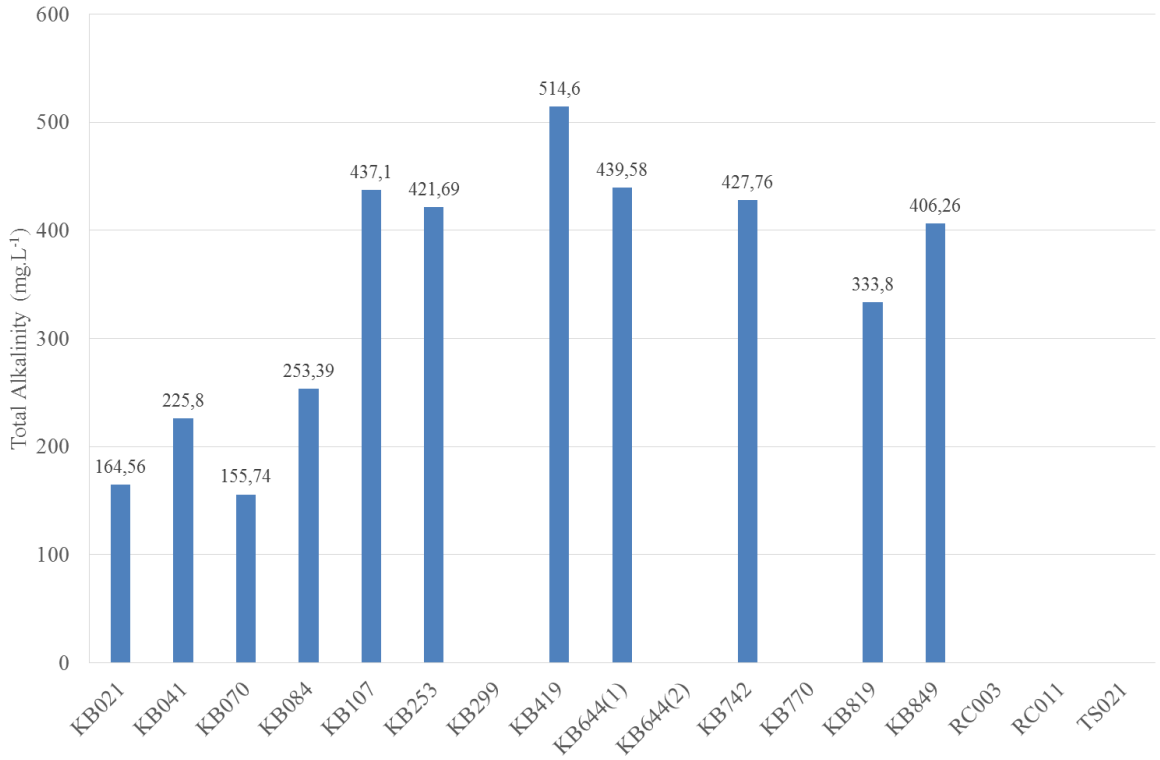

Figure 5-23: Total alkalinity bar graph.

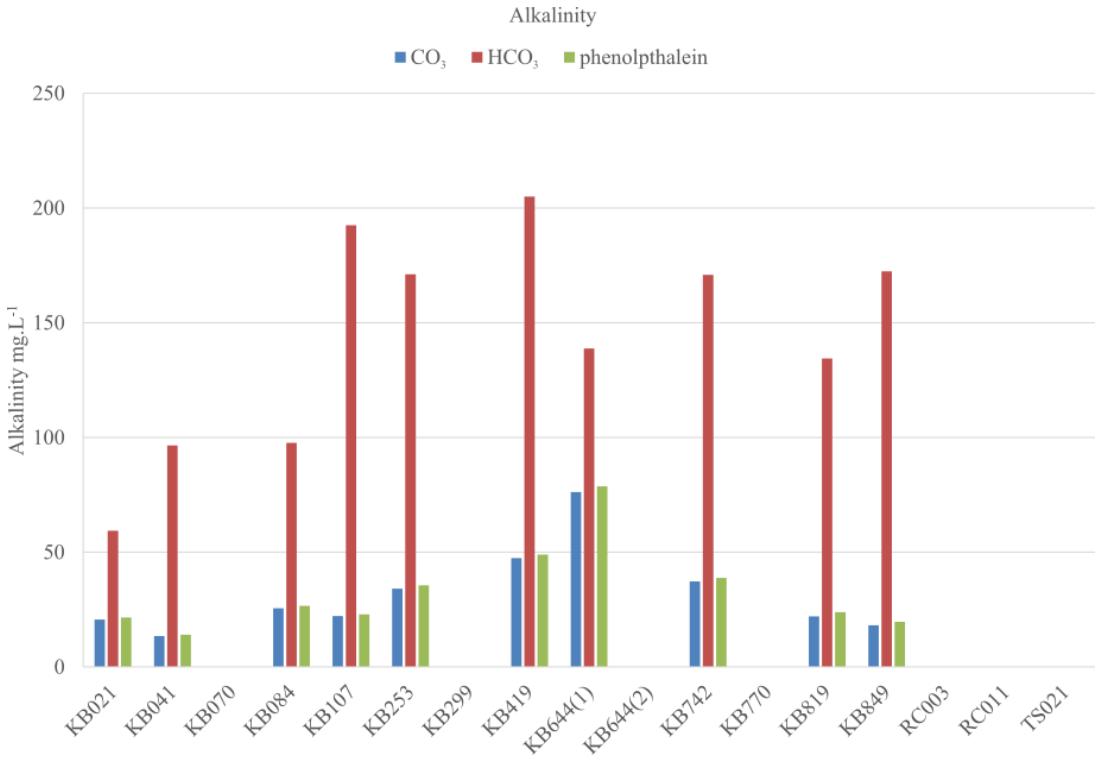

Figure 5-24: Alkalinity bar graph. Note that groundwater samples: KB070, KB299, KB644(2), KB770, RC003, RC011 and TS021 were not analysed for alkalinity.

5.3. Isotope Results

Groundwater isotope results are listed on Table 5-2. Figure 5-25 is a plot of δ^2H vs. $\delta^{18}O$ for the sampled groundwater and global meteoric waters. The linear correlation between δ^2H and $\delta^{18}O$ for the sampled groundwater is strong ($R^2 = 0.66$). The linear correlation between δ^2H and $\delta^{18}O$ for global meteoric waters is significantly stronger ($R^2 = 1$). The minimum and maximum for the δ^2H (‰) data-set is -26.6 ‰ and -9.9 ‰, respectively (Figure 5-25). The range for this data-set is 16.6 ‰ and the mean is -20.3 ‰. The variance for the data-set is 19.6 and the standard deviation is 4.4 ‰ (Table 5-2). The range for the $\delta^{18}O$ (‰) data-set is 3.2 ‰. The mean is -3.0 ‰. The variance for the data-set is 0.4 and the standard deviation is 0.75 ‰ (Table 5-2).

Table 5-2 Isotope Results

Sample Identification	δ^2H (‰)	$\delta^{18}O$ (‰)	Tritium (T.U.)	±	Carbon-14 (pMC)	±	$\delta^{13}C$ (‰)
KB021	-21.6	-3.1	0.10	0.20	50.20	1.70	-14.65
KB041	-16.7	-2.1	1.00	0.30	77.40	1.90	-10.64
KB070	-24.0	-3.4	0.40	0.20	59.20	1.80	-13.14
KB084	-22.4	-3.5	0.30	0.20	74.70	1.90	-11.40
KB107	-24.4	-3.1	0.10	0.20	73.50	2.00	-12.54
KB253	-13.8	-2.5	2.70	0.40	95.70	2.10	-10.32
KB299	-26.6	-3.7	2.00	0.30	80.80	2.00	-10.04
KB419	-17.1	-3.2	0.90	0.20	78.80	2.00	-13.71
KB644(1)	-23.3	-2.9	0.80	0.20	96.60	2.10	-14.82
KB644(2)	-24.4	-3.2	0.50	0.20	100.30	2.10	-13.20
KB742	-20.6	-2.8	0.30	0.20	87.60	2.10	-13.81
KB770	-20.8	-3.1	1.10	0.30	83.40	2.00	-15.95
KB819	-9.9	-1.2	1.70	0.30	94.90	2.10	-13.43
KB849	-23.3	-3.5	1.20	0.30	92.40	2.10	-13.04
RC003	-16.7	-3.0	2.30	0.40	92.00	2.10	-14.05
RC011	-15.9	-2.7	1.50	0.30	107.60	2.20	-11.28
TS021	-24.5	-4.4	0.90	0.20	87.50	2.10	-15.61
Minimum	-26.6	-4.4	0.10		50.20		-15.95
Maximum	-9.9	-1.2	2.70		107.60		-10.04
Range	16.6	3.2	2.60		57.40		5.90
Mean	-20.3	-3.0	1.0		84.27		-13.04
Variance	19.6	0.4	0.56		201.83		3.01
Standard deviation	4.4	0.7	0.75		14.21		1.74

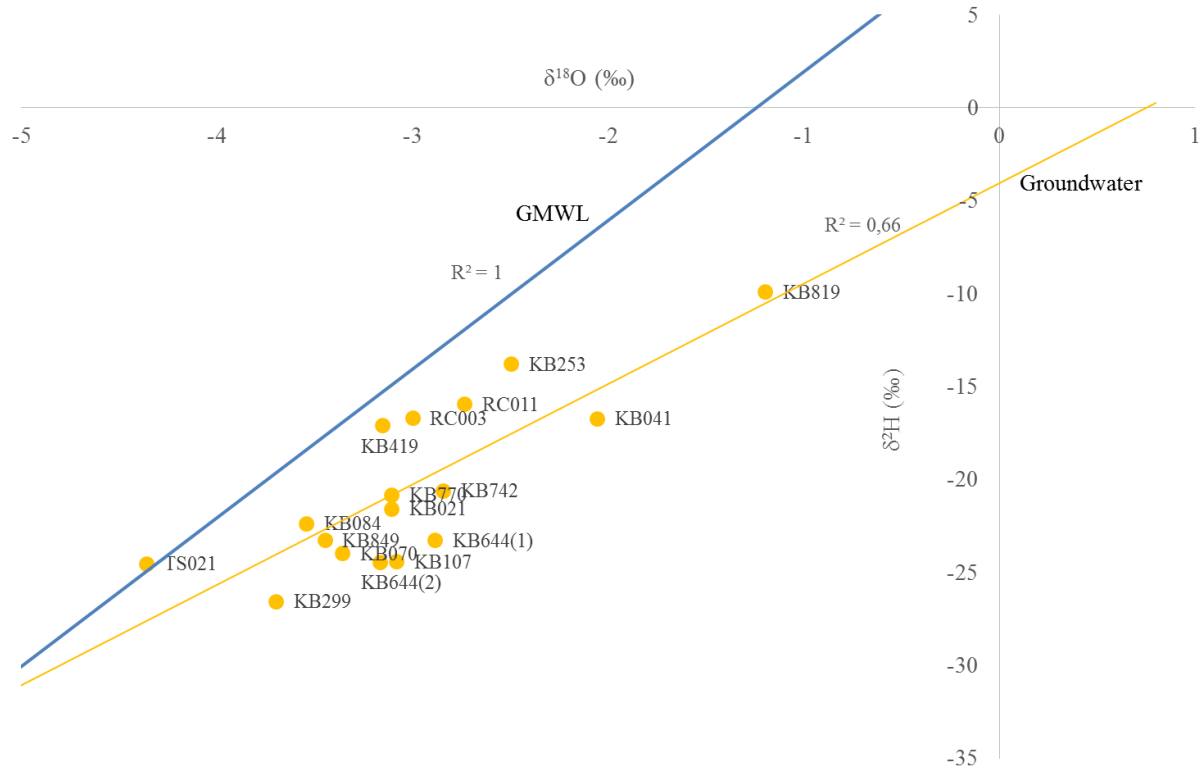

Figure 5-25: δ ^{18}O (‰) vs. δ ^{2}H (‰) for the sampled groundwater plotted against the Global Meteoric Water Line (GMWL) (Craig, 1961).

Carbon 13 ($\delta^{13}C_{DIC}$) results range from -15.95 ‰ to -10.04 ‰ (Figure 5-26) with an average of -13.04 ‰ (Table 5-2). The variance for $\delta^{13}C$ results is 3.01 and the standard deviation is 1.74 ‰ (Table 5-2). Tritium (^{3}H) (Figure 5-27) concentrations vary between 0.1 TU and 2.7 TU with a range of 2.60 TU (Figure 5-27). The average ^{3}H concentration is 1.0 TU. The variance for the tritium data-set is 0.56 and the standard deviation is 0.75 TU (Table 5-2). ^{14}C results range from 50.2 pMC to 107.6 pMC (Figure 5-28) with a range of 57.40 pMC (Figure 5-28). The average ^{14}C concentration is 84.72 pMC. The variance for this data-set is 201.83 and the standard deviation is 14.21 pMC (Table 5-2).

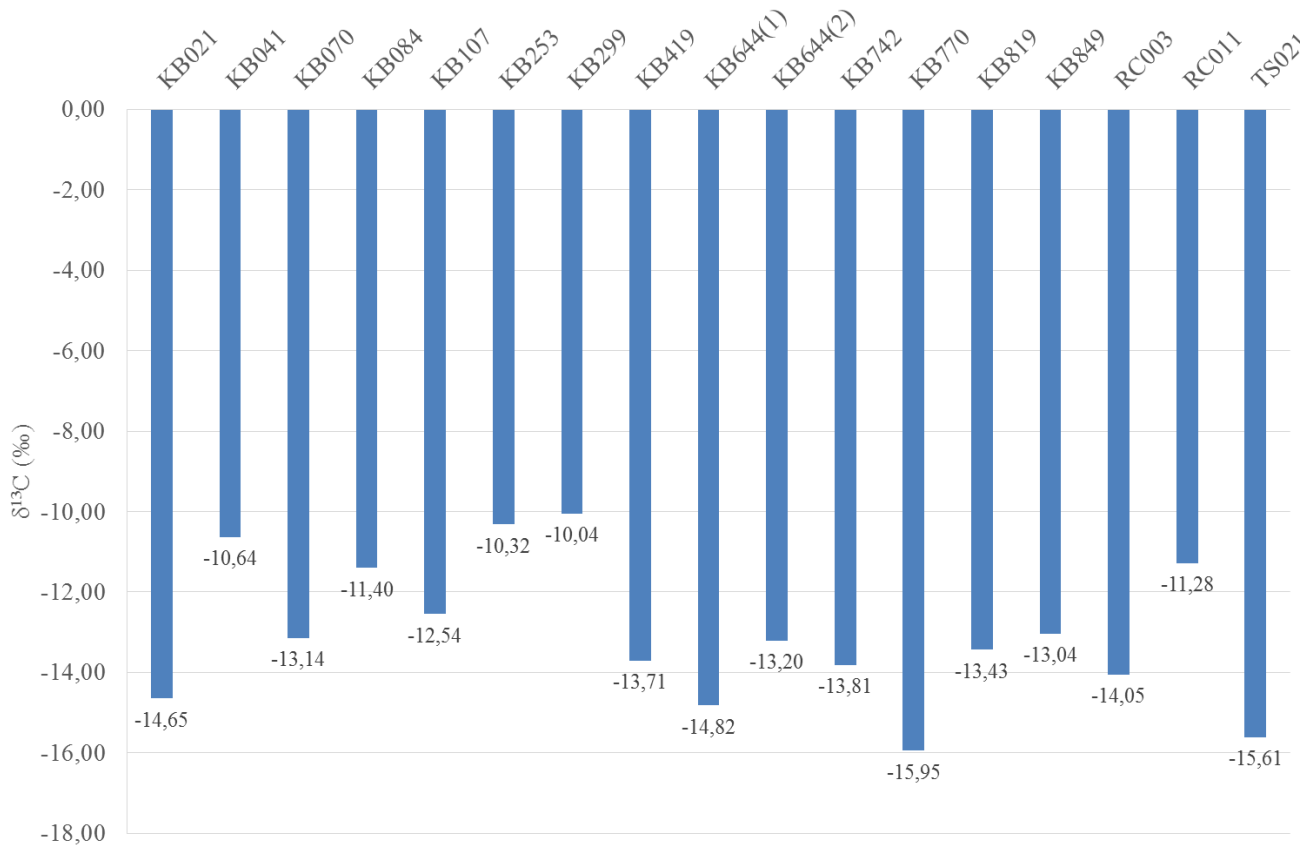

Figure 5-26: $\delta^{13}C$ (‰) bar graph for the sampled groundwater.

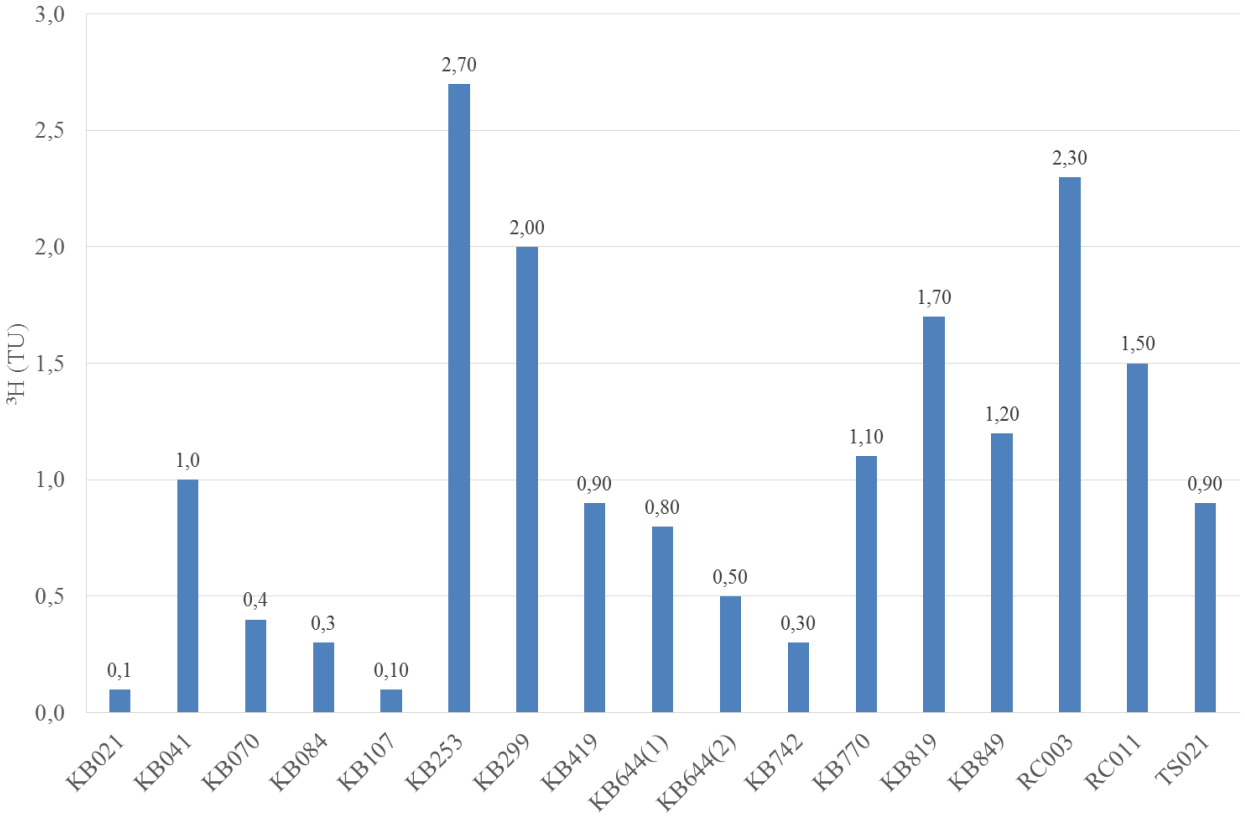

Figure 5-27: ^{3}H (TU) concentrations bar graph for the sampled groundwater.

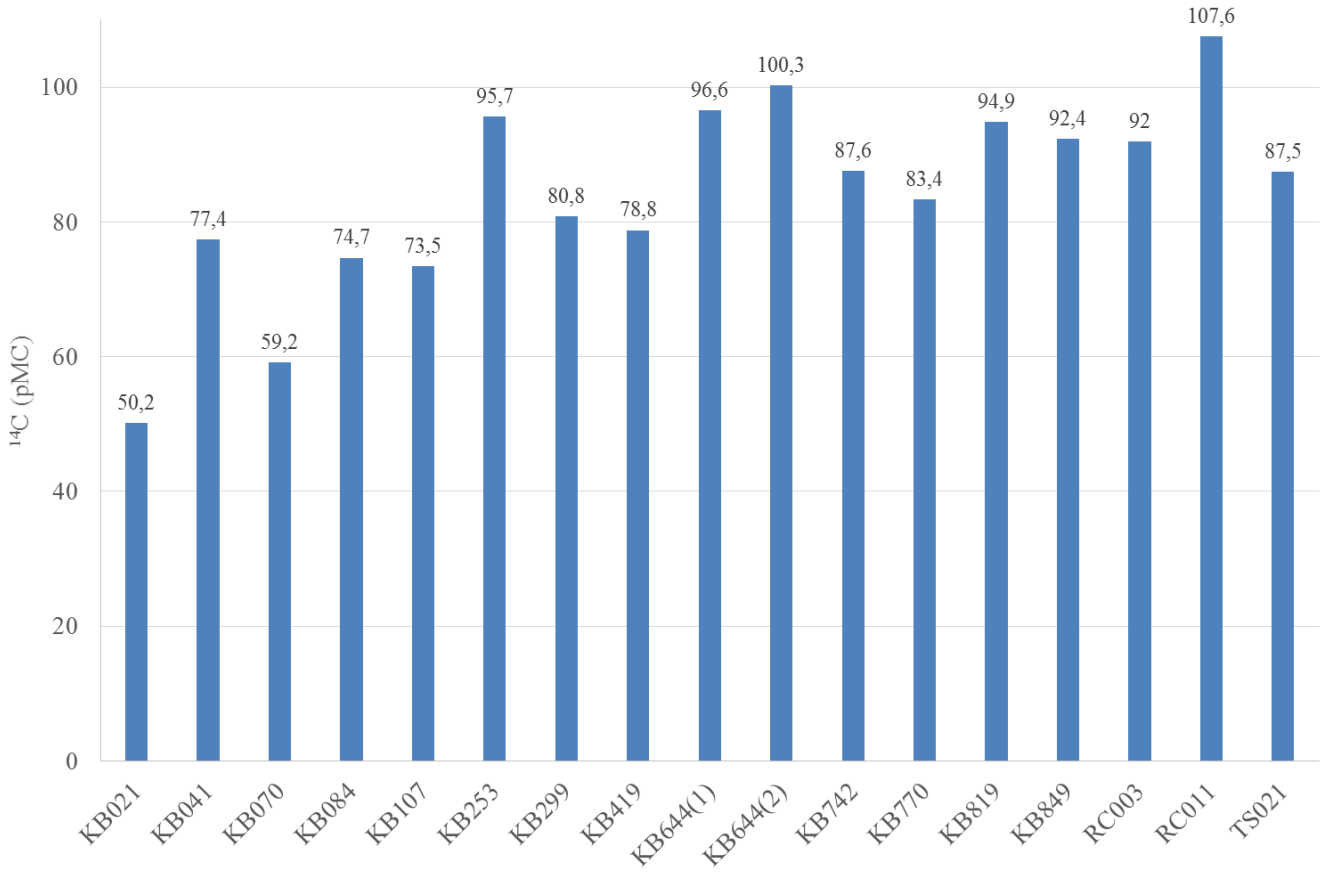

Figure 5-28: ^{14}C (pMC) concentration bar graph for the sampled groundwater.

6. Discussion

The previous chapter provided isotope ($\delta^{18}O$, $\delta^{2}H$, ^{3}H and $\delta^{13}C$) and general field parameter results (sampling depth (masl), temperature (°C), EC (µS/m) and sustainable yield (l/s)). Here, these results are discussed in order to primarily identify area(s) with potential natural reservoir connectivity and to gain insights about groundwater dynamics in the study area. The isotope results are correlated with sampling depth (masl), temperature (°C), EC (µS/m) and sustainable yield (l/s).

The elevation within the study area generally increases from south to north and west to east (Figure 3-1). Therefore, in addition to plotting sampling depths as mbgl (meters below ground level), they were also plotted as masl (meters above sea level) against the analysed isotope results to assess the influence of elevation on the observed isotope concentrations. The groundwater temperature within the study area varies between 18.3°C and 24.3°C (Table 5-1). This is below the minimum hot spring temperature in SA (25°C). In order to investigate if there is a relationship between the sampled groundwater temperature and isotope concentrations, temperature is correlated with the isotope concentrations. The same is done for EC, which varies between 414 and 9169 µS/m and sustainable yields (l/s) for the boreholes, which vary between 0.05 l/s to 4.93 l/s in order to gain insights about their influence on the observed isotope concentrations (Table 5-1).

Stable isotope results ($\delta^{18}O$, $\delta^{2}H$ and $\delta^{13}C$) were used in evaluating groundwater recharge, groundwater mineralisation and groundwater salinization mechanisms. Unstable isotopes (^{3}H and ^{14}C) gave insight about groundwater residence time and potential reservoir connectivity. Also, groundwater ages are calculated using ^{14}C (pMC). $\delta^{13}C_{DIC}$ is used to adjust ^{14}C ages for carbonate dissolution through using the Pearson Model. Groundwater ages were not calculated using tritium concentrations because the tritium groundwater age formula (Equation 2-6) is linked to helium concentrations, which were not analysed because at the time of sample analysis for this project there were no facilities available in South Africa to analyse helium concentrations in water samples.

6.1. ^{14}C (Carbon-14/ Radiocarbon)

The average ^{14}C concentration is 84.2 pMC. 76% of groundwater samples for this project have modern ^{14}C concentrations (>74 pMC) (Figure 6-1). There is no linear correlation between ^{14}C

(pMC) and sampling depth (mbgl) (R^2=0.01). KB021 is an old/deep groundwater sample (< 53 pMC) and, KB070; KB107 and KB084 are mixed groundwater samples (<74 pMC). These four older groundwater samples were collected from boreholes that are aligned parallel to and north-east of the Cape Mountains in the southern part of the study area (Figure 3-2). This suggests that, the deep set active and passive faults within the Cape Mountains and the basement of the southern part of the Karoo Basin (Egle 1996; Booth & Shone 2002; Linol & de Wit 2016) act as preferential pathways for deep groundwater migration to shallower depths (<60 mbgl) (Figure 6-1). These fault systems also conduct deep groundwater to shallower depths through thermal springs in the Cape Mountains (e.g. Egle 1996; Diamond & Harris 2000). Therefore, it is possible that some of the high temperature groundwater (> 25°C) from thermal springs may cool during their upward flow (KGEG 2013) or may be connected through shallow fault systems with low temperature potable groundwater.

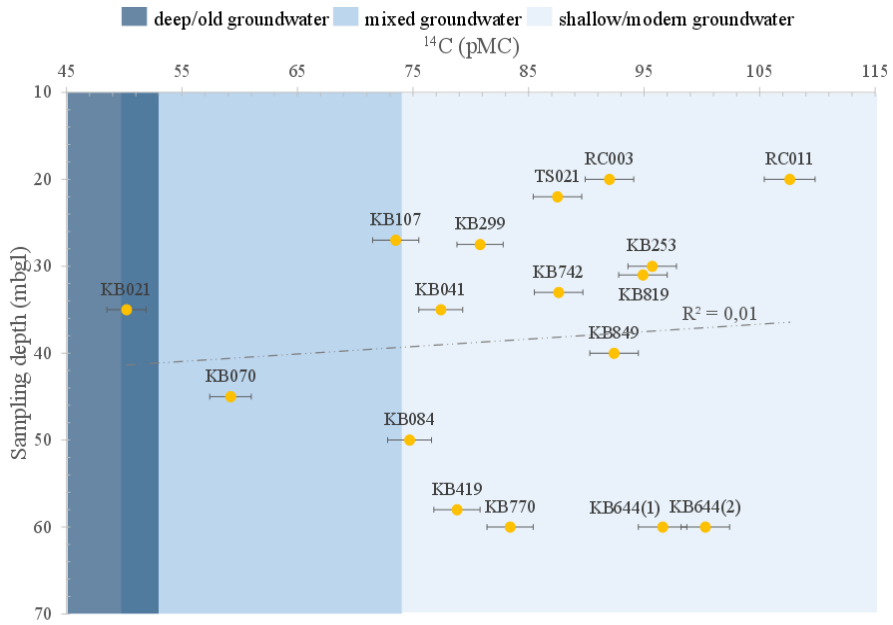

Figure 6-1: Sampling depth (mbgl) vs. ^{14}C (pMC) (R^2 = 0.01). 76% of the sampled groundwater is modern. The groundwater sampled for this project is sampled at shallow water strikes (<60 mbgl). This suggests that older groundwater in this area migrates to shallower depths.

The linear correlation between sampling depth (masl) and ^{14}C (pMC) concentrations is significantly stronger (R^2 = 0.38) (Figure 6-2) than the linear correlation between sampling depth (mbgl) and ^{14}C (pMC) (R^2 = 0.01) (Figure 6-1). Also, groundwater samples collected at

lower elevations (encircled with a red boarder-Figure 6-2) generally have lower ^{14}C (pMC) concentrations. These samples were collected across the southern part of the study area. The eastern side of the study area, partly due to its generally higher elevations, receives more rainfall compared to the western side (Figure 2-2). Thus, the eastern side of the study area has groundwater which has high ^{14}C (pMC) concentrations possibly due to relatively frequent groundwater recharge. However, it must be noted that although the influence of elevation on the analysed isotopic concentrations has the highest linear correlation (R^2=0.38) amongst all isotope-parameter relationships inferred in this study, this relationship is generally low by normal standards and thus it is possible that another factor (possibly reservoir connectivity) at least contributes to the observed behaviour of the isotope concentrations.

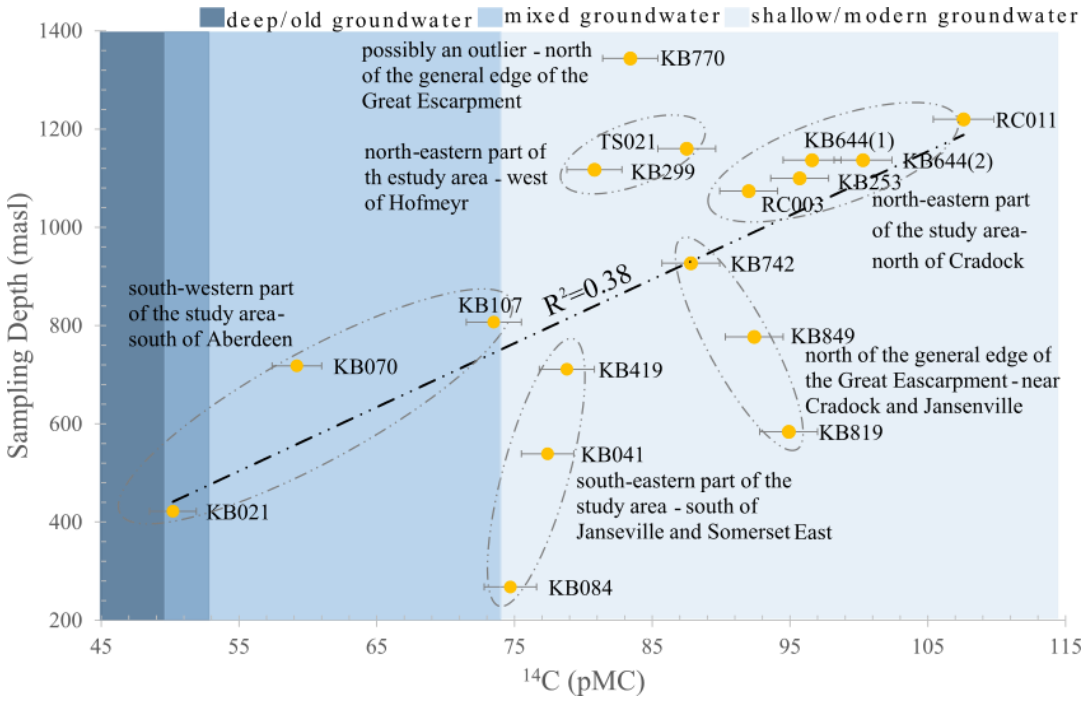

Figure 6-2: Sampling depth (masl) vs. ^{14}C (pMC) for the sampled groundwater (R^2=0.38). The majority of the groundwater samples were collected from water strikes that are at elevations > 600 masl. Groundwater sampled at lower elevations (sampling depth < 800 masl, south of the general edge of the Great Escarpment) are encircled with a red boarder (Figure 6-2). These groundwater samples have relatively older ages (^{14}C < 79 pMC) with KB084, KB107, KB070 falling in the mixed groundwater group, and KB021 at the border between the mixed groundwater group and old groundwater (darker blue colour between mixed groundwater and shallow/modern groundwater). Note groundwater sample-groupings according to geographic sampling location (dotted lines).

Groundwater Group A - KB107; KB070 and KB021 samples were collected in the south-western part of the study area (south of Aberdeen) at sampling depths between 422 masl and 807 masl. These samples have the lowest ^{14}C (pMC) concentrations (50.2 pMC ± 1.7 to 73.5 pMC ± 2). Groundwater Group B - KB419; KB041 and KB084 samples were collected on the south-eastern part of the study area (south of Jansenville and Somerset East) at sampling depths between 268 masl and 711 masl. These samples have ^{14}C (pMC) concentrations between 74.7 pMC ± 1.9 and 78.8 pMC ± 2. Groundwater Group C – KB742; KB849 and KB819 samples have ^{14}C concentrations between 87.8 pMC ± 2.1 and 94.9 pMC ± 2.1, and were collected at various distances immediately north of the general edge of the Great Escarpment (between 584 masl and 927 masl). Groundwater Group D – RC003; KB253; KB644 (1); KB644 (2) and RC011 samples were collected in the north eastern part of the study area (between 1074 masl and 1220 masl), north of Cradock. These have ^{14}C concentrations between 92.0 ± 2.1 and 107.6 ± 2.2. Groundwater Group D – KB299 and TS021 samples were collected in the north eastern part of the study area, west of Hofmeyr. These have ^{14}C concentrations of 80.8 pMC ± 2.0 and 87.5 pMC ± 2.1, respectively. Groundwater sample KB770 was collected close to Group C. However, KB770 was collected at a significantly higher elevation than Group C samples. It is possible that this borehole is located on a hill.

Figure 6-3 is a temperature (°C) vs. ^{14}C (pMC) plot. This shows that the linear trend between temperature (°C) and ^{14}C (pMC) for the sampled groundwater is poor ($R^2 = 0.01$). This lack of correlation is likely due to the uniformity of the temperature of the sampled groundwater. Six groundwater samples have temperatures above 22°C (encircled with a dotted line Figure 6-3). These six samples were all collected on the western side of the study area except for KB021 and KB070 which have lower temperatures (Figure 6-3).

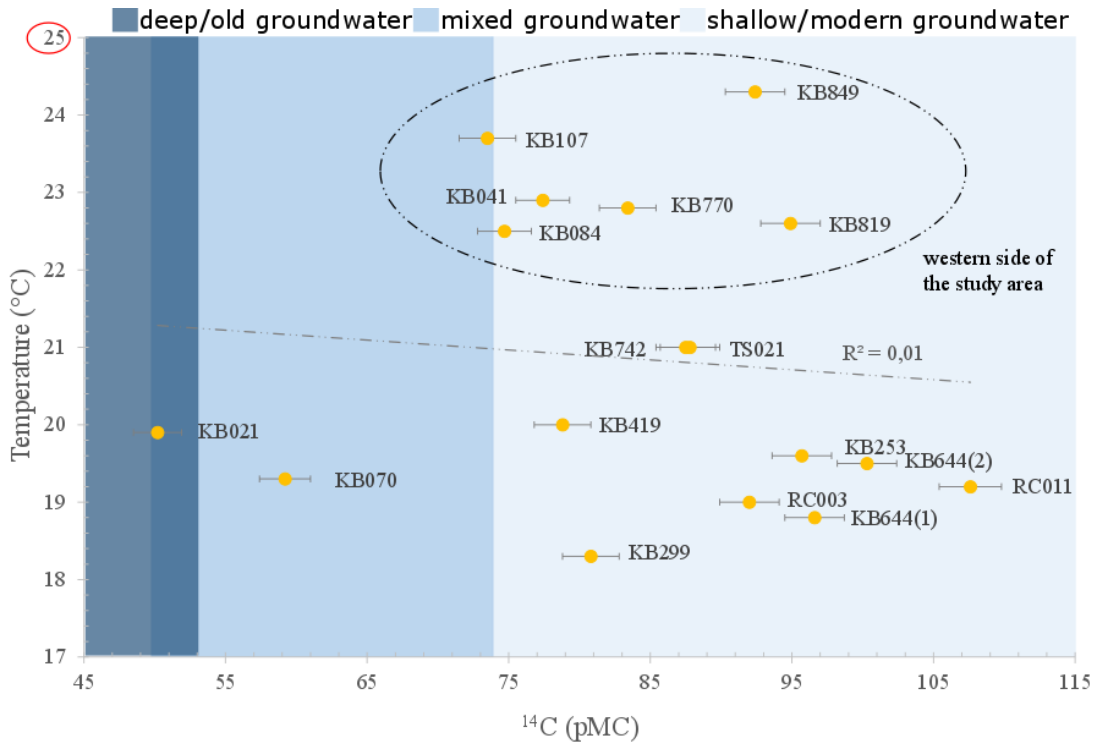

Figure 6-3: Temperature (°C) vs. ^{14}C (pMC) for the sampled groundwater (R^2=0.01). Overall the sampled groundwater is below the minimum hot-spring temperature in South Africa (encircled with a red line on the y-axis of the figure). Encircled with a dotted line are groundwater samples that occur in the western part of the study area (excluding KB021 and KB070). This shows that although the majority of the groundwater samples for this project have overall modern ^{14}C (pMC) signatures, the groundwater samples that occur in the western part of the study area have higher temperatures.

Figure 6-4 below is an EC vs. ^{14}C plot. This shows that EC has a low linear correlation with ^{14}C (pMC) (R^2 = 0.06). The groundwater samples encircled with a dotted line (Figure 6-4) were collected north of the general edge of the Great Escarpment, mostly on the eastern part of the study area. As mentioned earlier, this part of the study area receives relatively more rainfall partly due to its higher elevation (Figure 2-2). This may be a contributing factor affecting the groundwater's low EC (µS/m) values and high ^{14}C (pMC) concentrations (Figure 6-4).

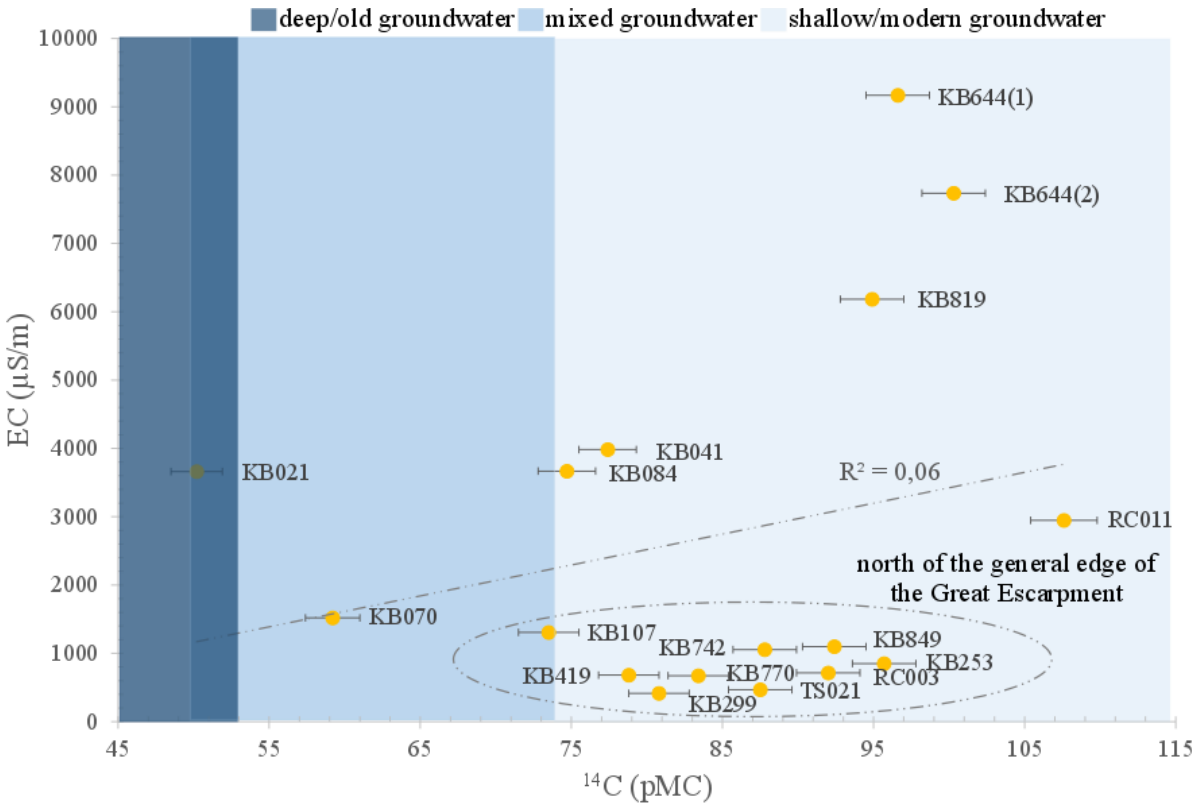

Figure 6-4: EC (µS/m) vs. ^{14}C for the sampled groundwater (R^2 = 0.06). The encircled groundwater samples are collected north of the general edge of the Great Escarpment, mostly on the eastern part of the study area. KB644(1) and KB64.4(2) have the highest EC values because they were collected within 5 km of a salt pan in Hofmeyr.

Figure 6-5 is a plot of sustainable yield (l/s) vs. ^{14}C (pMC). It shows that the older groundwater samples (KB021, KB070, KB107 and KB084) were collected from boreholes with sustainable yields of 4.93; 0.74; 1.49 and 0.35 l/s, respectively. KB021 has the highest sustainable yield (l/s) and could be an outlier reflecting an experimental error. Eliminating KB021 from the sample pool shows that, while other samples show an increase in sustainable yield with increasing ^{14}C (pMC) concentration, groundwater samples with sustainable yields (l/s) below 0.5 (l/s) group at ^{14}C (pMC) concentrations above or equal to 75 pMC (Figure 6-6). This suggests that groundwater with low sustainable yields (=<0.5 l/s) is often modern and groundwater with higher sustainable yields (=> 0.5 l/s) could be either modern or mixed groundwater within the study area.

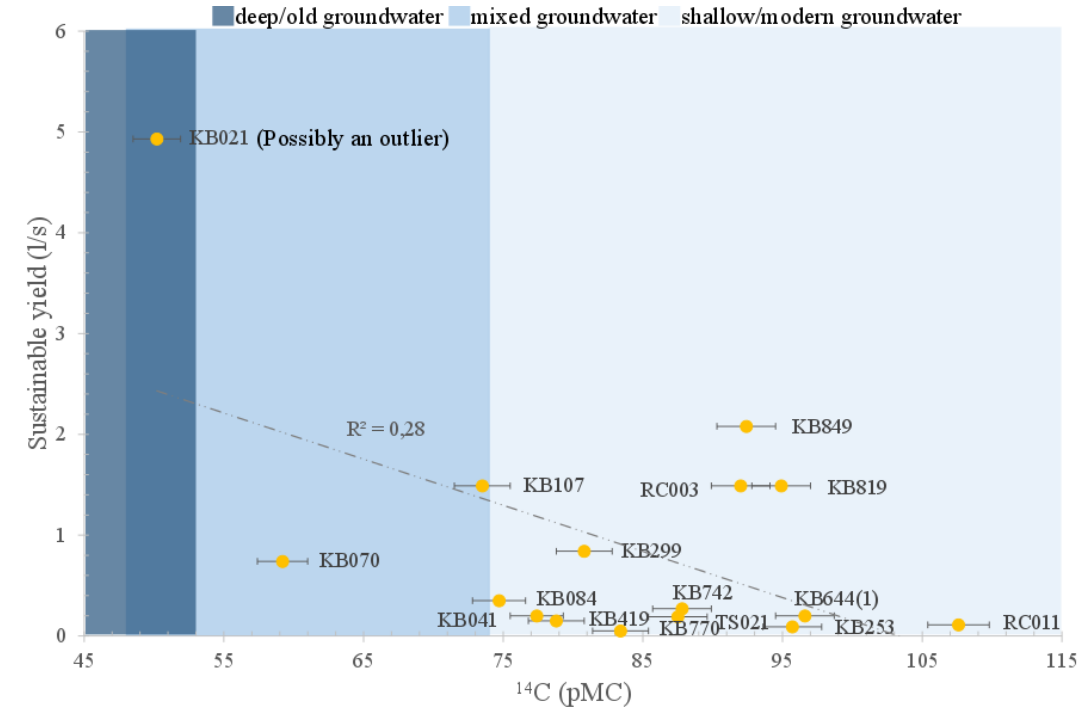

Figure 6-5: Sustainable yield (l/s) vs. ^{14}C (pMC) for the sampled groundwater (R^2 = 0.28). KB021 is possibly an outlier.

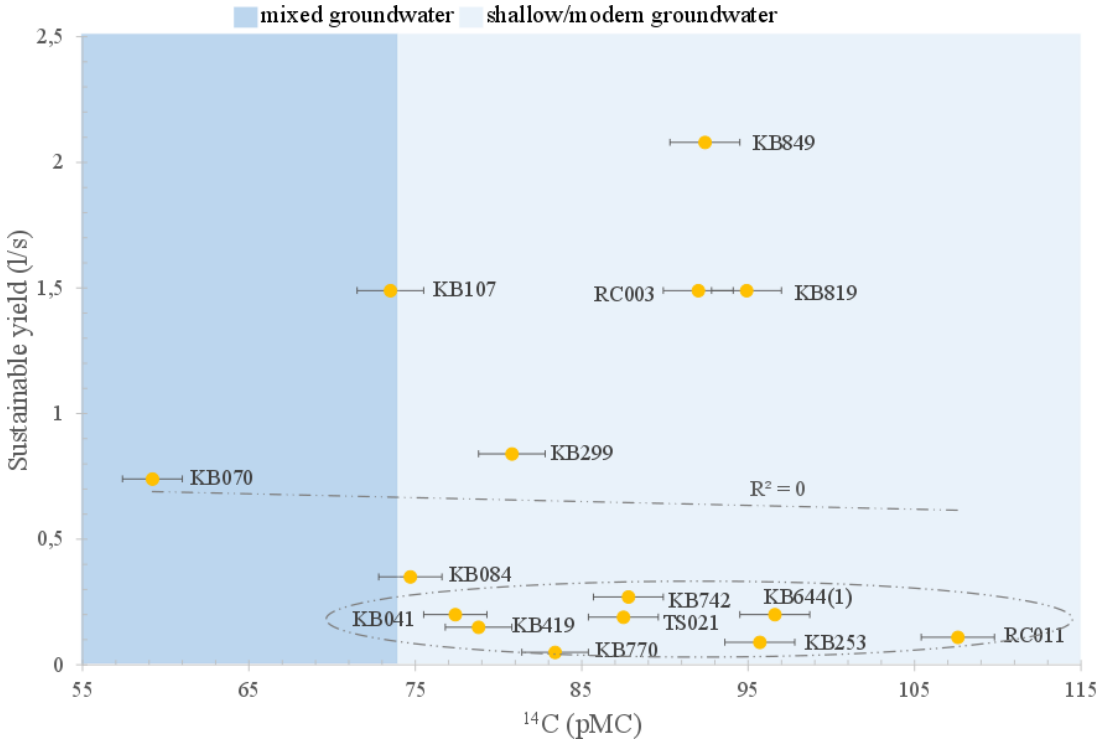

Figure 6-6: Sustainable yield (l/s) vs. ^{14}C (pMC) for the sampled groundwater (without the possible outlier) (R^2 = 0). In this figure three different trends are noticed in the sample pool.

6.2. $\delta^{13}C_{DIC}$ (Carbon 13 in Dissolved Inorganic Carbon)

The lack of linear correlation (R^2 = 0.01-Figure 6-7) between $\delta^{13}C$ (‰) and ^{14}C (pMC) is likely due to a poor performance for differentiating between deep and shallow groundwater for ^{13}C (‰) compared to ^{14}C (pMC) (see chapter 1).

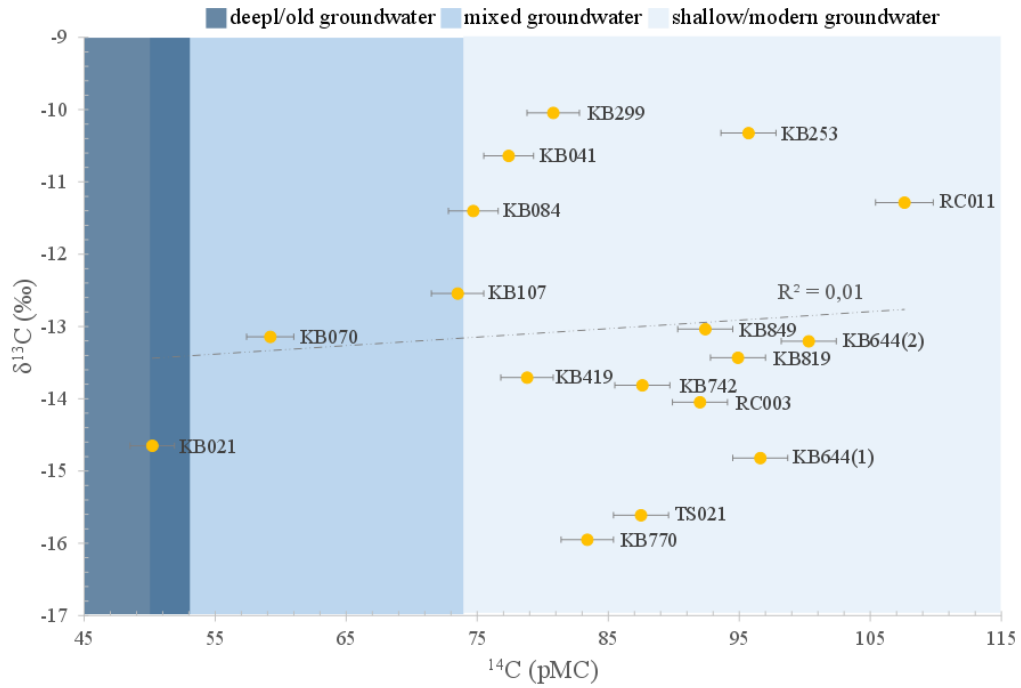

Figure 6-7: $\delta^{13}C$ (‰) vs. ^{14}C (pMC) for the sampled groundwater (R^2 = 0.01). The poor correlation between $\delta^{13}C$ (‰) and ^{14}C (pMC) is likely due to the poor performance of $\delta^{13}C$ (‰) in differentiating between different groundwater groups according to aquifer depth.

The average $\delta^{13}C_{DIC}$ concentration is -13.04 ‰. This value suggests that the DIC of the groundwater largely evolved from biogenic carbon (Diamond & Harris 2000) and is close to the $\delta^{13}C$ value of soil-respired $CO_2(g)$ derived from the decay of C4 plants in the Karoo Basin (e.g. Vogel et al. 1978; Verhagen et al. 2009; Swana 2016). Other contributions to DIC in groundwater may include carbonates, which were not analysed in this thesis. ^{14}C (pMC) results established that the majority of the sampled groundwater is modern. This suggests that the majority of the sampled groundwater evolved in the upper soil-zone (open system conditions of the CZ). This is supported by the high average pH (7.57) and high average total alkalinity (343.6 $mg.L^{-1}$), which suggest that the major ion contributing to alkalinity and DIC is HCO_3^- (Adams et al. 2001).

6.2.1. Calculating Groundwater Age Using ^{14}C and $\delta^{13}C$

^{14}C (pMC) concentrations were used to calculate groundwater ages (Table 6-1). The Pearson model (Ingerson & Pearson 1964) was used to account for ^{14}C dilution. The model takes into account the $\delta^{13}C$ values of soil-respired CO_2 (δ_g), of carbonates within the aquifer (δ_c) and of DIC (δ_{DIC}) to calculate carbonate dilution factors (q values) for each groundwater sample. For this project, only the δ_{DIC} was analysed and, values of δ_g and δ_c were acquired from Swana (2016). The calculated dilution factors are in turn used to determine calculated ages. To calculate the minimum dilution factor, the lowest $\delta^{13}C$ value for C4 plants (-13 ‰) and the highest $\delta^{13}C$ value for carbonates (2 ‰) were used. To calculate the maximum dilution factor, the highest $\delta^{13}C$ value for C4 plants (-12 ‰) and the lowest $\delta^{13}C$ value for carbonates (1.4 ‰). The resultant q values were used to calculate minimum, median and maximum ages (Lemay 2002).

Calculated ages are corrected for carbonate dissolution but not corrected for the nuclear bomb effects that took place after the 1950s. Equation 2-15 was used to account for this effect to determine a final corrected age (Table 6-1). The oldest groundwater sample (KB021) has a corrected median age of 6735 years, a minimum age of 6173 years and a maximum age of 7328 years. Negative ages (KB253 and RC011) mean that the groundwater is very young and possibly meteoric water (Swana 2016). The average difference between the minimum corrected age and median age is 470 years and the average difference between the maximum corrected and median age is 497 years (Table 6-2). These differences were used to determine error bars for the median corrected ages (Figure 6-8 & Figure 6-9). The linear correlation between calculated groundwater ages (years) and measured ^{14}C (pMC) concentrations is significantly strong ($R^2 = 0.72$). Some groundwater samples have the same calculated ages (years) but different ^{14}C concentrations (pMC) (encircled with dotted lines-Figure 6-8). The groundwater samples with the lowest ^{14}C concentrations (<74 pMC) have calculated ages equal to and above 1700 years. In addition to these older groundwater samples, groundwater samples KB742, KB419, TS021, KB770 also have calculated groundwater ages ≥ 1700 years although they have significantly higher ^{14}C concentrations (>74 pMC). This is likely due to the influence of adjusting the ^{14}C content in DIC based on its dilution by ^{14}C free carbonates and implies that older groundwater occurs in other parts of the study area possibly due to other fault systems between deep and shallow aquifers. This is not surprising as the Karoo Basin is dominated by secondary aquifers (Woodford & Chevallier 2002).

Table 6-1 Radiocarbon age calculations

$$q = \frac{(\delta_{DIC} - \delta_c)}{(\delta_a - \delta_c)}$$

				max q value	med q value	min q value	$calculated\ age(years) = -8033 \times \ln(\frac{^{14}C(pMC)}{q \times 100})$			$corrected\ age(years) = calculated\ age + (2016 - 1950)$		
				(δ_g) δ^{13}C of soil respired CO_2 (‰)								
				-12	-12,5	-13						
				(δ_c) δ^{13}C of carbonates (‰)								
Sample Label	(δ_{DIC}) δ^{13}C (‰)	^{14}C (pMC)	±	1.4	1.7	2	max	med	min	max	med	min
KB021	-14.65	50.2	1.70	1.20	1.15	1.11	7262	6669	6107	7328	6735	6173
KB041	-10.64	77.4	1.90	0.90	0.87	0.84	1398	930	488	1464	996	554
KB070	-13.14	59.2	1.80	1.09	1.05	1.01	5115	4565	4045	5181	4631	4111
KB084	-11.4	74.7	1.90	0.96	0.92	0.89	2182	1695	1235	2248	1761	1301
KB107	-12.54	73.5	2.00	1.04	1.00	0.97	3012	2496	2007	3078	2562	2073
KB253	-10.32	95.7	2.10	0.87	0.85	0.82	-545	-986	-1402	-479	-920	-1336
KB299	-10.04	80.8	2.00	0.85	0.83	0.80	644	184	-250	710	250	-184
KB419	-13.71	78.8	2.00	1.13	1.09	1.05	3085	2571	2084	3151	2637	2150
KB644(1)	-14.82	96.6	2.10	1.21	1.16	1.12	1989	1494	1025	2055	1560	1091
KB644(2)	-13.2	100.3	2.10	1.09	1.05	1.01	835	362	-84	901	428	-18
KB742	-13.81	87.6	2.10	1.14	1.09	1.05	2276	1772	1296	2342	1838	1362
KB770	-15.95	83.4	2.00	1.29	1.24	1.20	3728	3205	2710	3794	3271	2776
KB819	-13.43	94.9	2.10	1.11	1.07	1.03	1415	930	472	1481	996	538
KB849	-13.04	92.4	2.10	1.08	1.04	1.00	1420	935	476	1486	1001	542
RC003	-14.05	92	2.10	1.15	1.11	1.07	1999	1502	1032	2065	1568	1098
RC011	-11.28	107.6	2.20	0.95	0.91	0.89	-866	-1310	-1729	-800	-1244	-1663
TS021	-15.61	87.5	2.10	1.27	1.22	1.17	3184	2664	2171	3250	2730	2237

Table 6-2 Difference of maximum (+) and minimum ages (-) (years) from median ages.

		corrected age (years)					
Sample Label	^{14}C (pMC)	max	med	min	+	age (years)	-
KB021	50.2	7328	6735	6173	594	6735	562
KB041	77.4	1464	996	554	468	996	442
KB070	59.2	5181	4631	4111	550	4631	520
KB084	74.7	2248	1761	1301	487	1761	460
KB107	73.5	3078	2562	2073	516	2562	488
KB253	95.7	-479	-920	-1336	441	-920	417
KB299	80.8	710	250	-184	459	250	434
KB419	78.8	3151	2637	2150	514	2637	487
KB644(1)	96.6	2055	1560	1091	495	1560	468
KB644(2)	100.3	901	428	-18	472	428	447
KB742	87.6	2342	1838	1362	504	1838	477
KB770	83.4	3794	3271	2776	523	3271	495
KB819	94.9	1481	996	538	485	996	458
KB849	92.4	1486	1001	542	485	1001	459
RC003	92.0	2065	1568	1098	497	1568	470
RC011	107.6	-800	-1244	-1663	444	-1244	419
TS021	87.5	3250	2730	2237	521	2730	493
Average	84.3	2309	1812	1341	497	1812	470

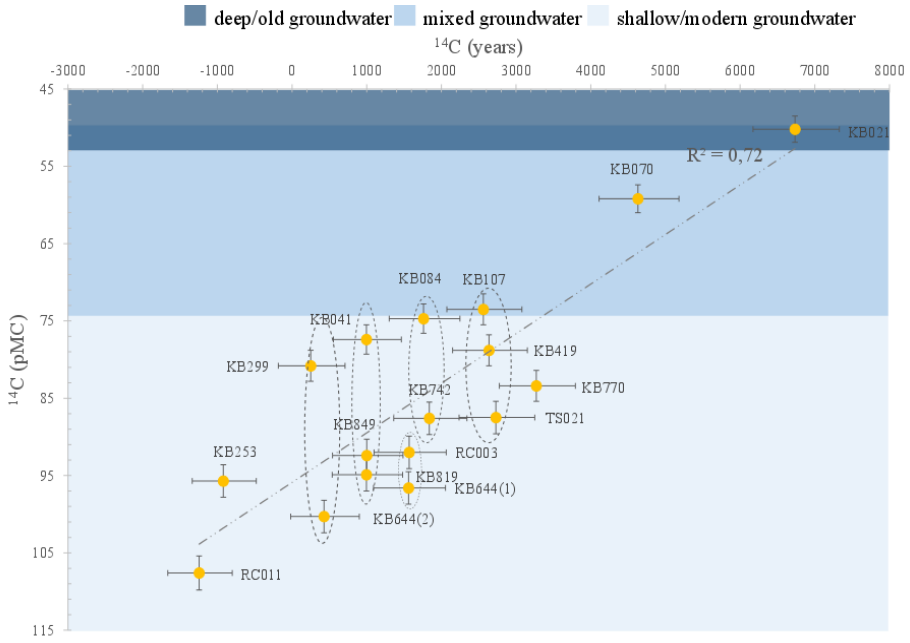

Figure 6-8: ^{14}C (pMC) vs. Final Corrected ^{14}Age (years) plot of sampled groundwater. Also shown are groundwater samples with similar calculated ages (years) but different ^{14}C (pMC) concentrations (R^2 = 0.72).

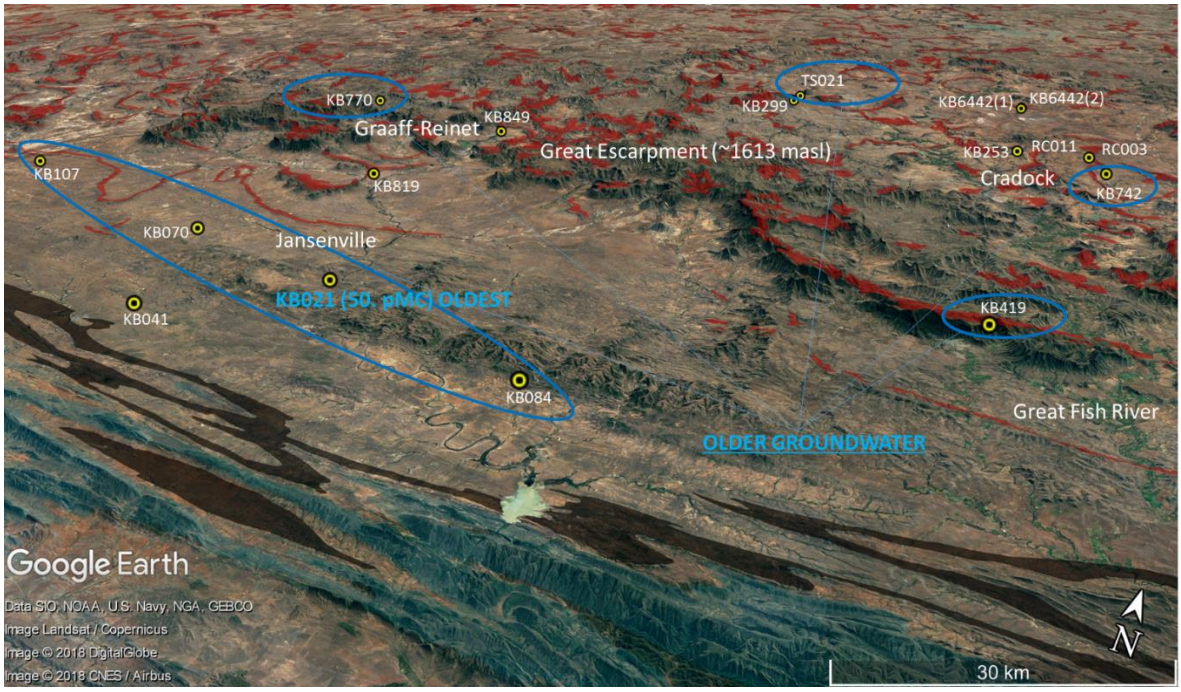

Figure 6-9: Map of the study area highlighting areas where reservoir connectivity possibly occurs. The blue shade on the terrain symbolises the Witterberg Group, the brown shade symbolises the surface exposure of the Whitehill Formation and the red shade symbolises the Karoo Dolerite. Note the intense folding of the Whitehill Formation and its intersection with the quartzites of the Witteberg Group (of the Cape Supergroup) implying folding and thrust faulting along these sections

6.3. ^{3}H (Tritium)

Although the four groundwater samples with the lowest ^{14}C (pMC) concentrations (KB084, KB021, KB070 and KB107) also have the lowest ^{3}H (TU) concentrations, the linear relationship between ^{14}C (pMC) and ^{3}H (TU) for the sampled groundwater is poor ($R^2 = 0.28$). Also, ^{3}H TU classifies that 47% of the sampled groundwater as modern as opposed to 76% (as classified by ^{14}C (pMC)). These discrepancies may be due to the shortness of the half-life of ^{3}H (TU) ($t_{1/2}$ = 12.43 years), which means that the ^{3}H (TU) that was liberated in the 1960s completely decayed over time, thus making ^{3}H (TU) a less effective groundwater residence-time tracer. In addition, there are considerable overlaps between aquifer depths when using ^{3}H (TU) as a groundwater residence time constraint (Figure 6-10). These overlaps make it difficult to precicely classify groundwater according to age and aquifer depth.

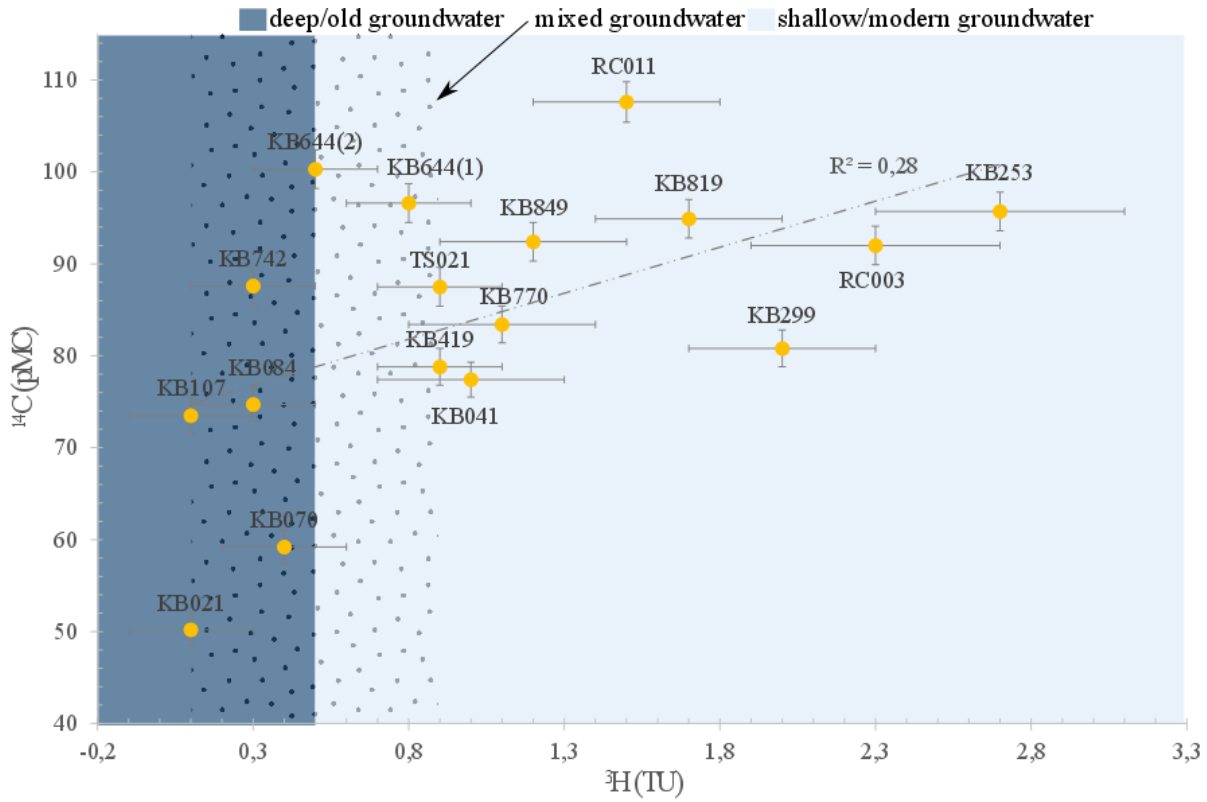

Figure 6-10: ^{14}C (pMC) vs. ^{3}H (TU) for the sampled groundwater (R^2 = 0.28). ^{3}H (TU) classifies that 47% of the sampled groundwater is modern. Note that the mixed groundwater group (dotted) overlaps with both the shallow/modern groundwater group and deep/old groundwater group when using ^{3}H as a groundwater residence time constraint.

Figure 6-11 shows that generally sampling depth (masl) for the groundwater samples increases steeply from 268 (masl) to 1137 (masl) for groundwater samples with ^{3}H (TU) concentrations less than 0.5 (TU) and "plateaus" thereafter with increasing ^{3}H (TU) concentrations. Exceptions to this relationship are groundwater samples: KB041, KB819, KB419 and KB849, which have sampling depths between 539 (masl) and 777 (masl) and ^{3}H (TU) concentrations between 1.0±0.3 (TU) and 1.70±0.3 (TU). If the mixed groundwater group is ignored, groundwater samples with sampling depths (masl) below 800 masl (collected south of the general edge of the Great Escarpment) have half of their groundwater samples plotting within the deep/old groundwater field, and the other half plotting within the shallow/modern groundwater field, whilst groundwater samples with sampling depths above 800 (masl) (collected in the north-eastern part of the study area) have ^{3}H (TU) concentrations exclusively resembling shallow/modern groundwater.

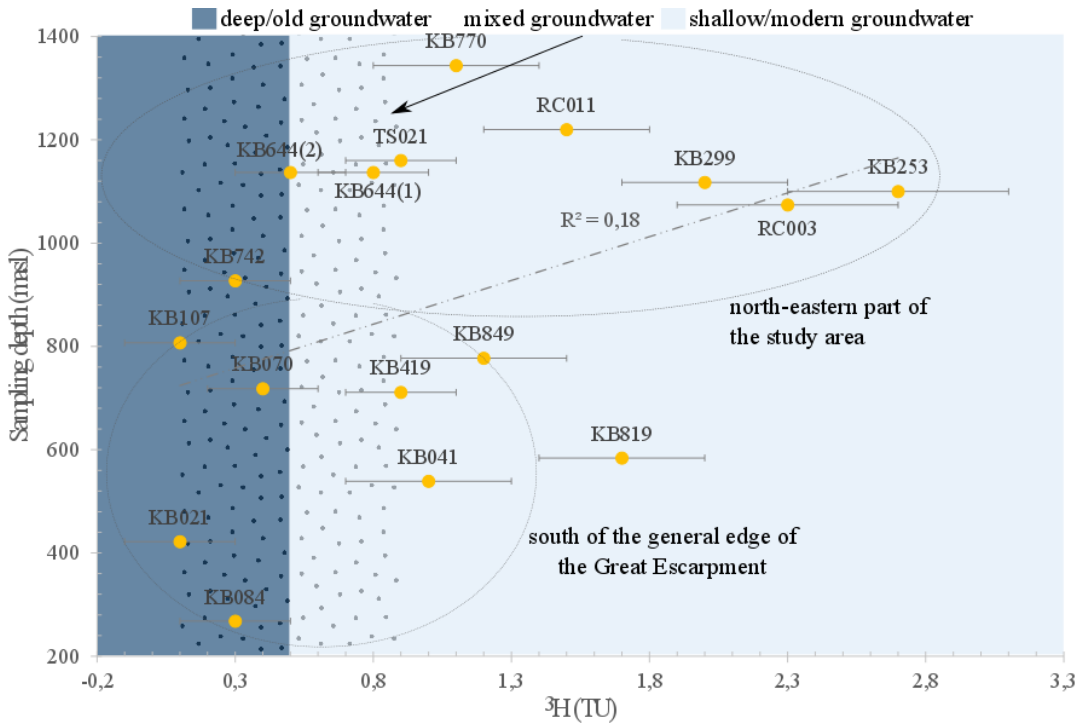

Figure 6-11: Sampling Depth (masl) vs. ^{3}H (TU) for the sampled groundwater (R^2 = 0.18). Sampling depth (masl) steeply increases between 268 (masl) and 1137 (masl) and thereafter plateaus with increasing ^{3}H (TU) concentration.

Figure 6-12 is a temperature vs. ^{3}H (TU) plot. There is no linear relationship between temperature (°C) and ^{3}H (TU) (R^2 = 0.08). Groundwater samples with temperatures > 22.5°C and collected from the western part of the study area, which falls exclusively within the mixed and shallow/modern groundwater group when using ^{14}C (pMC) as a groundwater residence time tracer (Figure 6-3), spans all three groundwater groups when using ^{3}H as a constraint (Figure 6-12). Similarly on Figure 6-13 where the group of groundwater samples that were collected north of the general edge of the Great Escarpment span all aquifer depth groups as opposed to dominating the just the shallow/modern groundwater group as shown on Figure 6-4. On Figure 6-14 it is shown that the linear correlation between sustainable yield (l/s) and ^{3}H (TU) is poor (R^2 = 0.06) and lower than that between sustainable yield (l/s) and ^{14}C (pMC) (R^2 = 0.28-Figure 6-5)

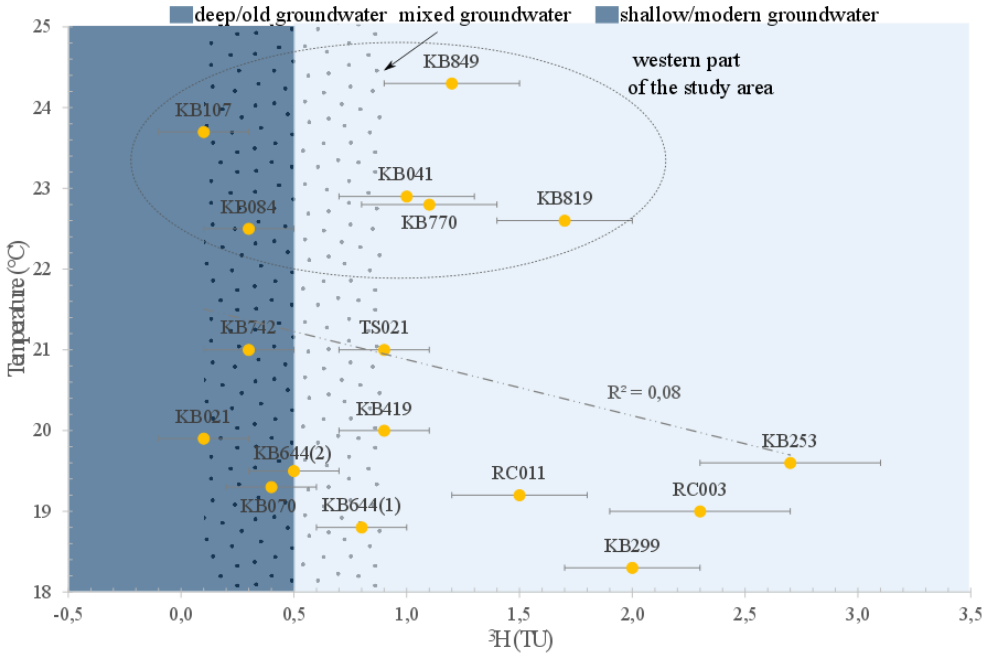

Figure 6-12: Temperature (°C) vs. ^{3}H (TU) for the sampled groundwater. The warmer groundwater samples collected from the western part of the study area (encircled with a dotted line) span all three aquifer depth groups (R^2 = 0.08).

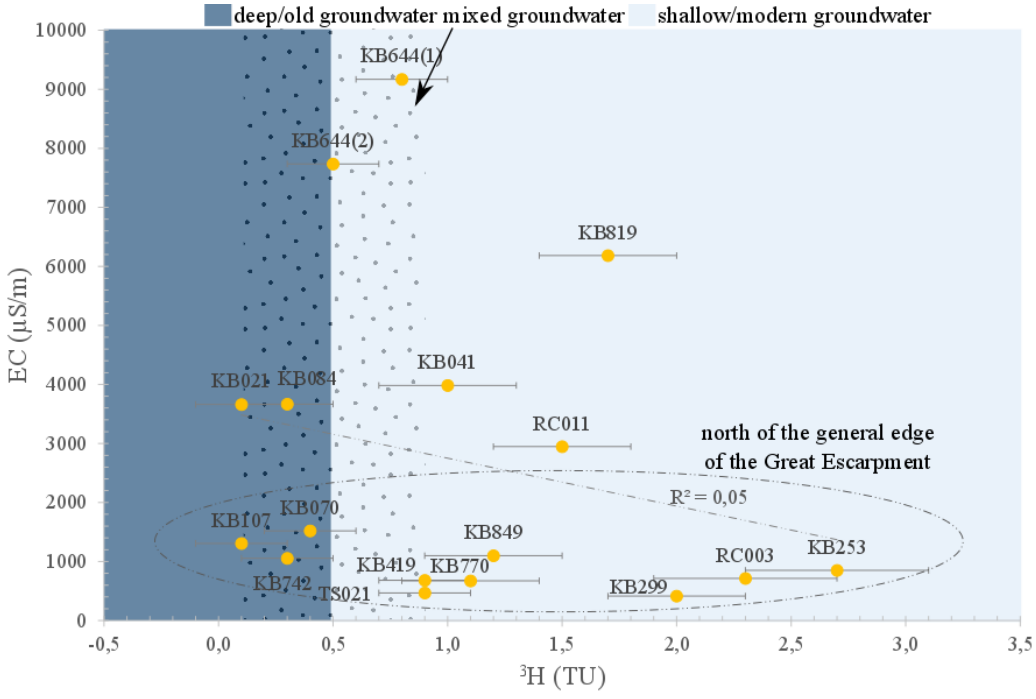

Figure 6-13: EC (µS/m) vs. ^{3}H (TU) for the sampled groundwater. The group of samples that were collected above the general edge of the Great Escarpment span all aquifer/groundwater groups.

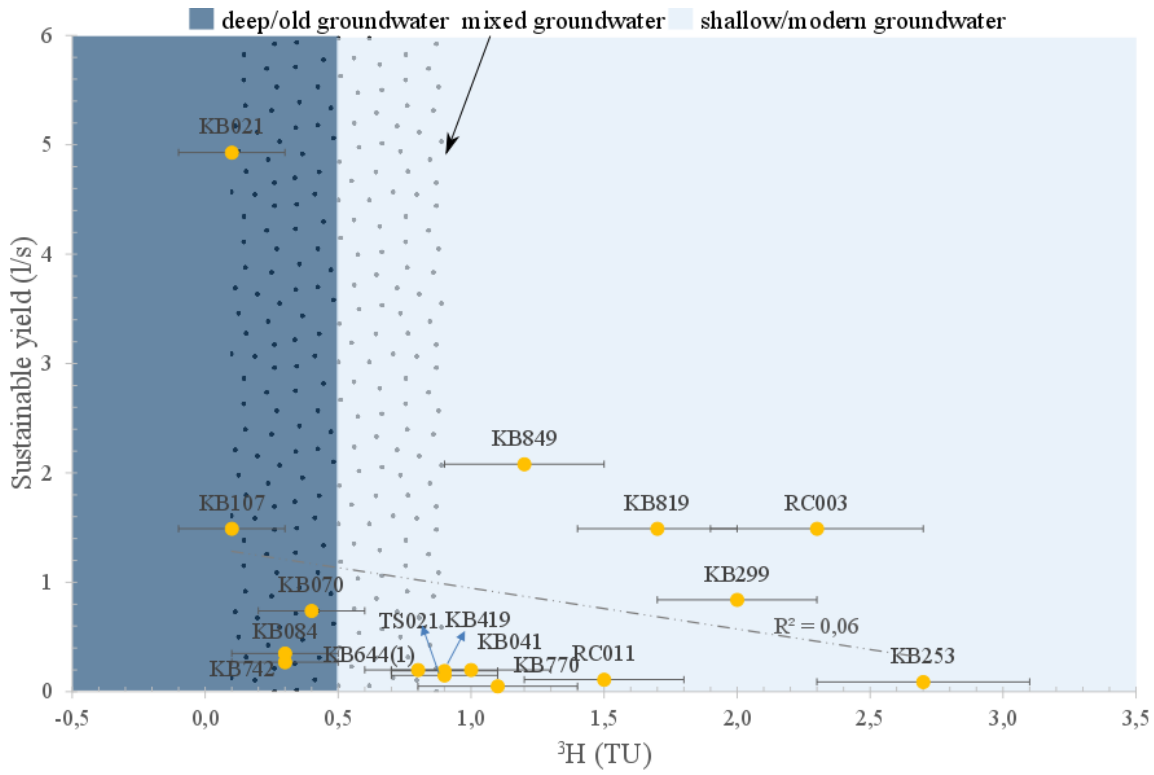

Figure 6-14: Sustainable yield (l/s) vs. ^{3}H (TU) for the sampled groundwater.

6.4. $\delta^{2}H$ and $\delta^{18}O$ (Deuterium and Oxygen 18)

Average $\delta^{18}O$ and $\delta^{2}H$ for the sampled groundwater is -3.02 ‰ and -20.35 ‰, respectively. This enriched isotope concentration suggests that the majority of the sampled groundwater systems for this project is modern (Miller et al. 2015; Murray et al. 2015; Swana 2016). It is difficult to distinguish older groundwater from modern groundwater using $\delta^{18}O$ and $\delta^{2}H$ in the Karoo Basin because there tends to be overlaps between modern groundwater and mixed groundwater isotope signatures (Table 1-1). $\delta^{18}O$ and $\delta^{2}H$ were not analysed in rainwater for this project and were attained from Sami (1992), who used the South African regional meteoric water line (from Kirchner & Van Tonder 1991) for a groundwater study in Bedford (~ 140 km east of study area) (Equation 2-5; Figure 6-15).

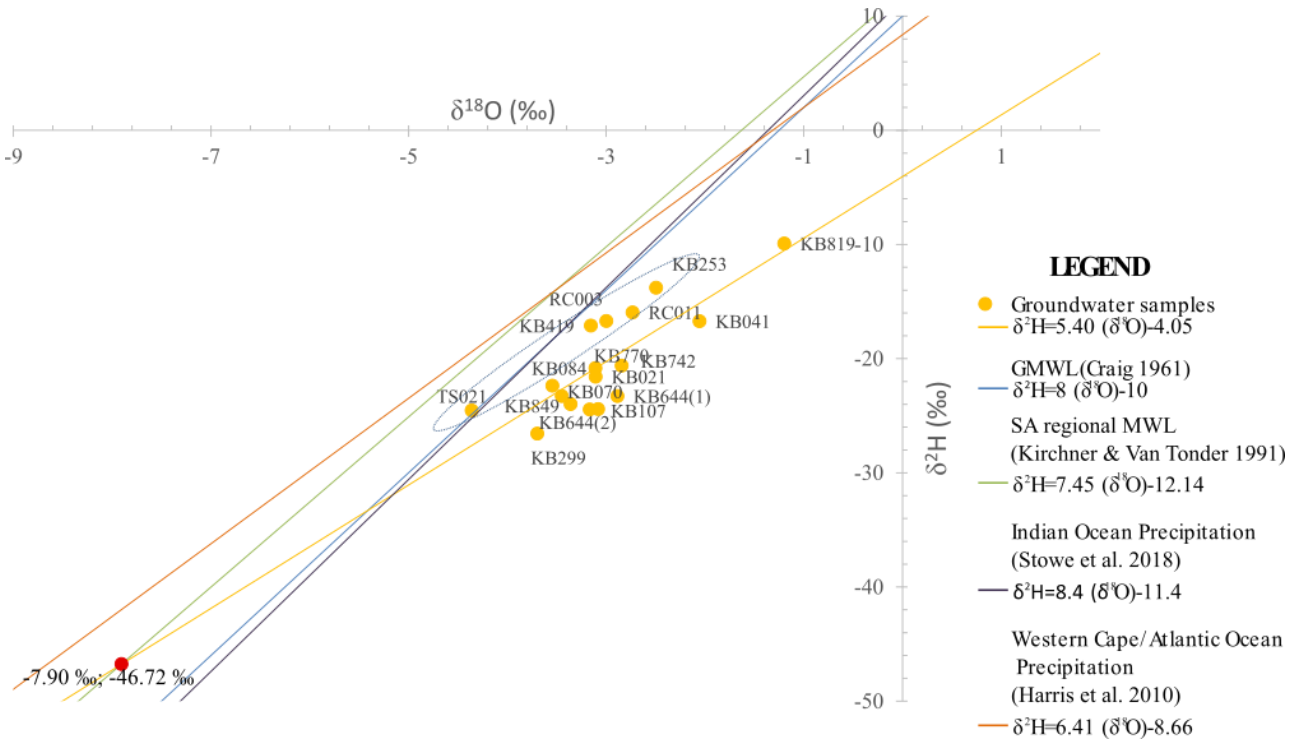

Figure 6-15: δ^2H vs $\delta^{18}O$ for the sampled groundwater. Also shown on is the GMWL (Craig, 1961), SA regional meteoric water line (Kirchner & Van Tonder 1991), the linear relationship for the sampled groundwater ($\delta^2H = 5.40(\delta^{18}O) – 4.05$), isotope concentration of rainwater in the Indian Ocean (Stowe et al. 2018) and the Atlantic Ocean (Harris et al. 2010). The encircled groundwater samples represent meteoric groundwater collected within the main drainage of the Great Fish River. The red dot represents the average isotope concentration of the recharging meteoric water ($\delta^{18}O$ = -7.90 ‰; δ^2H = -46.72 ‰).

The LMWL diverges marginally from the assumed equilibrium relationship of GMWL (Equation 2-4) suggesting that the relationship between δ^2H and $\delta^{18}O$ in rainwater for this area is slightly out of equilibrium (Figure 6-15) (Craig 1961; Dansgaard 1964). 70% of the sampled groundwater plot along the groundwater $\delta^{18}O$-δ^2H relationship line, which has a smaller gradient compared to the GMWL and LMWL (Figure 6-15). The small gradient likely reflects the evaporative isotope depletion that occurred in the recharging water (Sami 1992). This implies that the recharging water experienced surface evaporation before or during groundwater recharge (Adams et al. 2001; Kim & Lee 2011; Vogel & van Urk 1975; Sami 1992). This includes groundwater in eastern part of the study area. Considering that the sampled groundwater is overall modern. 30% of the sampled groundwater (TS021; RC003; RC011; KB253 and KB419) is isotopically enriched and plots closer to the GMWL and

LMWL. This implies that the recharging water to this groundwater did not experience significant evaporation and may have thus been recharged rapidly. Additionally, these groundwater samples were collected within the main drainage of the Great Fish River. The approximate composition of the recharging water for all the groundwater sampled for this project is calculated at the intersection between the sampled groundwater $\delta^{18}O$-$\delta^{2}H$ line and the GMWL (Sami 1992). The result is -7.90 ‰ and -46.72 ‰ for $\delta^{18}O$ and $\delta^{2}H$, respectively (red dot-Figure 6-15). This isotope result plots half-way between the $\delta^{18}O$-^{2}H relationship line of rainfall in the Indian Ocean and the $\delta^{18}O$-^{2}H relationship line of rainfall in the Atlantic Ocean, suggesting that the recharging water to the sampled groundwater was derived from rainwater which evolved from both the the Indian Ocean and Atlantic Ocean.

Figure 6-16 below is a plot of sampling depth (mbgl) vs. $\delta^{18}O$ (‰). The linear correlation between sampling depth (mbgl) and $\delta^{18}O$ (‰) is 0.01. This figure shows that the groundwater samples that plot close to the GMWL (Figure 6-15) were collected at shallow sampling depths between (20 mbgl) and 33 (mbgl) (Figure 6-16). This implies that this groundwater that does not experience significant evaporation upon or after recharge possibly due to rapid recharge within the main drainage of the Great Fish River is recharged through shallow preferential pathways. These groundwater samples are also collected at high elevations (1074 masl - 1220 masl) (Figure 6-17).

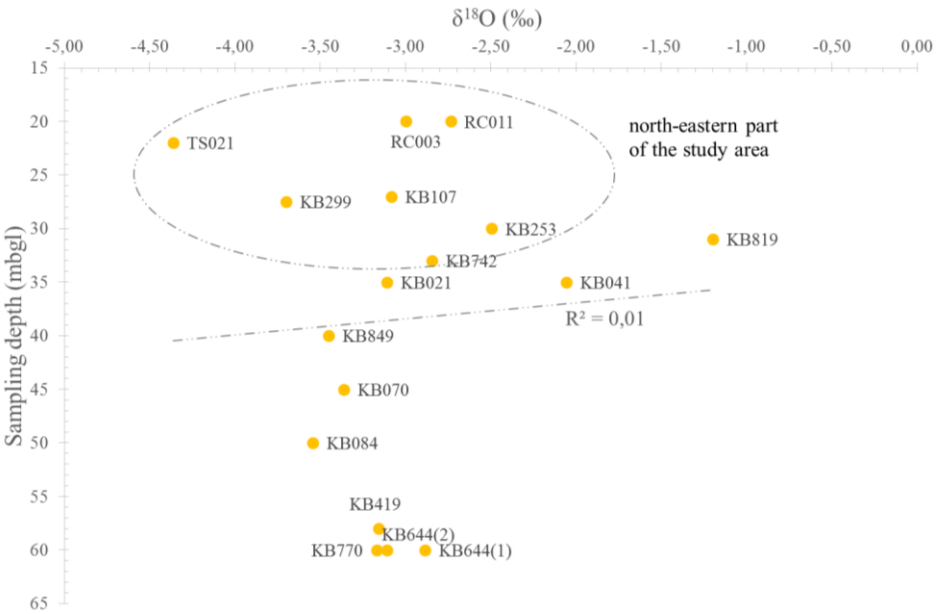

Figure 6-16: Sampling depth (mbgl) vs. $\delta^{18}O$ (‰). The groundwater that was recharged by meteoric water that does not experience significant evaporation (Figure 6-15) was collected at shallow sampling depths in the north-eastern part of the study area.

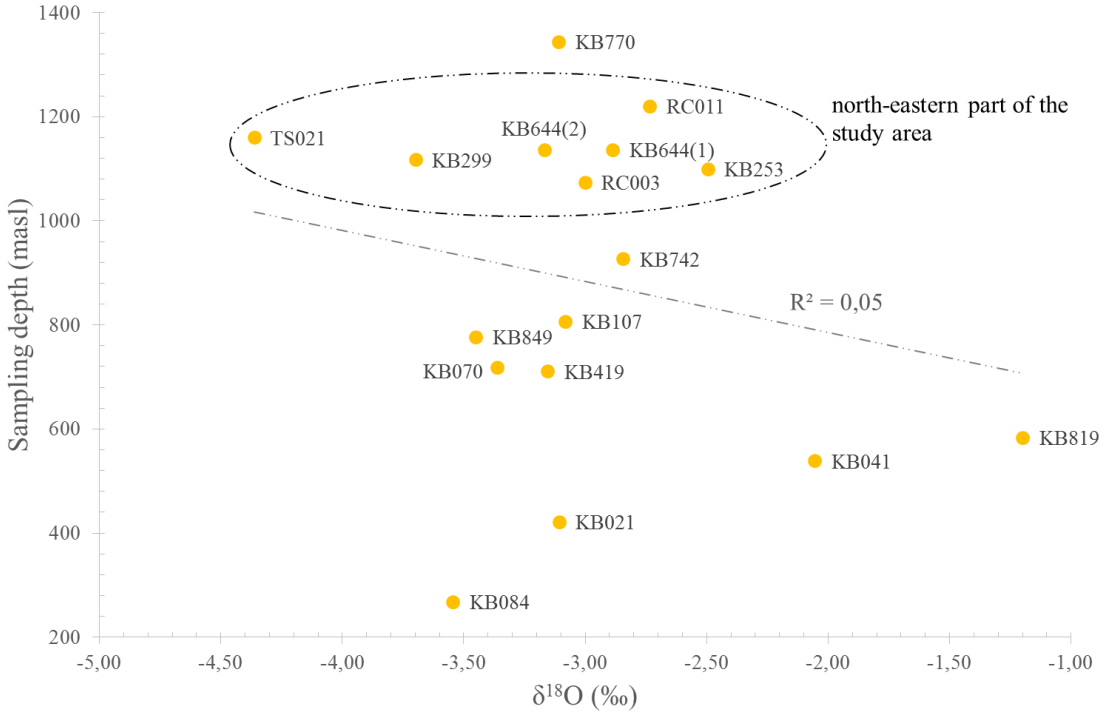

Figure 6-17: Sampling depth (masl) vs. $\delta^{18}O$ (‰). The groundwater that was recharged by meteoric water that does not experience significant evaporation (Figure 6-15) was collected at shallow sampling depths (Figure 6-16) and high elevations.

The salinization of the groundwater in the study area was studied using EC (µS/cm) as a salinity indicator (Sami 1992; Nakwafila 2015). Figure 6-18 is a plot of EC (µS/cm) vs. $\delta^{18}O$ (‰). It shows that EC (µSc/m) has a poor linear correlation with $\delta^{18}O$ (‰) (R^2=0.16). This suggests that there are multiple factors that contribute to groundwater salinity (Nakwafila 2015). Examples may include the lithology, fertilisers and other pollutants. Although site specific solute sources could not be identified, it can be reported that KB644(1) and KB644(2) have the highest EC (µS/cm) values because they were sampled approximately 5 km from a salt pan close to Hofmeyr. There is no linear correlation between EC (µS/cm) and $\delta^{18}O$ (‰) (R^2 = 0.16-Figure 6-18). The same is true for temperature (R^2 = 0.03 Figure 6-19) and sustainable yield (l/s) vs. $\delta^{18}O$ (‰) (R^2 = 0.01) (Figure 6-20).

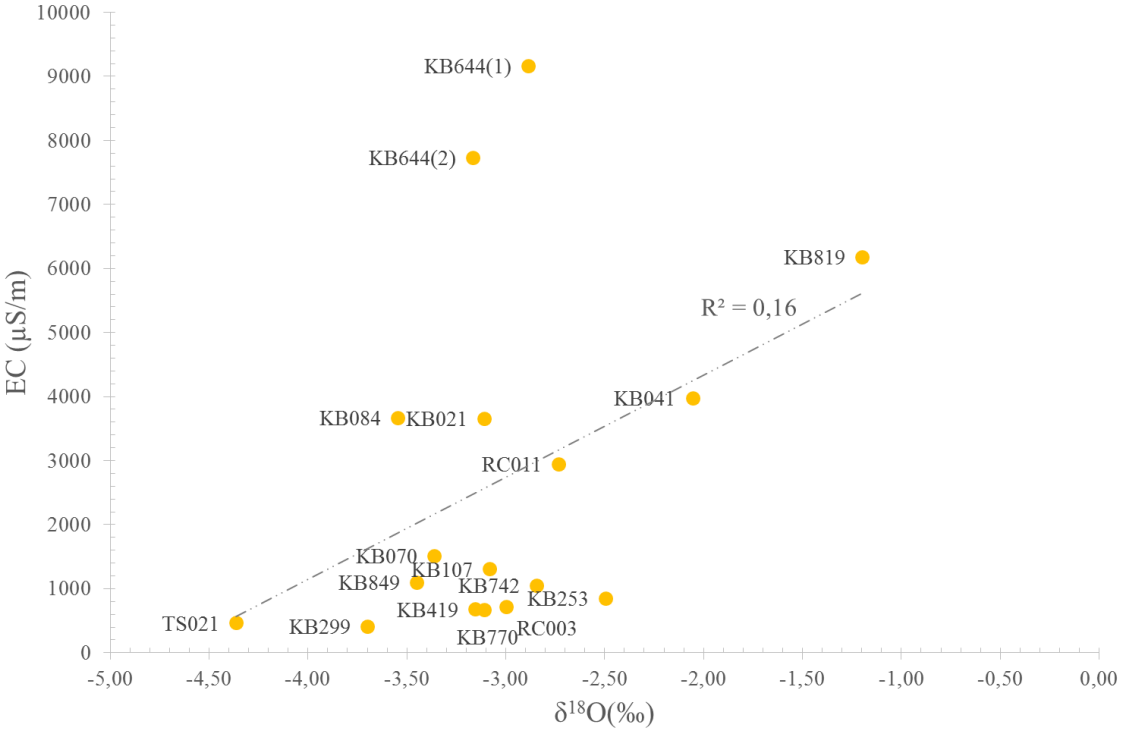

Figure 6-18: EC (µS/m) vs. $\delta^{18}O$ (‰) for the sampled groundwater. This shows the poor linear correlation between EC (µS/m) and $\delta^{18}O$ (‰) (R^2 = 0.16).

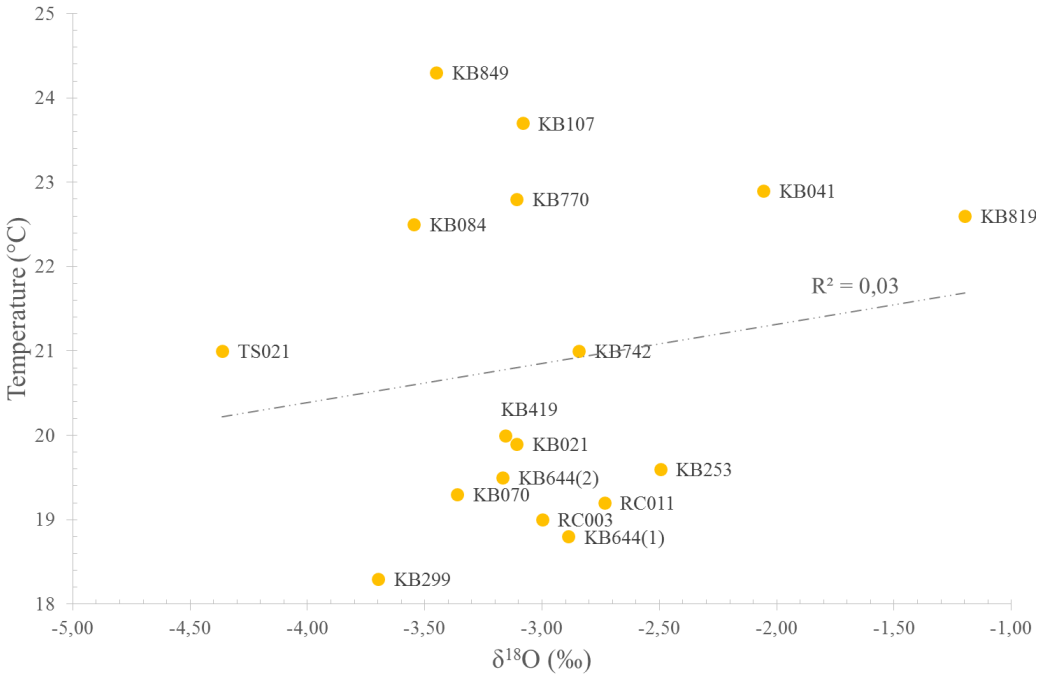

Figure 6-19: Temperature (°C) vs. $\delta^{18}O$ (‰) for the sampled groundwater (R^2 = 0.03).

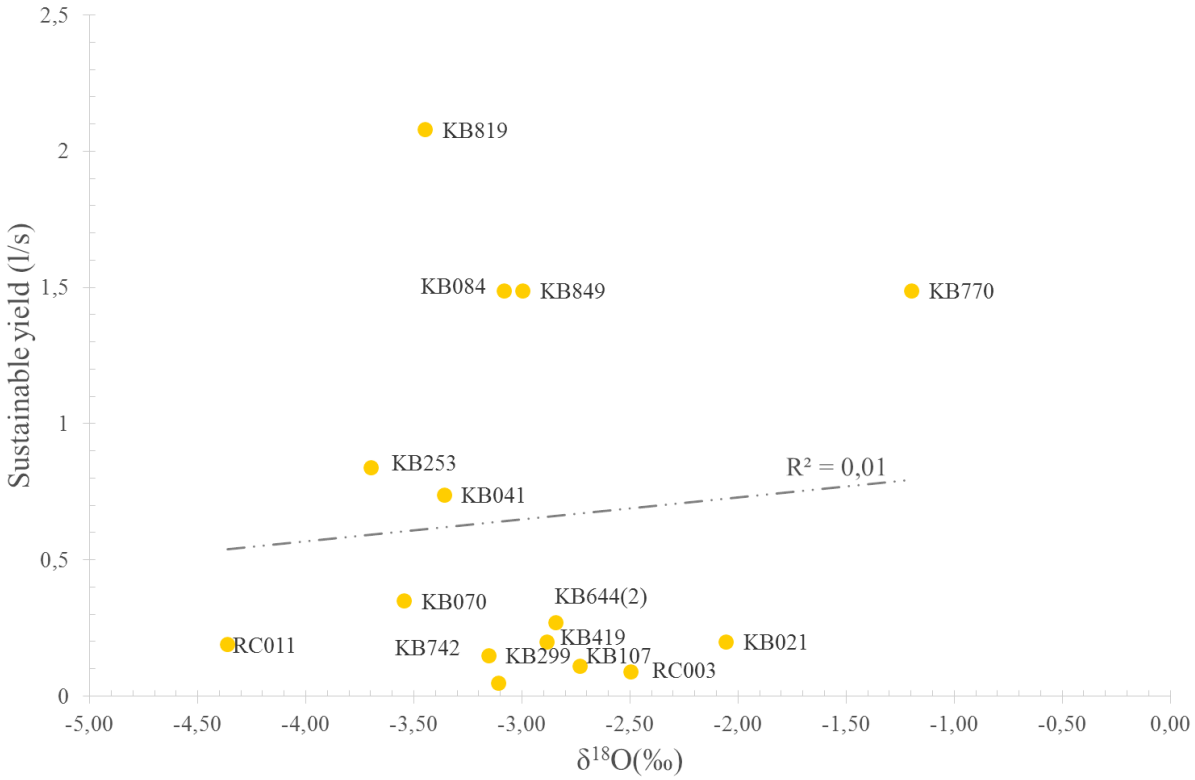

Figure 6-20: Sustainable yield (l/s) vs. ^{18}O (‰) for the sampled groundwater ($R^2 = 0.01$).

7. Conclusion

The aim of this project was to use isotopes (^{14}C, $\delta^{13}C$, ^{3}H and ($\delta^{18}O$ and $\delta^{2}H$)) in conjunction with general field parameters (sampling depth (masl), temperature (°C), EC (µS/m) and sustainable yield (l/s)) to evaluate connectivity between modern groundwater from shallow aquifers (<300 m) with old groundwater from the deep aquifers (> 300 m) in the southern part of the Karoo Basin. The proficiency of using isotopes in defining groundwater groups according to their aquifer origin in the Karoo Basin is discussed in Murray et al. (2015); Miller et al. (2015) and Swana (2016). In Murray et al. (2015) ^{14}C (pMC), $\delta^{18}O$ (‰) and alkalinity are described as having 100% success rate for identifying deep groundwater, ^{3}H (TU), pH and temperature as having a 50-75% success rate, and $\delta^{13}C$ as having a less than 50% success rate (see chapter 1).

There are inconsistencies among the results discussed as shown by the weak correlation factors among the isotope concentrations and field parameters analysed. The inconsistencies, particularly between ^{14}C and ^{3}H suggests that in the Karoo Basin, young or modern groundwater (with detactable tritium concentrations) mixes with old groundwater (low and even undetectable tritium concentrations and ^{14}C<50pMC) (Jasechko et al. 2017). Depsite these inconsistencies, it is a recurring theme that at least 50% of the sampled groundwater is modern. Among all the analysed isotopes and general field parameters, ^{14}C is the only isotope that exclusively classifies four groundwater samples as older groundwater (old/deep groundwater and mixed groundwater). $\delta^{18}O$ (and $\delta^{2}H$) and ^{3}H, due to overlaps among the determining criteria, cannot precicely determine the origin or age of the analysed groundwater. The outcomes of ^{14}C in regards to aquifer connectivity are preferred because ^{14}C has a 100% success rate in dilineating the origin groundwater and has the least amount of overlaps between the constraints of its defining criteria.

The four groundwater samples that are classified as older groundwater (mixed groundwater < 74 pMC and old groundwater < 60 pMC) were collected in the western part of the study area and are aligned parallel to- and north-east of the Cape Mountains (Figure 3 2 & Figure 7-1). Upon ^{14}C age (years) calculations, three more groundwater samples (KB742, KB419 and TS021) were determined to have ^{14}C age (years) similar in age as the groundwater samples with less ^{14}C concentration (≥1700 years), although these samples have modern ^{14}C (pMC) concentrations (>74 pMC). This implies that dilution factors, which are determined when calculating ^{14}C age in groundwater, play an important role in controlling and adjusting the

content of ^{14}C in DIC; and that there is possibly other areas in the study area where older groundwater mixes with younger groundwater or cools during its migration to shallower depths. Figure 7-1 is a 3-d model of the study area, which consolidates the outcomes of this project.

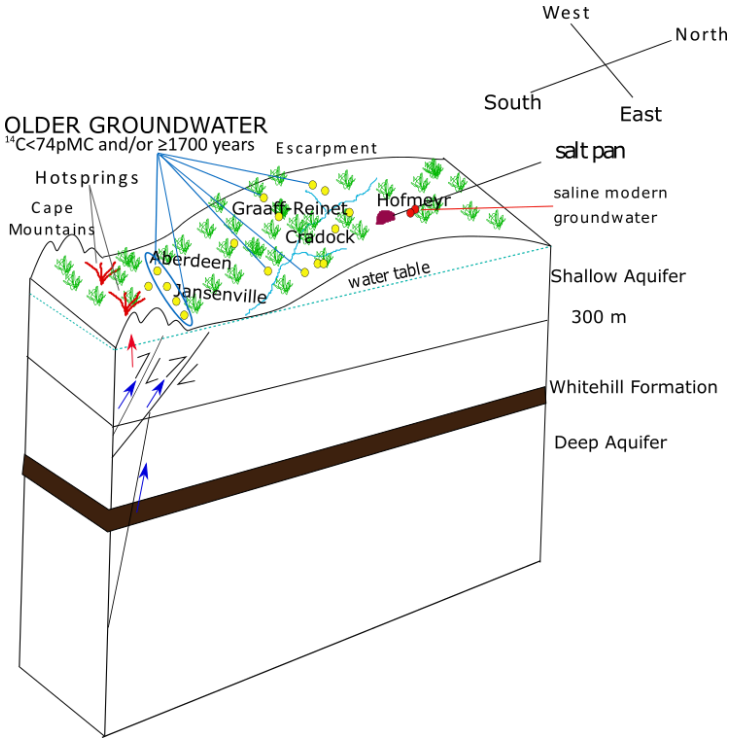

Figure 7-1: Conceptual model for the study area (not to scale). Shown on the figure is the identified area with potential reservoir connectivity in the southern part of the study area, close to the Cape Mountains. A few possibly older groundwater samples (^{14}C (age) $\geq$ 1700 years) also occur at higher elevations across the Great Escarpment.

The groundwater within the main drainage of the Great Fish River generally plots on or close to the GMWL. This suggests that this groundwater is likely meteoric water and did not experience significant evaporation during or after recharge. This groundwater was collected at shallow sampling depths (<35 mbgl). All of the general field parameters have poor linear correlations with the analysed isotopes. The strongest linear correlation (R^2 = 0.38) was between ^{14}C (pMC) and sampling depth (masl). This suggests elevation influences the observed isotope concentrations. The weak linear correlation (R^2 = 0.16) between $\delta^{18}O$ (‰) and EC (µS/cm) suggests that there are multiple factors contributing to the salinisation of groundwater (such as for example contact with the salt pan in Hofmeyr).

8. Recommendations for Future Research

Based on isotopes, this project suggests that there is potential natural reservoir connectivity between shallow aquifer(s) and deep aquifer(s) in the southern part of the Karoo Basin. However, the sample population for this study area is sparse and may explain the poor correlations among the sampled isotopes and other parameters. This implies that further research is needed using isotopes to study groundwater connectivity in the Karoo Basin with increased sample density.

A few key factors pertaining to isotopes in groundwater were not analysed in the sampled groundwater. This includes the analyses of $\delta^{18}O$ and $\delta^{2}H$ in rainwater in the study area, which was substituted with a South African regional MWL (Kirchner & Van Tonder 1991) as was also done by Sami (1992) who conducted a study in Bedford (~ 140 km east of study area). However considering that Bedford is ~140 km from the study area and that the MWL is from nearly 30 years ago there is an urgency to analyse $\delta^{18}O$ and $\delta^{2}H$ in rainwater in the study area and the Karoo Basin as a whole for future studies. It is also suggested that mixing proportions of old groundwater and modern groundwater by using mass-balance and mixing models be resolved (e.g. Schramke et al. 1996). This will assist with determining how much natural reservoir connectivity contributes towards groundwater pollution and, how much anthropogenic activities might contribute to groundwater pollution. Also, it will be useful to determine site specific salinity sources to groundwater systems in the Karoo Basin before the on-set of hydraulic fracturing. This should allow scientists to better delineate the environmental footprint of hydraulic fracturing from natural pollutants or pollutants from other sources.

It is suggested that the abovementioned recommendations be incorporated into future transdisciplinary monitoring efforts that will take place before and after hydraulic fracturing is implemented. Conducting these recommendations before hydraulic fracturing will assist the South African government with developing a legislative framework that urges companies to take extra caution when fracking around areas with high contamination risk. Conducting these recommendations after the implementation of hydraulic fracturing will assist with determining the footprint of hydraulic fracturing after implementation. As referenced in this thesis MT surveys can be instrumental in delineating where older groundwater is likely migrating to shallower depths. Thus, it is recommended that in the future groundwater studies such as this one incorporate MT surveys and other geophysical applications to study reservoir connectivity.

Reference List

Academy of Science of South Africa (ASSAf) (2016) South Africa's Technical Readiness to Support the Shale Gas Industry. doi:10.17159/assaf.2016/0003.

Adams S (2011) Groundwater use potential for South Africa. Water Research Commission, Pretoria. http://www.wrc.org.za/News/Pages/GroundwaterusepotentialforSouthAfrica.aspx.

Adams S, Titus R, Pietersen K, Tredoux G and Harris C (2001) Hydrochemical characteristics of aquifers near Sutherland in the Western Karoo, South Africa. Journal of Hydrology 241: 91-103. doi:10.1016/S0022-1694(00)00370-X.

Adelana SMA (2005) Environmental Isotopes in Hydrogeology. In: Lehr J(ay), Keeley J, and Lehr J(anet) (editors) Water Encyclopedia p. 227-233. doi:10.1002/047147844X.gw211.

African Ministries‟ Council on Water (AMCOW) (2008) Roadmap for the Africa Groundwater Commission. United Nations Environment Programme (UNEP) / United Nations Educational, Scientific and Cultural Organization (UNESCO) / UWC.

Aggarwal PK (2013) Introduction: Chapter 1 In: Suckow A, Aggarwal PK and Araguas-Araguas L (editors) Isotope methods for dating old groundwater. International Atomic Energy Agency (IAEA). http://www-pub.iaea.org/MTCD/Publications/PDF/Pub1587_web.pdf.

Aggarwal PK, Alduchov OA, Froehlich KO, Araguas-Araguas LJ, Sturchio NC and Kurita N (2012) Stable isotopes in global precipitation: A unified interpretation based on atmospheric moisture residence time. Geophysical Research Letters 39(11):L11705. doi:10.1029/2012GL051937.

Appelo CAJ and Postma D (2005) Geochemistry, Groundwater and Pollution (2nd Edition). AA Balkema Publishers. 634p.

Atkinson AP, Cartwright I, Gilfedder BS, Cendon DI, Unland NP and Hofmann H (2014) Using ^{14}C and ^{3}H to understand groundwater flow and recharge in an aquifer window. Hydrology and Earth System Sciences 18:4951–4964. doi:10.5194/hess-18-4951-2014.

Barbetti M (1980) Geomagnetic strength over the last 50 000 years and changes in atmospheric ^{14}C concentration: Emerging trends. Radiocarbon 22(2):192-199. doi:10.1017/S0033822200009450.

Berman ES, Levin NE, Landais A, Li S and Owano T (2013) Measurement of $\delta^{18}O$, $\delta^{17}O$, and ^{17}O-excess in Water by Off-Axis Integrated Cavity Output Spectroscopy and Isotope Ratio Mass Spectrometry. Analytical Chemistry 85(21):10392−10398.

Black D, Booth P and de Wit M (2016) Petrographic, geochemical, and petro-physical analysis of the Collingham Formation in the context of shale gas from a borehole (STT 2) near Jansenville, Eastern Cape, South Africa-potential cap rock to shale gas in the Karoo. South African Journal of Geology 119(1). doi:10.2113/gssajg.119.1.0.

Booth PWK and Shone RW (2002) A review of thrust faulting in the Eastern Cape Fold Belt, South Africa, and the implications for current lithostratigraphic interpretation of the Cape Supergroup. Journal of African Earth Sciences 34(3-4):179-190. doi:10.1016/S0899-5362(02)00017-9.

Bordy EM (2008) Enigmatic trace fossils from the aeolian lower Jurassic Clarens Formation, Southern Africa. Palaeontologia Electronica, [Online]. 11(3), 16A-16p. Available at: https://palaeo-electronica.org/2008_3/150/intro.html [Accessed 15 October 2018].

Bordy E and Eriksson P (2015) Lithostratigraphy of the Elliot Formation (Karoo Supergroup), South Africa. South African Journal of Geology 118(3):311-316. doi:10.2113/gssajg.118.3.311.

Branch T, Ritter O, Weckmann U, Sachsenhofer RF, Schilling F (2007) The Whitehill Formation – a high conductivity marker horizon in the Karoo Basin. South African Journal of Geology 110(2-3):465-476. doi:10.2113/gssajg.110.2-3.465.

Branch T (2013) Electrical conductivity experiments on carbon-rich Karoo shales and forward modelling of aeromagnetic data across the Beattie Anomaly. Unpublished MSc Thesis. Nelson Mandela Metropolitan University.

Brantley SL, Goldhaber MB, and Ragnarsdottir KV (2007) Crossing disciplines and scales to understand the Critical Zone. Elements 3(5):307-314. doi:10.2113/gselements.3.5.307.

Braune E, Adams S and Fourie F (2014) 20 years of groundwater research development and implementation in South Africa, 1994-2014. Report No. SP 78/14. Water Research Commission, Pretoria.

Butler MJ (1998) Groundwater pollution at sanitary landfill sites: geohydrological, environmental isotope and hydrochemical studies. Unpublished MSc thesis. Witwatersrand University.

Button TW (1991) Stable Carbon Isotope Ratios of Natural Materials: II. Atmospheric, Terrestrial, Marine, and Freshwater Environments. In: D. C. Coleman & B. Fry , eds. Carbon Isotope Techniques Volume 1 of Isotopic techniques in plant, soil, and aquatic biology series. s.l.:Academic Press, pp. 173-183.

Cagniard L (1953) Basic Theory of the Magneto-Telluric Method of Geophysical Prospecting. Geophysics 18(3):605-635. doi:10.1190/1.1437915.

Cai X, Altchenko Y and Chavula G (2017) Availability and use of water resources In: Lautze J, Phiri Z, Smakhtin V and Saruchera D (editors) The Zambezi River Basin: Water and sustainable development-Earthscan Series on Major River Basins of the World. Routledge, New York, p 7-28.

Carbone MS and Trumbore SE (2007) Contribution of new photosynthetic assimilates to respiration by perennial grasses and shrubs: residence times and allocation patterns. New Phytologist 176(1):124-135. doi:10.1111/j.1469-8137.2007.02153.x.

Cerling TE, Solomon DK, Quade J and Bowman JR (1991) On isotopic composition of carbon in soil carbon dioxide. Geochimica et Cosmochimica Acta 55(11):3403-3405. doi:10.1016/0016-7037(91)90498-T.

Chere N, Linol B, Sculz HM and de Wit (2017) Lateral and temporal variations of black shales across the southern Karoo Basin-Implications for shale gas exploration. South African Journal of Geology (in press).

Chiu TC, Fairbanks RG, Cao L and Mortlock RA (2007) Analysis of the atmospheric ^{14}C record spanning the past 50 000 years derived from high-precision $^{230}Th/^{234}U/^{238}U$, $^{231}Pa/^{235}U$and ^{14}C dates on fossil corals. Quaternary Science Reviews 26(1-2):18-36.

Chorover J, Kretzschmar R, Garcia-Pichel F and Sparks DL (2007) Soil Biogeochemical Processes within the Critical Zone. ELEMENTS 3:321-326.

Clark CE, Horner RM and Harto CB (2013) Life cycle water consumption for shale gas and conventional natural gas. Environmental science and technology 47(20): 11829-11836.

Clark ID (2015) Groundwater geochemistry and isotopes. CRC Press, Boca Raton. 456p.

Clark ID and Fritz P (1997) Environmental Isotopes in Hydrogeology. Lewis Publishers, Boca Raton, 290p.

Clark ID and Fritz P (2000) Chapter 2: Tracing the Hydrological Cycle http://mysite.science.uottawa.ca/eih/ch2/ch2.htm#tei.

Craddock JP, McKiernan AW and de Wit MJ (2007) Calcite twin analysis in syntectonic calcite, Cape Fold Belt, South Africa: Implications for fold and cleavage formation within a shallow thrust front

Craig H (1961) Isotopic Variations in Meteoric Waters. Science 133(3465):1702-1703.

Dansgaard W (1964) Stable isotopes in precipitation. Tellus 16(4):436-468. doi:10.1111/j.2153-3490.1964.tb00181.x.

Davies RJ, Almond S, Ward RS, Jackson RB, Adams C, Worrall F, Herringshaw LG, Gluyas JG and Whitehead MA (2014) Oil and gas wells and their integrity: Implications for shale and unconventional resource exploitation. Marine and Petroleum Geology 56:239-254. doi:10.1016/j.marpetgeo.2014.03.001.

Davis C (2010) A Climate Change Handbook for North-Eastern South Africa. Council for Scientific and Industrial Research (CSIR), Pretoria. https://researchspace.csir.co.za/dspace/bitstream/handle/10204/4088/Davis_2010.pdf ?se quence=1&isAllowed=y.

De Wit (2016) Organic Carbon Isotope Stratigraphy of the Karoo Supergroup In: Linol B and de Wit MJ (editors) Origin and Evolution of the Cape Mountains and Karoo Basin. Springer International Publishing, Switzerland, pp.169-180.

Department of Environmental Affairs (2015) Climate change adaptation plans for South African Biomes https://www.environment.gov.za/sites/default/files/reports/climatechangeadaptation_plansforsouthafricanbiomes_report.pdf.

Department of Mineral Resources (2012) Investigation of hydraulic fracturing in the Karoo of South Africa.

https://www.gov.za/sites/www.gov.za/files/investigation_hydraulic_fracturing_Karoo_asin_sa_executive_summary.pdf.

Department of Water Affairs (2004) Groundwater Protection - Involving Community Members in a Hydrocensus http://www.dwa.gov.za/Groundwater/NORADToolkit/3.1%20Involving%20community%20in%20hydrocensus.pdf.

Department of Water Affairs and Forestry (1996). South African Water quality guidelines Volume 1: Domestic Use. http://www.dwa.gov.za/iwqs/wq_guide/Pol_saWQguideFRESH_vol1_Domesticuse.PDF.

Department of Water and Sanitation (2016) National Groundwater Strategy. http://www.dwa.gov.za/Groundwater/Documents/NGS_Draft-Final_04012017.pdf.

Department of Water and Sanitation (2018). *dwa.gov*. http://www.dwa.gov.za/National%20Water%20and%20Sanitation%20Master%20Plan/Documents/NWSMP_Vol%201_Call%20to%20Action_Ver%208.2_20180112.pdf.

Dhansay T (2017) On the evolution and mechanics of the brittle upper crust below South Africa: implications toward the sustainable transformation of exploration/exploitation in the Critical Zone. Unpublished PhD Thesis. Nelson Mandela University.

Diamond RE (2014) Stable Isotope Hydrology of the Table Mountain Group. Unpublished PhD Thesis. University of Cape Town.

Diamond RE and Harris C (2000) Oxygen and hydrogen isotope geochemistry of thermal springs of the Western Cape, South Africa: Recharge at high altitude? Journal of African Earth Sciences 31(3-4):467-481. doi:10.1016/S0899-5362(00)80002-0.

Director of Central Intelligence NIE 22-64 (1964) The French Advanced Weapons Program. https://nsarchive2.gwu.edu/NSAEBB/NSAEBB184/FR23.pdf.

Du Toit (2013) Fracking: Groundwater Threats to Karoo Towns. Karoo Space http://karoospace.co.za/fracking-groundwater-threats-to-karoo-towns/.

Du Toit AL (1954) The Geology of South Africa (3rd edition). Oliver and Boyd, Edinburgh.

Duncan RA, Hooper PR, Rehacek J, Marsh JS and Duncan AR (1997) The timing and duration of the Karoo igneous event, southern Gondwana. Journal of Geophysical Research 102(B8):18127-18138. doi:10.1029/97JB00972.

Dupont LM, Rommerskirchen F, Mollenhauer G and Schefuß E (2013) Miocene to Pliocene changes in South African hydrology. Earth and Planetary Science Letters 375:408-417.

Eamus D (2006) Ecohydrology: Vegetation Function, Water and Resource Management. Csiro Publishing, Clayton South, 348p.

Eastern Cape Socio Economic Consultative Council (ECSC) (2016) Highlights of the community survey 2016: selected findings for the Eastern Cape http://www.ecsecc.org/documentrepository/informationcentre/community-survey_73473.pdf.

ECOMETRIX Incorporated in association with Rowan Williams Davies and Irwin Incorporated (2009) Investigation of the Environmental Fate of Tritium in the Atmosphere, Ottawa: Canadian Nuclear Safety Commission. http://nuclearsafety.gc.ca/pubs_catalogue/uploads/Investigation_of_Environmental_Fate_of_Tritium_in_the_Atmosphere_INFO-0792_e.pdf.

Egle S (1996) Paleo-hydrology of the Cape Fold Belt and the Karoo Basin, South Africa. Unpublished PhD thesis. University of Vienna.

Engelder T (2013) The fracking debate: Terry Engelder at TEDxPSU (YouTube). https://www.youtube.com/watch?time_continue=2&v=BBSVLGf7zPI.

Engelkemeir AG, Hamill WH, Inghram MG and Libby WF (1949) Half-life of radiocarbon (^{14}C). Physical Review 75(12):1825-1833. doi:10.1103/PhysRev.75.1825.

Erasmus SW, Muller M, van der Rijst M and Hoffman LC (2016) Stable isotope ratio analysis: A potential analytical tool for the authentication of South African lamb meat. Food Chemistry 192:997-1005. doi:10.1016/j.foodchem.2015.07.121.

Fabbri P, Ortombina M, Piccinini L (2012) Estimation of Hydraulic Conductivity Using the Slug Test Method in a Shallow Aquifer in the Venetian Plain (NE, Italy). Aqua Mundi 3(2):125-133.

Fan Y (2015) Groundwater in the Earth's critical zone: relevance to large-scale patterns and processes. Water Resources Research 51(5):3052-3069. doi: 10.1002/2015WR017037.

Fetter CW (2001) Applied Hydrogeology (4th edition). Prentice-Hall Incorporated, New Jersey. 598p.

Fontes JC and Garnier JM (1979) Determination of the initial ^{14}C activity of the total dissolved carbon: A review of the existing models and a new approach. Water Resources Research 15(2):399-413.

Fowler WA, Burbidge GR and Burbidge EM (1955) Stellar Evolution and the synthesis of the elements. Astrophysical Journal 122:271-285.

Froehlich K, Gibson JJ and Aggarwal P (2002) Deuterium excess in precipitation and its climatological significance. International Atomic Energy Agency (IAEA) 34(10). https://inis.iaea.org/search/search.aspx?orig_q=RN:34017972.

Gallegos TJ, Varela BA, Haines SS and Engle MA (2015) Hydraulic fracturing water use variability in the United States and potential environmental implications. Water Resources Research 51(7): 5839-5845. doi:10.1002/2015WR017278.

Garstang M, Coleman AD and Therrell M (2014) Climate and the Mfecane. South African Journal of Science 110(5/6):1-7.

Gat JR (1996) Oxygen and hydrogen isotopes in the hydrologic cycle. Annual Review of Earth and Planetary Sciences 24(1):225–262. doi:10.1146/annurev.earth.24.1.225.

Gauch Jr. HG (2012) Scientific method in brief. Cambridge University Press, New York. 270p.

Geel C, Schulz HM, Booth P, de Wit M and Horsfield B (2013) Shale gas characteristics of Permian black shales in South Africa: results from recent drilling in the Ecca Group, Eastern Cape. Energy Procedia 40:256-265. doi:10.1016/j.egypro.2013.08.030.

Geel C, Schulz HM, Booth P, de Wit M and Horsfield B (2015) Palaeo-environment, diagenesis and characteristics of Permian black shales in the Lower Karoo Supergroup flanking the Cape Fold Belt near Jansenville, Eastern Cape, South Africa:implications for the shale gas potential of the Karoo Basin. South African Journal of Geology 118(3):249-274. doi:10.2113/gssajg.118.3.249.

Geyh MA (2000) An overview of ^{14}C analysis in the study of groundwater. Radiocarbon 42(1):99-114.

Gil L (2017) Scientists Explore Groundwater in the Sahel with Nuclear Technology.International Atomic Energy Agency (IAEA). https://www.iaea.org/newscenter/news/scientists-explore-groundwater-in-the-sahel-with-nuclear-technology.

Godwin H (1962) Half-life of radiocarbon. Nature 195(4845):984. doi:10.1038/195984a0.

Graven HD (2015) Impact of fossil fuel emissions on atmospheric radiocarbon and various applications of radiocarbon over this century. Proceedings of the National Academy of Sciences of the United States of America 112(31):9542-9545.doi:10.1073/pnas.1504467112.

Ground Water Division of the Geological Society of South Africa (2008) Groundwater Aspects. Parliamentary Portfolio Committee on Water Affairs and Forestry: Review of the National Water Act (Act No.36 of 1998). http://pmg-assets.s3-website-eu-west-1.amazonaws.com/docs/081022groundwater.pdf.

Harris C, Burgers C, Miller JA and Rawoot F (2010) O- and H-isotope record of Cape Town rainfall from 1996 to 2008, and its application to recharge studies of Table Mountain groundwater, South Africa. South African Journal of Geology 113(1): 33-56.

Harris C, Stock WD and Lanham J (1997) Stable isotope constraints on the origin of CO_2 gas exhalations at Bongwan, Natal. South African Journal of Geology 100(3):261-266. doi:10.2113/gssajg.113.1.33.

Herbst P (2013) South African‟s Water Conservation and Water Demand Management (WCWDM) Overview Presentation. African Water Summit, Bloemfontein.

Hoefs (1997) Stable isotope geochemistry (4th edition). Springer-Verlag, Berlin. 213p.

Holzförster F (2007) Lithology and depositional environments of the Lower Jurassic Clarens Formation in the eastern Cape, South Africa. South African Journal of Geology 110(4):543-560.

Horton CW and Hoffman AAJ (1962) Magnetotelluric Fields in the Frequency Range 0.03 to 7 Cycles Per Kilosecond: Part 1. Power Spectra. Journal of Research of the National Bureau of Standards-D. Radio Propagation 66(4):487-494.

Hua Q (2016) Vignette Collection: Radiocarbon calibration https://serc.carleton.edu/36729.

Hussain SD (1991) Measurement of Carbon-14 in Hydrological samples (No. PINSTECH-RIAD-129). Pakistan Institute of Nuclear Science and Technology http://www.iaea.org/inis/collection/NCLCollectionStore/_Public/24/022/24022324.pdf.

Ingerson E and Pearson FJ (1964) Estimation of age and rate of motion of ground water by the ^{14}C method In: Miyake Y and Koyama T (editors) Recent Researches in the fields of Hydrosphere, Atmosphere and Nuclear Chemistry. Maruzen, Tokyo, 263-283.

Ingraffea AR, Wells MT, Santoro RL and Shonkoff SBC (2014) Assessment and risk analysis of casing and cement impairment in oil and gas wells in Pennsylvania, 2000–2012. Proceedings of the National Academy of Sciences 111(30): 10955-10960. doi: 10.1073/pnas.1323422111.

Jasechko S, Perrone D, Befus KM, Cardenas B, Ferguson G, Gleeson T, Luijendijk E, McDonnell JJ, Taylor RG, Wada Y, Kirchner JW (2017) Global aquifers dominated by fossil groundwaters but wells vulnerable to modern contamination. NATURE GEOSCIENCE 10. www.nature.com/naturegeoscience.

Johnson MR (1966) Stratigraphy of the Cape and Karroo Systems in the Eastern Cape Province. Unpublished MSc Thesis. Rhodes University.

Johnson MR, van Vuururen CJ, Visser JNJ, Cole DI Wickens HDV, Christie ADM and Roberts DL (1997) The Foreland Karoo Basin, South Africa In: Selley RC (editor) Sedimentary basins of the World: African Basins. Elsevier, Amsterdam, pp. 269–317.

Jury MR (2013) Climate trends in southern Africa. South African Journal of Science 109(1-2):1996-7489. http://www.scielo.org.za/pdf/sajs/v109n1-2/13.pdf.

Kalin RM (1999) Radiocarbon dating of groundwater systems In: Cook PG and Herczeg AL (editors) Environmental Tracers in Subsurface Hydrology. Springer Science and Business Media, LLC, New York, pp.111-144.

Kane RP (2009) Periodicities, ENSO effects and trends of some South African rainfall series: an update. South African Journal of Science 105(5-6):199-207.

Kargbo DM, Wilhelm RG, Campbell DJ (2010) Natural gas plays in the Marcellus shale: challenges and potential opportunities. Environment Science and Technology 44(15):5679-5684. doi:10.1021/es903811p.

Karoo Groundwater Expert Group (KGEG) (2013). Karoo Groundwater Atlas (Volume 2). Shell. http://gwd.org.za/sites/gwd.org.za/files/KGEG_Karoo%20Groundwater%20Atlas%20V olume%202_Final_12Aug13_opt_opt.pdf.

Katz JI (2008) Lessons Learned from Nonproliferation Successes and Failures. Comparative Strategy 27(5):426-430. doi:10.1080/01495930802358398.

Keke Z (2006) Groundwater research needs in the Eastern Cape Province. http://www.wrc.org.za/Lists/Knowledge%20Hub%20Items/Attachments/3718/TT%228 6-06-EXECUTIVE%20SUMMARY.pdf.

Key RM (2001) Radiocarbon Measurements. Uranium-Thorium Decay Series in the Oceans Overview. doi:10.1006/rwos.2001.0162.

Kim K and Lee X (2011) Isotopic enrichment of liquid water during evaporation from water surfaces. Journal of Hydrology 399(3-4):364-375. doi:10.1016/j.jhydrol.2011.01.008.

Kirchner J, van Tonder, GJ and Lukas E (1991) Exploitation Potential of Karoo Aquifers. Report No. 170/1/91. Water Research Commission, Pretoria.

Kruger AC, Goliger AM, Retirf JV and Sekele S (2010) Strong wind climatic zones in South Africa. Wind and Structures 13(1):37-55.

Lavoisier A (1783) Report of a memoir read by M. Lavoisier at the public session of the Royal Academy of Sciences of November 12, on the nature of water and on experiments which appear to prove that this substance is not strictly speaking an element but that it is susceptible of decomposition and recomposition. Observations sur la Physique 23:452-455.

Lemay TG Carbon-14 Dating of Groundwater from Selected Wells in Quaternary and Quaternary–Tertiary Sediments, Athabasca Oil Sands (In Situ) Area, Alberta. Alberta Energy and Utilities Board, Alberta Geological Survey, Geo-Note 2002-03.

Libby WF (1946) Atmospheric Helium Three and Radiocarbon from Cosmic Radiation. Physical Review 69(11-12):671-672. doi:10.1103/PhysRev.69.671.2.

Libby WF, Anderson EC and Arnold JR (1949) Age Determination by Radiocarbon Content: World-Wide Assay of Natural Radiocarbon. Science 109(2827):227-228. doi:10.1126/science.109.2827.227.

Lin H (2010). Earth's Critical Zone and hydropedology: concepts, characteristics, and advances. Hydrology and Earth System Science 14(1):25-45. doi: 10.5194/hess-14-25-2010.

Lindeque AS and de Wit MJ (2009) Revealing the Beattie Magnetic Anomaly and the anatomy of the crust of southernmost Africa: Geophysics and deep surface geology where the Cape Fold Belt and Karoo Basin meet. 11th SAGA Biennial Technical Meeting and Exhibition pp. 490-499, Swaziland.

Linol B and de Wit MJ (2016) Origin and Evolution of the Cape Mountains and Karoo Basin. Springer International Publishing, Switzerland. 193p.

Linol B, Chere N, Muedi T, Nengovhela V, de Wit MJ (2016) Deep Borehole Lithostratigraphy and Basin Structure of the Southern Karoo Basin Re-Visited In: Linol B and de Wit M (editors) Origin and Evolution of The Cape-Karoo Mountains. Springer International Publishing, Switzerland, pp. 3-13.

Lucas LL and Unterweger MP (2000) Comprehensive Review and Critical Evaluation of the Half-Life of Tritium. Journal of Research of the National Institute of Standards and Technology 105(4):541-549. doi:10.6028/jres.105.043.

Lynch SD (2004) Development of a raster database of annual, monthly and daily rainfall for Southern Africa. Report No. 1156/1/04. Water Research Commission, Pretoria.

Mazor E (2003) Chemical and Isotopic Groundwater Hydrology (3rd edition). Mercel Dekker, New York. 352p.

Mazor E and Verhagen B (1983) Dissolved ions, stable and radioactive isotopes and noble gases in thermal waters of South Africa. Journal of Hydrology 63(3-4):315-329.

McGuire K and McDonnell J (2007) Stable Isotope Tracers in Watershed Hydrology. In: Michener R and Lajtha J (editors) Stable Isotopes in Ecology and Environmental Science. Blackwell Publishing, Malden, pp. 335-365.

Merkel BJ and Planer-Friedrich B (2008) Groundwater Geochemistry: A Practical Guide to Modeling of Natural and Contaminated Aquatic Systems (2nd edition). Springer-Verlag, Berlin Heidelberg. 200p.

Meyer R, Talma AS, Duvenhage AWA, Eglington BM, Taljaard J, Botha JP, Verwey J and van der Voort I (2001) Geohydrological investigation and evaluation of the Zululand Coastal Aquifer. Report No. 221/1/1. Water Research Commission, Pretoria.

Midgley JJ, Scott DF (1994) The use of stable isotopes of water (D and ^{18}O) in hydrological studies in the Jonkershoek Valley. Water SA 20(2):151-154.

Miller JA, Swana K, Talma S, Vengosh A, Butler M, Tredoux G, Murray R and Butler MJ (2015) O, H, C_{DIC}, Sr, B and ^{14}C Isotope fingerprinting of deep groundwaters in the Karoo Basin, South Africa as a precursor to shale gas exploration. Procedia Earth and planetary Science 13:211-214. doi:10.1016/j.proeps.2015.07.050.

Milton SJ (2004) Grasses as invasive alien plants in South Africa. South African Journal of Science 100(1-2):69-74.

Mook WG (editor) (2000) Environmental Isotopes in the Hydrological Cycle: Principles and Applications. International Atomic Energy Agency (IAEA) and United Nations Educational Scientific and Cultural Organization (UNESCO), Paris/Viena, 280p.

Mook WG and van der Plicht J (1999) REPORTING ^{14}C ACTIVITIES AND CONCENTRATIONS. RADIOCARBON, 41(3):227-239.

Moore RD, Richards G, Story A (2008) Electrical Conductivity as an Indicator of Water Chemistry and Hydrologic Process. Streamline: Watershed Management Bulletin 11(2):25-29.

Morkel B and de Wit (2017) Trying not to repeat history: Are shale gas development and broad-based economic development compatible? (Country Chapter/South Africa) In: Gamper-Rabindram S (editor) The Shale Dilema: A Global Perspective on Fracking and Shale Development. University of Pittsburgh University Press (in press).

Mucina L, Rutherford MC, Palmer AR, Milton SJ, Scott L, Lloyd JW (2006) Nama-Karoo Biome. In Mucina L and Rutherford MC (editors) The Vegetation of South Africa, Lesotho and Swaziland. South African National Biodiversity Institute Strelitzia 19, Pretoria, pp. 324-347.

Münnich KO (1957) Messung des ^{14}C Gehaltes von hartem Grundwasser. Naturwissenschaften 34:32-33.

Murray R, Baker K, Ravenscroft P, Musekiwa C and Dennis R (2012) A groundwater-planning toolkit for the main Karoo Basin: Identifying and quantifying groundwater-development options incorporating the concept of wellfield yields and aquifer firm yields. Water S.A 38(3):407-416.

Murray R, Swana K, Miller JA, Talma S, Tredooux G, Vengosh A and Darrah T (2015) The Use of Chemistry, Isotopes and Gases as Indicators of Deeper Circulating Groundwater in the Main Karoo Basin. Report No. 2254/1/15. Water Research Commission, Pretoria.

Myers (2012) Potential Contaminant Pathways from Hydraulically Fractured Shale to Aquifers. Groundwater 50(6):872-882. doi:10.1111/j.1745-6584.2012.00933.x.

Naidu GD (2012) Magnetotellurics: Basic Theoretical Concepts In G. D. Naidu (editor) Deep Crustal Structure of the Son-Narmada-Tapti Lineament, Central India. Springer, Berlin, Heidelberg, pp. 3-35.

Nakwafila AN (2015) Salinisation sources and mechanisms in shallow alluvial aquifers along the Buffels River, Northern Cape Province, South Africa. Unpublished MSc thesis. Stellenbosch University.

National Planning Commission (2011) National Development Pan: Vision for 2030. https://heaids.org.za/site/assets/files/1267/npc_national_development_plan_vision_2030 _-lo-res.pdf.

National Research Council (NRC) (2009) Frontiers in Soil Science Research: Report of a Workshop. National Academies Press, Washington. 80p.

Netshishivhe S (2014) The Karoo Fracking Scenario: Can Development and Environmental Wellbeing Coexist, or Must One of Them Prevail? Policy Brief No.109. Africa Institute of South Africa. http://www.hsrc.ac.za/uploads/pageContent/5293/The%20Karoo%20Fracking%20Scenario.pdf.

Ola SA, Fadugba OG, Uduebor MA (2016) Slug Tests for Determination of Hydraulic Conductivity of Contaminated Wells. Environment and Natural Resources Research 6(2):156-165.

Ostle N, Ineson P and Sleep D (2000) Carbon assimilation and turnover in grassland vegetation using an in situ $^{13}CO_2$ pulse labelling system. Rapid Communications in Mass Spectrometry 14(15):1345-1350.

Parsekian AD, Singha K, Minsley BJ, Holbrook WS, and Slater L (2014) Multiscale geophysical imaging of the Critical Zone. Reviews of Geophysics 53(1):1-26.

Penna N, Stenni B, Sanda M, Wrede S, Gobbi A, Borga M, Fischer BMC, Bonazza M, Bogaard TA and Charova Z (2010) On the reproducibility and repeatability of laser absorption spectroscopy measurements for δ^2H and $\delta^{18}O$ isotopic analysis. Hydrology and Earth System Sciences Discussions 14(8): 1551-1566. doi:10.5194/hessd-7-2975-2010.

Plummer LN and Glynn PD (2013) Radiocarbon dating in groundwater systems: Chapter 4 In: Suckow A, Aggarwal PK and Araguas-Araguas L (editors) Isotope methods for dating old groundwater. International Atomic Energy Agency (IAEA), pp. 33-89.

Plummer LN, Sanford WE and Glynn PD (2013) Characterization and conceptualization of groundwater flow systems: Chapter 2. In: Suckow A, Aggarwal PK and Araguas-Araguas L (editors) Isotope methods for dating old groundwater. International Atomic Energy Agency (IAEA), pp. 5-17.

Pourimani R and Aghamohammadi M (2014) Determination of tritium concentration in heavy water. World Journal of Nuclear Science and Technology 4:170-176. doi:10.4236/wjnst.2014.43022.

Praˇvaˇlie R (2014) Nuclear Weapons Tests and Environmental Consequences: A Global Perspective. Ambio 43(6):729-744. doi:10.1007%2Fs13280-014-0491-1.

Ramnarine R, Wagner-Riddle C, Dunfield KE and Voroney RP (2012) Contributions of carbonates to soil CO_2 emissions. Canadian Journal of Soil Science 92(4):599-607. doi:10.4141/cjss2011-025.

Reason CJ and Jagadheesha D (2005) Relationships between South Atlantic SST Variability and Atmospheric Circulation over the South African Region during Austral Winter. Journal of Climate 18:3339-3355. doi:10.1175/JCLI3474.1.

Rozanski K, Araguás-araguás L and Gonfiantini R (1993) Isotopic Patterns in Modern Global Precipitation. Climate change in continental isotopic records 78:1-36.

Ruben S and Kamen MD (1941) Long-lived Radioactive Carbon: ^{14}C. Physical Review 59:349-354. doi:10.1103/PhysRev.59.349.

Rubidge BS, Day MO, Barbolini N, Hancox PJ, Choiniere JN and Bamford MK (2016) Advances in Nonmarine Karoo Biostratigraphy: Significance for Understanding Basin Development In: Linol B and de Wit MJ Origin and Evolution of the Cape Mountains and Karoo Basin. Springer International Publishing, Switzerland, pp. 141-149.

Sami K (1992) Recharge mechanisms and geochemical processes in a semi-arid sedimentary basin, Eastern Cape, South Africa. Journal of Hydrology 139(1-4):27-44. doi:10.1016/0022-1694(92)90193-Y.

Sanford WE (2011) Calibration of models using groundwater age. Hydrogeology Journal 19(1):13-16. doi:10.1007/s10040-010-0637-6.

Schlosser P, Stute M, Dorr H and Munnich KO (1988) Tritium/^{3}He dating of shallow groundwater. Earth and Planetary Science Letters 89(3): 353-362. doi:10.1016/0012-821X(88)90122-7.

Schramke JA, Murphy EM and Wood BD (1996) The use of geochemical mass-balance and mixing models to determine groundwater sources. Applied Geochemistry 11(4):523-539. doi: 10.1016/0883-2927(96)00007-8.

Schulz HM, Chere N, Geel C, Booth P and de Wit MJ (2016) Is the Postglacial History of the Baltic Sea an Appropriate Analogue for the Formation of Black Shales in the Lower Ecca Group (Early Permian) of the Karoo Basin, South Africa? In: Linol B and de Wit MJ (editors) Origin and Evolution of the Cape Mountains and Karoo Basin. Springer International Publishing, Switzerland, pp. 111-116.

Selley RC (1997) African Basins: Volume 3 of Sedimentary Basins of the World. Elsevier. 391p.

Shiklomanov (1993) World fresh water resources In: Gleick PH (editor) Water in Crisis: A Guide to the World"s Fresh Water Resources. Oxford University Press, New York, pp. 13-24.

Simon MH, Ziegler M, Bosmans J, Barker S, Reason CJ and Hall IR (2015) Eastern South African hydroclimate over the past 270,000 years. Scientific Reports 5(18153). doi:10.1038/srep18153.

Sims WE and Bostick Jr. FX (1969) Methods of Magnetotelluric Analysis. Technical Report No.58. Texas University at Austin Electronics Research Center. http://www.dtic.mil/dtic/tr/fulltext/u2/685130.pdf.

Smith BN (1972) Natural Abundance of the Stable Isotopes of Carbon in Biological Systems. Bioscience 22(4):226-231. doi:10.2307/1296391.

Smith RM and Botha-Brink J (2014) Anatomy of a mass extinction: Sedimentological and taphonomic evidence for drought-induced die-offs at the Permo-Triassic boundary in the main Karoo Basin, South Africa. Palaeogeography, Palaeoclimatology, Palaeoecology 396:99-118.

Smith RMH (1980) The lithology, sedimentology and taphonomy of flood-plain deposits of the lower Beaufort (Adelaide Subgroup) strata near Beaufort West. Transactions of the Geological Society of South Africa 83(3):399-413.

Snoeyik V and Jenkins D (1980) Water Chemistry. New York: John Wiley.

Snyman HA (1998) Dynamics and sustainable utilization of rangeland ecosystems in arid and semi-arid climates of southern Africa. Journal of Arid Environments 39(4):645-666.

Soddy F (1913) The Radio-Elements and the Periodic Law. Nature 91:57-58. doi:10.1038/091057a0.

Soeder (2012) Shale Gas Development in the United States In: Al-Megren H (editor) Advances in Natural Gas Technology. In Tech, pp.3-28 http://www.intechopen.com/books/advances-in-natural-gas-technology/shale-gas-development-in-the-unitedstates.

Soeder DJ (2017) Unconventional: Natural Gas Development from Marcellus Shale. Geological Society of America Special Paper 527, Colorado, pp. 143.

South African Department of Environmental Affairs (2015). Climate Change Adaptation Plans for South African Biomes https://www.environment.gov.za/sites/default/files/reports/climatechangeadaptation_plansforsouthafricanbiomes_report.pdf.

Stewart MK (1975) Stable isotope fractionation due to evaporation and isotopic exchange of falling waterdrops: Applications to atmospheric processes and evaporation of lakes. Journal of Geophysical Research 80(9):1133-1146. doi:10.1029/JC080i009p01133.

Stowe MJ, Harris C, Hedding D, Eckardt F and Nel Werner (2018) Hydrogen and oxygen isotope composition of precipitation and stream water on sub-Antarctic Marion Island. Antarctic Science 30(2):83-92. doi:10.1017/S0954102017000475

Swana K (2016) Application of Hydrochemistry and Residence Time Constraints to Distinguish Groundwater Systems in the Karoo Basin prior to shale-gas exploration. Unpublished MSc thesis. Stellenbosch University.

Swatuk LA (2017) Water in Southern Africa. University of KwaZulu-Natal Press, KwaZulu-Natal. 130p.

Tadross M. and Johnston P (2012) Climate Systems Regional Report: Southern Africa. ICLEI-Local Governments for Sustainability. 38p.

Talma AS and van Wyk E (2013) Rainfall and Groundwater Isotope Atlas. Report No. TT 570/13. Water Research Commission.

Thomas D and Shaw PA (1991) The Kalahari Environment. Cambridge University Press, Cambridge, 284p.

Thomas RJ, von Brunn V and Marshall CG (1990) A tectono-sedimentary model for the Dwyka Group in southern Natal, South Africa. South African Journal of Geology 93(4):809-817.

Trumbore SE, Schiff SL, Aravena R and Elgood R (1992) Sources and Transformation of Dissolved Organic Carbon in the Harp Lake Forested Catchment: The Role of Soils. Radiocarbon 34(3):626-635. doi:10.1017/S0033822200063918.

Turner BR (1983) Braidplan deposition of the Upper Triassic Molteno Formation in the main Karoo (Gondwana) Basin, South Africa. Sedimentology 30:77-89.

Unsworth M, Soyer W and Tuncer V (2005) Magnetotelluric measurements for determining the subsurface salinity and porosity structure of Amchitka Island, Alaska. Draft Report June 28 2005. Martyn Unsworth and CRESP. http://www.cresp.org/Amchitka/Amchitka_Final_Report/finalreport/06Append_magneto/6A_MT_report_june2_2C.pdf.

Van der Kemp WJM, Appelo C and Walraevens K (2000) Inverse chemical modelling and radiocarbon dating of palaeogroundwaters: Tertiary Ledo-Paniselian aquifer in Flanders, Belgium. Water Resource Research 36(5):1127-1287. doi:10.1029/1999WR900357.

Van Tonder G, de Lange F, Steyl G and Vermeulen D (2013) Potential Impacts of Fracking on Groundwater in the Karoo Basin of South Africa. Proceedings of the 13th Biennial Conference of the Groundwater Division of the Geological Society of South Africa, Durban, pp. 17-18. http://gwd.org.za/sites/gwd.org.za/files/04_G%20vTonder_Potential%20%20Impacts%20of%20Fracking%20on%20Groundwater.pdf.

Van Wyk E, van Tonder GJ and Vermeulen D (2011) Characteristics of local groundwater recharge cycles in South African semi-arid hard rock terrains-rainwater input. Water SA 37(2):147-154.

Verhagen BT, Butler MJ, van Wyk E and Mutheiwana S (2009) A multi-tracer study of the origins, systematics and hydrological linkages of high nitrate concentrations in groundwater in Bochum District, Limpopo Province. Report No. 1328/1/09. Water Research Commission, Pretoria.

Visser JNJ (1987) The palaeogeography of part of southwestern Gondwana during the Permo-Carboniferous glaciation. Palaeogeography Palaeoclimatology Palaeoecology 61(3-4):205-219.

Vogel JC (1971) Radiocarbon in nature. South African Journal of Science 67(2):32-42.

Vogel JC and Ehhalt D (1963) The Use of the Carbon Isotopes in Groundwater Studies In:International Atomic Energy Agency (editor) Radioisotopes in hydrology, pp. 383-395.

Vogel JC and van Urk H (1975) Isotopic Composition of Groundwater in Semi-Arid Regions of Southern Africa. Journal Of Hydrology 25(1-2):23-36. doi:10.1016/00221694(75)90036-0.

Vogel JC, Ellis RP and Fuls A (1978) The geographical distribution of Kranz grasses in South Africa. South African Journal of Science 74(6):209-215.

Vogel JC, Fuls A and Visser E (2002) Accurate dating with radiocarbon from the atom bomb tests. South African Journal of Science 98:437-438.

Vogel JC, Thilo L and van Dijken M (1974) Determination of Groundwater Recharge with Tritium. Journal of Hydrology 23(1-2):131-140. doi:10.1016/0022-1694(74)90027-4.

Vörösmarty CJ, Green P, Salisbury J and Lammers RB (2000) Global Water Resources: Vulnerability from Climate Change and Population Growth. Science 289(5477):284-288. doi: 10.1126/science.289.5477.284.

Warner NR, Jackson RB, Darrah TH, Osborn SG, Down A, Zhao K, White A and Vengosh A (2012) Geochemical evidence for possible natural migration of Marcellus Formation brine to shallow aquifers in Pensylvania. Proceedings of the National Academy of Sciences of the Unitesd States of America 109(30):11961-11966.

Wassenaar LI, Kumar B, Douence C, Belachew DL and Aggarwal PK (2016) Measurement of extremely ^{2}H-enriched water samples by laser spectrometry: application to batch electrolytic concentration of environmental tritium samples. Rapid Communications in Mass Spectrometry 30(3):415–422. doi:10.1002/rcm.7459.

Weckmann U, Ritter O, Chen X, Tietze K and de Wit M (2012) Magnetotelluric image linked to surface geology across the Cape Fold Belt, South Africa. Terra Nova 24(3):207-212. doi:10.1111/j.1365-3121.2011.01054.x.

Weckmann U, Ritter O, Jung A, Branch T, and de Wit M (2007) Magnetotelluric measurements across the Beattie magnetic anomaly and the Southern Cape Conductive Belt, South Africa. Journal of Geophysical Research: 112(B5) doi:10.1029/2005JB003975.

West AG, February EC and Bowen GJ (2014) Spatial analysis of hydrogen and oxygen stable isotopes ("isoscapes") in ground water and tap water across South Africa. Journal of Geochemical Exploration 145: 213-222. doi:10.1016/j.gexplo.2014.06.009.

Woodford AC and Chevallier L (2002) Hydrogeology of the Main Karoo Basin: Current knowledge and future research needs. Report No. K5/860. Water Research Commission, Pretoria.

Wright DB and London K (2009) First (and second) steps in statistics (2nd edition). Sage Publications, Los Angeles. 250p.